



Technische Universität München

Institut für molekulare Immunologie & Experimentelle Onkologie

Characterization of myeloid cells inducing local T cell activation and proliferation in the hepatic environment

Kim Melissa Pawelka

Vollständiger Abdruck der von der Fakultät für Medizin der Technischen Universität München zur Erlangung des akademischen Grades eines Doktors der Naturwissenschaften (Dr.rer.nat.) genehmigten Dissertation.

Vorsitzender: Prof. Dr. Dirk Busch

Prüfende der Dissertation:

1. Prof. Dr. Percy A. Knolle
2. Prof. Dr. Dirk Haller

Die Dissertation wurde am 22.12.2020 bei der Technischen Universität München eingereicht und durch die Fakultät für Medizin am 13.04.2021 angenommen.

Index

1	Introduction	7
1.1	The 24-hour factory of the body – the liver	7
1.1.1	Storehouse, manufacturing hub and processing plant	7
1.1.2	Immune surveillance with a default to tolerance	7
1.1.3	Immune cell recruitment to the liver	13
1.2	The myeloid cells of the mononuclear phagocyte system (MPS)	14
1.2.1	Origin and differentiation	14
1.2.2	Monocytes	15
1.2.3	Macrophages	16
1.2.4	Dendritic cells	17
1.3	Intrahepatic myeloid cell aggregates for T cell population expansion (iMATE)	19
2	Aim of the study	21
3	Material and Methods	22
3.1	Material	22
3.1.1	Equipment	22
3.1.2	Consumables	23
3.1.3	Chemicals and Reagents	24
3.1.4	Buffer and Media	27
3.1.5	Antibodies	29
3.1.6	Kits	32
3.1.7	Dextramer	33
3.1.8	Enzymes	33
3.1.9	Recombinant cytokines and proteins	34
3.1.10	Beads	34
3.1.11	Mice	34
3.1.12	Software	35
3.2	Methods	35
3.2.1	Injections	35
3.2.2	Preparation of murine tissue	36
3.2.3	Single cell isolation from tissues	36
3.2.4	Surface marker staining and FACS analysis	37
3.2.5	Granzyme B staining	37
3.2.6	Intracellular staining	37
3.2.7	CFSE staining	37
3.2.8	Cell Sorting	38
3.2.9	RNA-sequencing and bioinformatic analysis	38
3.2.10	ELISA	39
3.2.11	BrdU pulse chase	40
3.2.12	DilC ₁ (5)	40
3.2.13	MitoTracker® Green	40
3.2.14	Cross-presentation assay	40
3.2.15	T cell coincubation assay	40
3.2.16	Hexokinase assay	41
3.2.17	Measurement of the extracellular acidification rate (ECAR)	41
3.2.18	2-NBDG assay	42
3.2.19	ProcartaPlex™ multiplex Immunoassay	42
3.2.20	Immunohistochemistry of liver sections	42

3.2.21	Immunofluorescence of liver tissue	42
3.2.22	Statistical Analyses	43
4	Results	44
4.1	Dynamics of myeloid cell composition after TLR9-L application	44
4.1.1	Transient disappearance of Kupffer cells and increase influx of CD11b ⁺ cells	44
4.1.2	TLR9-L application does affect other lymphoid organs as well	45
4.2	The disappearance of CD11b ⁺ Clec4F ⁺ Ly6C ^{neg} Kupffer cells is not a prerequisite for iMATE formation	47
4.3	iMATE formation is only induced by TLR9-L	49
4.4	iMATE forming myeloid cells originate from the circulation	50
4.5	TRL9L induces a specific cytokine expression profile not only in the liver.	51
4.6	Phenotypical plasticity observed after the application of TLR9-L in the liver	52
4.6.1	Four markers display the heterogenous nature of myeloid cells	53
4.6.2	Additional phenotypical characterization did not result in an iMATE-specific marker	54
4.7	Genetic profiling of iMATE tissue identifies CD40 as a potential biomarker	56
4.7.1	Potential iMATE specific markers	58
4.7.2	Overall differentially expressed genes	61
4.8	Validation of the potential role of CD40 as a biomarker	62
4.8.1	Transient expression of CD40 on hepatic CD11b ⁺ Ly6C ⁺ cells after TLR9-L application	62
4.8.2	CD40 expression on Ly6C ⁺ cells is only found in the liver	63
4.8.3	CD40 is the only TNF receptor that is significantly upregulated due to the application of TLR9-L	64
4.8.4	CD11b ⁺ Ly6C ⁺ CD40 ⁺ cells form a rather homogenous cell population	65
4.8.5	CD11b ⁺ Ly6C ⁺ CD40 ⁺ cells are not found in the liver after the treatment with other TLR ligands	66
4.8.6	No elevated expression of CD40L was detected in the liver after the application of TLR9-L	67
4.8.7	CD11b ⁺ Ly6C ⁺ CD40 ⁺ cells have a specific cytokine expression profile	67
4.8.8	CD40 expression is not necessary for iMATE formation and CD8 ⁺ T cell expansion	68
4.9	mRNA sequencing identifies a unique set of genes that is differentially expressed by CD11b ⁺ Ly6C ⁺ CD40 ⁺ cells	69
4.9.1	Comparing Ly6C ⁺ CD40 ⁺ myeloid cells to Clec4F ⁺ Kupffer cells identifies fundamental differences	69
4.9.2	Data generated by RNA sequencing are partially found in the gene array	73
4.9.3	Pathway and gene set enrichment analysis illustrated the pro-inflammatory nature of CD11b ⁺ Ly6C ⁺ CD40 ⁺ cells	74
4.9.4	Transcription factor analysis detects an IRF8 core signature	75
4.9.5	An elevated glycolytic capacity in CD11b ⁺ Ly6C ⁺ CD40 ⁺ cells is detected by weighted gene correlation analysis (WGCNA)	77
4.9.6	The strong differences in gene expression cannot be found when compared to other cell types.	78
4.10	CD11b ⁺ Ly6C ⁺ CD40 ⁺ cells display a glycolytic phenotype and an increased capacity to induce CD8 ⁺ T cell proliferation	79
5	Discussion	84
5.1	iMATEs arise within an immunogenic window	84
5.2	The dynamic changes in the composition of hepatic myeloid cells after TLR9-L application	85
5.3	iMATE specific gene set reflect its local microenvironment	87
5.4	CD40 is a surrogate marker for a distinct myeloid cell population with specific properties involved in iMATE formation	88

5.5	Implications for future research	91
6	<i>Supplementary</i>	93
6.1	References	93
6.2	Table of figures	113
6.3	Index of tables	114
6.4	Supplementary Tables	114
6.5	Index of supplementary Tables	123
6.6	Abbreviations	127
6.7	Prior publications	128
7	<i>Acknowledgement</i>	129

Summary

Intrahepatic myeloid-cell aggregates form in response to Toll-like receptor 9 (TLR9) signaling in a TNF-dependent fashion and provide a unique anatomic structure that drives local proliferation of cytotoxic CD8 T cells (iMATEs) and confers protection against viral infection. Yet, the identity and functional profile of the iMATE-defining myeloid cell population remained elusive. The current study was undertaken to identify the iMATE-forming myeloid cell population to gain mechanistic insights into iMATE-formation and T cell expansion and to characterize a molecular marker that predicts iMATE-formation.

The phenotype of myeloid cells in the murine liver after TLR9 activation was analyzed systematically using a set of different methodologies. Initial flow cytometric phenotypic characterization and tSNE analysis revealed a complex composition of monocytes and newly differentiating macrophages that hinted towards a sequential replacement of liver-resident macrophages followed by repopulation through bone marrow derived inflammatory monocytes. Laser-capture microdissection and genome wide analysis of gene expression identified a set of marker proteins that were validated by flow cytometry and led to the definition of a particular phenotype of CD40-expressing monocyte-derived macrophages that are exclusively found in iMATEs but not elsewhere in the host. Further genomic characterization employing RNA sequencing revealed substantial differences to liver-resident Kupffer cells and identified specific metabolic properties relevant for local induction of immunity. Functional assays of these iMATE-defining monocyte-derived macrophages revealed metabolic competence with high-level glycolysis and revealed that these cells are highly potent in the induction of CD8 T cell proliferation, in the differentiation towards GzmB expression rendering them efficient killer cells and in cross-presenting soluble antigens to CD8 T cells. Liver macrophages, in contrast, displayed a low glycolytic rate and failed to provide any support for T cell proliferation and did not show significant cross-presentation capacity. The transient presence of iMATE-defining monocyte-derived macrophages in the liver indicates that protective hepatic T cell immunity is determined by the dynamics of the changes in inhibitory vs stimulatory macrophage populations, that do not fall into the conventional M1/M2 categories but are related to iMATE formation.

Zusammenfassung

Intrahepatischer myeloider Zellaggregate (iMATEs) bilden sich auf Grund des durch Toll-like Rezeptor 9 (TLR9) induzierten TNF Signalings. Sie stellen einzigartige anatomische Strukturen da, die die lokale Proliferation zytotoxischer T Zellen fördern und Schutz gegen virale Infektionen darstellen. Die Identität und das funktionale Profil der iMATE-bildenden Zellen sind bis jetzt noch unbekannt. Sie sollten mit Hilfe der vorliegenden Studie identifiziert werden, um Einblicke in die mechanistischen Vorgänge der iMATE Bildung und T Zellexpansion zu gewinnen. Des Weiteren sollte ein molekularer Marker für die Prognostik der iMATE Formation bestimmt werden.

Der Phänotyp der myeloiden Zellen in der murinen Leber nach der Anwendung des Liganden für TLR9 wurde mit Hilfe verschiedener Methoden systematisch analysiert. Die initiale phänotypische Charakterisierung mit Durchflusszytometrie und tSNE Analyse offenbarte eine komplexe Zusammensetzung von Monozyten und neu differenzierten Makrophagen. Alles wies darauf hin, dass leberresidente Makrophagen nach und nach durch inflammatorische Monozyten aus dem Knochenmark ersetzt werden. Eine Gruppe von Markerproteinen wurden mit Laser-Mikrodissektion und anschließender genomweiter Analyse der Genexpression bestimmt und durchflusszytometrisch validiert. Dabei konnte ein bestimmter Phänotyp CD40 exprimierender von Monozyten abstammender Makrophagen definiert werden, der nur in iMATEs auftaucht. Weiterführende genomische Charakterisierung durch RNS Sequenzierung konnte zeigen, dass substanzielle Unterschiede zwischen CD40 exprimierender von Monozyten abstammender Makrophagen und leberresidenten Kupfferzellen bestehen. Des Weiteren wurde spezifische metabolische Fähigkeiten identifiziert, die für die Induktion lokaler Immunität von großer Bedeutung sind.

Die metabolische Kompetenz der iMATE definierenden von Monozyten abstammender Makrophagen wurde mit Hilfe funktioneller Assays untersucht und zeichnete sich vor allem durch eine hohe glykolytische Aktivität aus. Darüber hinaus sind diese Zellen äußerst potent in der Kreuzpräsentation löslicher Antigene zu T-Zellen und der Induktion von T-Zellproliferation und Differenzierung hin zur Granzyme B Expression, was diese Zellen zu effizienten Killerzellen macht. Im Gegensatz dazu konnte bei Lebermakrophagen nur eine geringe glykolytische Rate festgestellt werden. Die T-Zellproliferation wurde nicht unterstützt und eine signifikante Kreuzpräsentationskapazität konnte nicht festgestellt werden.

Die transiente Präsenz iMATE-definierender von Monozyten abstammenden Makrophagen in der Leber spricht dafür, dass die protektive hepatische T-Zellimmunität durch die dynamischen Veränderungen in den Populationen der inhibitorischen und stimulatorischen Makrophagen, die nicht in die konventionellen M1/M2 Kategorien fallen, bestimmt wird und mit der Bildung von iMATEs zusammenhängt.

1 Introduction

1.1 The 24-hour factory of the body – the liver

The liver is the largest solid internal organ in the body and has metabolic, clearance as well as immunological functions, thereby supporting other organs as well as impacting almost all physiological systems¹. Even though classically perceived as a non-immunological organ it is involved in complex immunological activities. It harbours the largest population of tissue resident macrophages and the greatest density of NK and NKT cells. The hepatic reticulo-endothelial network of immune sentinels and effector cells is highly dynamic and complex and forms the primary line of defence. Its size is unparalleled elsewhere in the body².

1.1.1 Storehouse, manufacturing hub and processing plant

The liver is central to a proper and efficient metabolism of nutrients and clearance of toxins. It is involved in the formation and secretion of bile as well as the metabolism of carbohydrates, fats and proteins³. It clears the body from drugs, toxins, steroids and hormones and synthesizes plasma proteins like albumin or clotting factors. It is constantly exposed to high levels of fat and carbohydrates⁴. Whereas carbohydrates are taken up and stored as glycogen within hepatocytes, dietary fats are broken down to lipoproteins that are used as cholesterol and triglycerides throughout the whole body⁵.

Glucose, the basic element of carbohydrates, is stored within muscles and the liver as glycogen. Whereas the hepatic glycogen is used to regulate the blood glucose levels the muscular glycogen can only be used for muscle activity. Therefore, it is of great importance that the hepatic glycogen reservoirs get restored continuously⁶. Glucose coming from the intestines over the portal blood is taken up by hepatocytes via Glut transporter molecules. The glucokinase will phosphorylate glucose to glucose-6-phosphate that can be either used in glycolysis or stored as glycogen. Even though glycolysis can provide energy, most of the hepatic energy need is covered by amino and fatty acid oxidation. Therefore, most of the absorbed glucose will be stored. The liver is also the main site of gluconeogenesis, a process similar to glycolysis just reverse⁷.

The liver has a central role in the lipid metabolism, as it is the main site for fatty acid and lipoprotein synthesis, conversion and regulation of the energy balance⁸. It produces the bile that is needed for intestinal lipid absorption, secretes the cholesterol that is used in lipid metabolism and produces as well as clears lipoproteins from the circulation⁹.

The metabolic processes are tightly linked to inflammation. Excessive metabolite production or dysregulated processes can induce inflammatory processes. Metabolites like succinate or cholesterol as well as triglycerides can have inflammatory effects as well^{8,10}, inducing fatty liver disease^{11,12}, chronic inflammation¹⁰ or NASH¹³.

1.1.2 Immune surveillance with a default to tolerance

1.1.2.1 Hepatic architecture

The liver has a unique microanatomical and immunological environment¹⁴. It is localized at the confluence of arterial blood from the hepatic artery and venous blood from the portal vein and filters around 30% of the total blood volume per minute¹⁵. About 80% of the blood is derived

from the portal vein, blood rich in nutrients and pathogen-derived molecules from the gut, that had bypassed primary immune sentinel structures like the spleen or lymph nodes. The remaining 20% are derived from the hepatic arteries¹⁶. This creates low oxygen tension and perfusion pressure as well as a slow irregular blood flow. Arterial blood entering the liver rapidly loses speed as the liver is permeated by a net of small sinusoids, that are capillary like vessels. The sudden increase in total cumulative vessel diameter slows down the blood flow, maximizing the immune cell – gut-derived antigen interaction time and enabling detection and uptake by immune cells like liver sinusoidal endothelial cells lining the sinusoids¹⁷. The immune cells create a fenestrated sinusoidal endothelium allowing for a direct contact of blood and hepatocytes.

1.1.2.2 Preferential induction of immune tolerance over immunity in the liver

The liver is a primary entity of immune surveillance for blood-borne pathogens and serves as a buffer between gut-derived antigens and the systemic circulation¹⁸. Despite the constant exposure to antigens as well as frequent tissue remodelling and changing metabolic activity, the liver is not in a constant state of inflammation¹⁹, but developed highly specialized mechanisms of immune tolerance¹ to assure tissue homeostasis²⁰. The inherent tolerogenicity of the liver is mainly due to its unique antigen presenting cell populations, cell autonomous molecular pathways that regulate inflammation and locally produced mediators that regulate innate and adaptive immunity¹⁴. Gut derived microbial antigens can trigger low-level inflammation that is rapidly regulated, allowing metabolic functions to be continued unaffected and leaving the tissue undamaged¹⁹. Additional activity is only tolerated under pathogenic conditions¹⁸. The liver needs to balance immune tolerance towards harmless molecules against being alert for possible infectious agents. The hepatic anatomy and a specific set of resident cell populations form a distinct local immune environment with a unique cytokine / growth factor milieu that favours a state of tolerance, which can be reversed to local immunity²¹. This is supported by a complex collaborative network between antigen presenting, lymphoid and nonparenchymal liver cells¹⁹. Immune tolerance in the liver is enabled by nonconventional immune cells, which maintain an immature phenotype and mainly produce tolerogenic cytokines like IL10 which was attributed to the specific microenvironment shaped by hepatic parenchymal cells²². Tolerance is not only defined by immunoregulatory cytokines but also by silencing of T cells in an antigen-specific fashion²³ or interaction with inhibitory molecules²⁴, as well as the failure of effective antigen presentation by nonconventional antigen presenting cells like hepatic stellate cells or hepatocytes¹⁶.

1.1.2.3 Antigen presenting cells in the liver

Antigen presentation systems have evolved to direct T cells towards possible threats as they cannot process free antigen by themselves²⁵. In the liver it is not only the classical professional antigen presenting cells like dendritic cell that presents antigen. Rather also liver cell populations, like liver sinusoidal endothelial cells (LSEC), hepatocytes, hepatic stellate cells and Kupffer cells have antigen presentation capacity²⁶. They recognize microbial associated molecular patterns (MAMP) as well as damage-associated molecular patterns (DAMP).

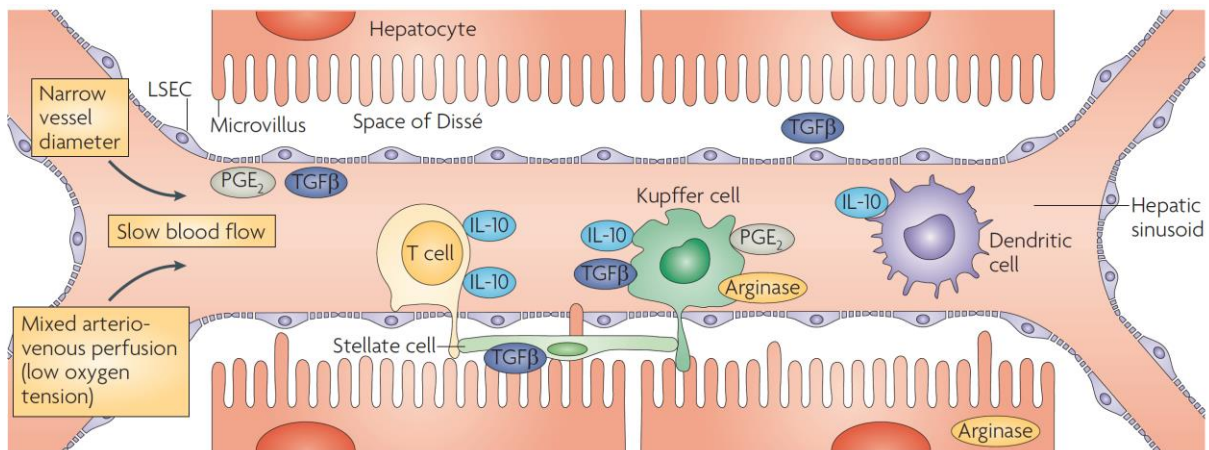


Figure 1: “Anatomical location of hepatic antigen-presenting cells (APCs) and the factors that regulate their function¹⁴.”

1.1.2.3.1 Dendritic cells

Several populations of dendritic cells (DCs) can be found in the liver primarily located in the periportal areas and around the central veins²⁶. They arise from bone-marrow derived hematopoietic stem cells that enter the liver in an immature state but also from circulating monocyte precursors²⁷. Within the liver they do not mature the same way DCs do in secondary lymphoid tissues and remain in less mature state with respect to their phenotype and function^{28–30}. Liver resident DCs are comprised out of myeloid/conventional (CD11b⁺; moDCs), crosspresenting (CD103⁺) and plasmacytoid (B220⁺; pDC) as well as CD11c⁺CD8⁺DCs. Like regular DCs, they internalize antigen and transport it to draining lymph nodes, where they induce T cell activation. However, this activation is not as efficient as compared to non-hepatic DCs. Most of the hepatic DCs have rather tolerogenic properties. This has been related to their unique functional properties and the local hepatic cytokine milieu that is high in IL-10 but low in IL-12²⁹ and constrains the expression of MHCs and co-stimulatory molecules to very low levels. Especially moDCs, monocytes that differentiate into dendritic cells, attenuate the T cell response by producing IL-10 and indoleamine 2,3-dioxygenase (IDO) instead of IL-12²⁹. They suppress local T cell proliferation and can induce apoptosis of cytotoxic T cells. The constitutive expression of PD-L1 by pDCs and PGE₂ by moDCs limit the effective onset of an adaptive immune response^{14,31}. It remains controversial whether monocytes represent DC precursors³². Most of them display an antigen-specific and transient hypo-responsiveness that had been termed endotoxin tolerance in the context of LPS³³. Another type of DCs found in the liver belongs to a rarely found subpopulation of DCs – the NK-DCs. Those cells have characteristics of both NK cells as well as DCs and are found to be enriched in the liver³⁴. Together with the CD11c⁺CD8⁺DCs they support the development and activation of cytotoxic T cells (CTLs). Their activation via pathogen-associated molecular patterns (PAMPs) can potentiate the immune response by production of large amounts of cytokines like IFNγ³⁵.

1.1.2.3.2 Liver sinusoidal endothelial cells

The first immune cells that get into contact with blood-borne pathogens are the liver sinusoidal endothelial cells (LSEC). LSECs account for 50% of liver non-parenchymal cells and line the liver sinusoids. They separate the hepatocytes from the blood and form a fenestrated endothelium. LSECs are able to detect, capture and present pathogenic particles to lymphocytes inducing the development and maintenance of T cell tolerance³⁶. LSECs express several adhesion molecules

like intercellular adhesion molecule-1 (ICAM-1), vascular cell adhesion molecule-1 (VCAM1) and vascular adhesion protein-1 (VAP-1) at higher levels than found in other tissues³⁷. Furthermore their expression of MHC class I and II and molecules for co-stimulation (CD80, CD86, CD40) that would make them really efficient in antigen presentation³⁸, if they were not expressed at low levels under steady state conditions³⁹. LSECs can activate T cells but IL-10 and PGE₂ that are expressed by Kupffer cells and the LSECs themselves impair their maturation to effector T cells. LSECs as well as dendritic cells remain at a rather immature level of differentiation and PAMPs cannot trigger their functional maturation¹⁴.

1.1.2.3.3 Hepatocytes

Hepatocytes are the parenchymal cells of the liver making up make up for 80% of all hepatic cells. They are primarily engaged in the metabolism, protein production and clearance of toxins. Nonetheless they can activate innate and adaptive immunity, as they can detect pathogens and present antigens. Hepatocytes mediate inflammation via complement and acute phase proteins such as C-reactive protein, transforming growth factor beta (TGF- β), tumour necrosis factor alpha (TNF α), IL-6 and opsonizing proteins. The acute phase proteins do not only trigger systemic inflammation for pathogen clearance but are also capable of limiting excessive inflammation^{40,41}. In addition, hepatocytes can directly activate naïve T cells via MHC class I and II expression. This activation commonly induces the apoptosis of activated T cells⁴². The IL-10 rich environment inducing the expression of PD-L1 also influences hepatocytes.

1.1.2.3.4 Hepatic stellate cells

Hepatic stellate cells (HSC) also known as Ito cells are another member of the hepatic sentinels. They are characterized by their astral phenotype and can be found between hepatocytes and LSECs. They account for 5-8% of all NPCs and are mainly involved in vitamin A and lipid storage as well as fibrinogenesis. On the other hand, they express molecules for antigen presentation like MHCs and co-stimulation like CD80/86 and are capable of direct T cell activation in the inflamed liver⁴³. Retinoic acid derived from vitamin A and TGF β is the tolerogenic driver of the HSCs next to their expression of PD-L1^{44,45}.

1.1.2.3.5 Kupffer cells

Kupffer cells form the largest tissue resident population of macrophages. They account for 80-90% of all tissue macrophages and 35% of the NPCs in the liver. Their ontogeny remains under debate. For a long time, they were described to originate from the bone marrow, entering the liver as monocytes and to differentiate locally in the liver⁴⁶. Nowadays, more and more evidence is found that Kupffer cells are yolk sac derived cells seeded in the liver during embryogenesis with self-renewing capacity⁴⁷. Nevertheless, if Kupffer cells are depleted for any reason, the Kupffer cell niche will be replenished by immigrating monocytes that re-differentiate to Kupffer cells. After a differentiation period⁴⁸ they reach the same functionality but may still differ in their transcriptomic signatures⁴⁹. Interestingly it is rather liver derived factors that imprint the Kupffer cell functionality than the constant exposure to microbial molecular patterns⁴⁸. Keeping the varying and dynamical environmental conditions in mind, it is not surprising that the Kupffer cells do not form a homogenous population⁵⁰.

Kupffer cells are stationary located in the vasculature and adhere to LSECs⁵⁰ where they stay adherent over a longer period of time. As competent sentinels, Kupffer cells capture and internalize pathogens and pathogenic molecules out of the blood stream with a massive array

of scavenger, Toll-like (TLR), complement and antibody receptors. Apart from the immune regulation they are also involved in tissue repair and liver regeneration⁵¹. Even though Kupffer cells can release pro-inflammatory cytokines like Il-1, Il-6 and TNF α and carry the full repertoire needed for antigen cross-presentation (MHC; co-stimulatory molecules) they are poor activators of the adaptive immune response⁵². Their production of additional inflammatory cytokines like Il-12 and Il-18 which activate NK cells is rapidly followed by production of anti-inflammatory Il-10⁵². Kupffer cells are continuously in contact with common gut bacteria and thus are more active in preventing immunity. Nevertheless, inflammatory cytokines or pathogen associated molecules can render them rapidly from tolerogenic to potent antigen presenting cells⁵³.

In addition to the clearance of pathogens, Kupffer cells bind to neutrophils, platelets and activated host cells. Depending on the receptor they are bound to this immune clearance can induce the secretion of anti- or pro-apoptotic cytokines⁵⁴ and mount an intravascular immunity¹⁴.

1.1.2.3.6 Liver resident lymphocytes

Apart from antigen presenting cells a set of heterogenous resident and transiting lymphocytes with many additional functional characteristics is also found in the liver. Especially innate lymphocytes are highly enriched⁵⁵ and differ in numbers and function from lymphocytes found in other tissues or the blood. Most of those lymphocytes belong to the group of unconventional T cells that express TCRs with a limited diversity and can influence both innate and adaptive immune responses⁵⁶. Up to 50% are natural killer (NK) cells, sentinels for viral and bacterial infections, found at unusual high numbers compared to the blood for example⁵⁷. The same is true for $\gamma\delta$ -T cells. In the rest of the body they are only found at low concentrations, in the liver they account for 15-20% of all hepatic lymphocytes and form one of the largest populations of $\gamma\delta$ T cells in the whole body⁵⁸. Natural killer T cells (NKT) make up for the remaining 20-30% of innate lymphocytes in the liver. The hepatic NKT cells actively patrol the vasculature and are activated by a diverse array of signals. They can be pro- or anti-inflammatory and rapidly produce cytokines upon activation. The hepatic innate lymphocytes are derived from the bone marrow and complete their maturation locally within the liver⁵⁹. Liver resident T cells do not undergo thymic selection. Only around 50% of the CD3⁺ cells express the T cell receptor at intermediate amounts. The ratio of CD4⁺ to CD8⁺ cells in the liver - 1:2 - is opposite to the ration in the blood.

NK cells are traditionally classified as either cytolytic or immunoregulatory⁶⁰. The hepatic NK cells are different from the conventional ones in terms of function, phenotype and origin and have been compared to innate lymphoid cells that present immunoregulatory properties⁶¹. $\gamma\delta$ T cells express rearranged antigen receptors and recognize stress-inducible proteins like MICA and MICB as well as glycolipids⁶². NKT cells are lymphocytes with a restricted set of $\alpha\beta$ TCR and NK cell markers and multiple cytotoxic activities⁶³. NKT cells recognize glycoproteins and lipids presented on CD1d and by MHCI and kill their target cells and secrete growth factors as well as cytokines^{64,65}.

T cells are the central players of the adaptive immune response. They are trapped within the liver by adhesion molecules like ICAM-1 or VCAM-1 expressed by LSECs or Kupffer cells. Upon

TCR ligation they activate B cells, lyse the target cells and release several cytokines like IL-2, IFN γ and TNF α that influences other immune cells. Some hepatic T cells also produce IL-4, a cytokine that has been linked to a rather regulatory T cell type. To further support the hypothesis of the unique hepatic environment a population of non-MHC restricted killer cells (lymphokine activated killing (LAK) cells) has also been discovered within the liver⁶⁶.

Mucosal-associated invariant T (*MAIT*) cells make up for one of the largest populations of T cells within the human liver where they have an important role in the hepatic firewall defending in the first line⁶⁷. In contrast to that the murine livers only harbors a very small population even though the highest frequency is found in the liver⁶⁸.

Regulatory T cells (T_{reg}S) are important for central and peripheral tolerance. In the liver they work together with Kupffer cells in creating a local immunosuppressive milieu by producing IL-10 and actively suppressing the activation of effector T cells⁶⁹.

1.1.2.4 Platelets

Not only liver resident cells participate in the immune surveillance but also components of the blood namely the platelets. Under steady state conditions they can shortly interact with Kupffer cells (touch & go) scanning for pathogens. If a pathogen is captured platelets not only touch but also adhere and form aggregates around the pathogen. This probably shields the pathogen from other immune cells and prevents an inflammatory immune response⁷⁰. In addition, platelets can produce defensins and other antimicrobial molecules. Altogether the mechanisms how platelets are involved in the immune response are in need for more detailed analysis.

1.1.2.5 Receptors for pathogen recognition

For the detection of pathogens immune cells are equipped with two types of receptors: pattern recognition (PRRs) and humoral receptors.

The PRRs identify endo- and exogenous, self- and pathogen-derived molecular patterns. This diverse class of multifunctional receptors is not specific for single pathogens but recognizes a limited set of pathogen-associated molecular patterns (PAMPs). The array includes scavenger, carbohydrate, cytoplasmic and Toll-like receptors (TLRs). Scavenger receptors are mainly found on LSECs and bind to PAMPs circulating in the blood. The mannose receptor, part of the carbohydrate receptor family, recognizes specific sugar tags on circulating particles and induces internalization. This receptor is also found on LSECs. The cytoplasmic receptors are expressed by hepatocytes and are important for the detection of intracellular infections. They bind to viral RNA (MDA-5, RIG-I) and parts of bacterial cell walls (NOD-like receptors) and induce the production of pro-inflammatory cytokines^{71,72}. TLRs can be found on the cell surface (1, 2, 4, 5, 6) and within endosomes (3, 7, 8, 9). They are key upstream mediators of inflammation and some of them are found on hepatic cells. Kupffer cells express TLR2, TLR4 and TLR9. Hepatocytes express TLR2 and 4 but their response to stimulation is rather weak. Hepatic stellate, dendritic and sinusoidal endothelial cells have been shown to express TLR4⁷³. They induce cellular activation, cytokine production and can modify cellular functions. And again, the immune response evoked by TLRs expressed in the liver differs from TLRs found in other organs. Lipopolysaccharide (LPS) for example that binds to TLR4 is a potent immuno-activator of circulating leukocytes. In the liver it induces the production of IL-10, an anti-inflammatory cytokine and interferes with antigen presentation³⁶. This immune evasion¹⁴ is essential as the

liver is constantly exposed to large amounts of bacteria-derived molecules from the gut within the portal blood. It has been proposed that common concentrations of TLR ligands detected by hepatic TLRs dampen the immune response. Higher concentrations, on the contrary, can overcome the tolerance and induce a fully blown immune response⁷⁴.

1.1.3 Immune cell recruitment to the liver

The recruitment of immune cells to the liver is induced by chemotactic cytokines like MCP1 and IL8⁷⁵ that are small protein mediators secreted by antigen presenting cells upon their activation due to hepatic injury or inflammation⁷⁶. Especially chemokines drive the migration of immune cells. The cells will migrate along a gradient of increasing chemokine concentrations in direction of the source of chemokine production⁷⁷. Recruited immune cells will produce further pro-inflammatory cytokines amplifying the inflammatory response. Their recruitment does not follow the classical pattern of leukocyte adhesion cascade and is tightly regulated⁷⁸. Several adhesion molecules are involved in this process that differ according to the site of adhesion, mainly the hepatic sinusoids. Neutrophils use selectins in postcapillary venules⁷⁹. Within the liver sinusoids hyaluronan has been shown to be a key ligand for the adhesion⁸⁰. Many leukocytes use CD44, Mac-1 and Icam-1⁸¹ for adhesion. The NKT cells rather rely on V α 4 and V β 1. For the recruitment of some monocytes subsets CCR1 and CCR2 seem to play an important role^{82,83}, for others it is rather CCR5, CX₃CR1 and CCR6⁸⁴⁻⁸⁶. Monocytes are not only recruited to the liver due to liver damage or ongoing inflammation. They can replenish the Kupffer cell niche and contribute to the macrophage pool in the liver. In addition to filling in the Kupffer cell niche they gradually adopt a Kupffer cell like transcriptional profile and become self-renewing, long-lived cells. They then strongly resemble embryonic yolk-sac derived Kupffer cells and even compete with them for niche repopulation⁸⁷. Monocytes are also recruited from the circulation to control infections and tissue repair⁸⁸. Many of them will differentiate into an alternatively activated phenotype with regulatory properties. They transiently contribute to local inflammation and promote its resolution until the homeostasis is restored^{89,90}. Myeloid derived suppressor cells (MDSCs) are attracted by serum amyloid A an acute phase protein⁷⁷. The main route of infiltration for immune cells into the liver is via the blood stream. However, recently J Wang et al. described mature peritoneal macrophages that rapidly infiltrated the liver at infectious sites, shedding light onto a different route of immigration into the liver⁹¹. Neutrophils that are recruited to the liver upon infection clear viruses and bacteria from the circulation. They will interact with the endothelium, crawl along the sinusoids and extravasate or remain sessile within. A tight regulation of neutrophil recruitment enables to balance pathogen control against immunopathology⁶³.

The liver is not a classical secondary lymphoid organ but as a frontline sentinel it has the unique capacity to induce immune tolerance and hypo-responsiveness on the one and a rapid and robust immune response on the other side. The complex interactions between the liver resident cell populations enable this finely tuned balance. The low abundance of MHCs and co-stimulatory molecules creates an environment that does not support induction of immunity. T cells can be primed locally in the liver, but typically are devoid of licensing cytotoxic effector functions. One of the inhibitory molecules involved in local induction of immune tolerance is PD-L1 that is expressed by LSECs and is operational to induce immune tolerance in T cells. Furthermore it has been described that DCs that directly interact with LSECs induce T cell

tolerance⁹². It can be described as a default to immune non-responsiveness or tolerance^{29,42,93}. The liver function relies on the balance between immunity and tolerance. Tissue damage and remodelling are induced by excessive inflammation due to non-pathogenic molecules. Insufficient immunity prepares the ground for chronic infections and cancer.

1.2 The myeloid cells of the mononuclear phagocyte system (MPS)

Myeloid cells are descendants from hematopoietic precursors in the bone marrow and key factors for innate and adaptive immune responses. The term mononuclear phagocyte system was introduced by Van Furth et al. 1972⁹⁴. It is used to condense all highly phagocytic mononuclear cells namely monocytes, macrophages and dendritic cells into one group. The classification is based on the similarities found in function, origin, morphology and phagocytic kinetics⁹⁴. Members of the MPS are immune cells of the innate immune system that originate from the bone marrow and are constantly released into the circulation. They are not only crucial effectors of the innate immune response but also important for the regulation of the adaptive immunity.

1.2.1 Origin and differentiation

Myeloid cells originate from multipotent hematopoietic stem cells in the bone marrow that are the origin of all blood and immune cells. The stem cells can develop into two different lineages – the myeloid and the lymphoid lineage with a common myeloid, dendritic cell and lymphoid progenitor. A transcription factor network tightly regulates commitment to the respective lineage. The myeloid progenitor, induced by PU.1⁹⁵, further differentiates into megakaryocytes, erythrocytes, mast cells and myeloblasts. The myeloblast gives rise to baso-, neutro- and eosinophil granulocytes as well as monocytes that mature into macrophages and dendritic cells (**Fig. 2**). Whereas transcription factors regulate the commitment to either differentiation, specific colony-stimulating factors determine the terminal maturation. The list of transcription factors is small and includes factors as PU.1, CCAAT/enhancer binding protein alpha (C/EBP α), C/EBP β , C/EBP ϵ , growth-factor independent 1 (GFI1), interferon regulating factor 8 (IRF8), the runt-related transcription factor 1 (Runx1) and others⁹⁶.

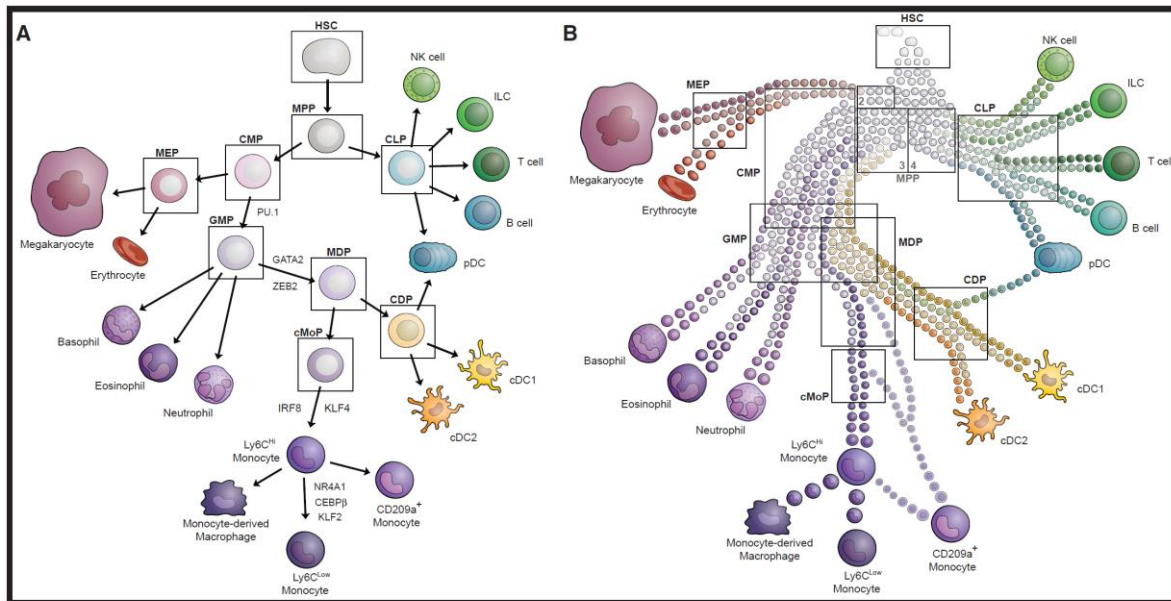


Figure 2: (A,B) Two different views on the hematopoietic development. “(A) Depiction of the classic hierarchical representation of hematopoietic development in the bone marrow; hematopoietic stem cells (HSC) or multipotent precursors (MPP); granulocyte macrophage precursors (GMP); monocyte-macrophage/dendritic cell precursors (MDP); dendritic cell precursors (CDP); common monocyte precursors (cMoP); plasmacytoid DC (pDC); common lymphocyte precursors (CLP); common myeloid precursors (CMP); megakaryocyte/erythrocyte progenitors (MEP); main transcription factors involved in monocyte development are shown (B) Development of the hematopoietic system based on single-cell analysis⁹⁷. ”

1.2.2 Monocytes

The term monocyte describes the third member of the MPS that consists of various distinct functional subsets that are shaped by different developmental pathways. Monocytes are active phagocytes that can differentiate into antigen-presenting cells (APC) like macrophages or dendritic cells⁹⁸. They are key players for both the innate and adaptive immune response and account for 4% of nucleated cells in the blood⁸⁵. Even though their short half-life is only about 20 hours they account for a cellular system of great plasticity and dynamic. Even within one organ they can be highly heterogenous and harbour a multitude of functional modules. According to the local microenvironment they can recapitulate their phenotype and functional features towards induction or resolution of inflammatory reactions⁹⁷. Activation by inflammatory stimuli induces rapid migration to the site of inflammation where the monocytes differentiate according to the tissue-specific factors into monocyte-derived effector cells⁹⁹ and complement the tissue-resident phagocytic compartment. Most physiological processes that monocytes have been described to be involved in so far, are macrophage or DC-like activities. Additional inherent monocytic activities are still under debate. Just recently it was suggested that they might promote angiogenesis and arteriogenesis¹⁰⁰.

Under steady state conditions most monocytes are found circulating in the blood in different states of differentiation relating to size, phenotype and function. They express a variety of receptors that sense environmental changes and induce the differentiation of inflammatory or anti-inflammatory subsets. Phenotypic profiling classified them into ‘patrolling’ ones which are CX₃CR1^{hi}, Ly6C^{low}, CCR2^{neg}, CD62L^{neg}CD43^{hi} and remain as sentinels in the vasculature. The ‘classical’ ones have a high phagocytic capacity due to TLRs and scavenger receptors for PAMP recognition, can be rapidly mobilized and are CX₃CR1^{mid}Ly6C^{hi}CCR2⁺CD62L⁺CD43^{low}¹⁰¹.

Monocytes remove pathogenic materials, lipids and dead cells and produce effector molecules like cytokines and superoxides which can initiate inflammation. The expression level of Ly6C indicates for how long the monocytes have already been circulating. Monocytes with high Ly6C expression just recently left the bone marrow. If they do not get recruited they greatly downregulate Ly6C¹⁰². Several distinct transient states that were discovered remain almost uncharacterized¹⁰³. Monocytes that get recruited and extravasate into tissues can differentiate into macrophage-like or DC-like cell types with comparable functional properties. Furthermore, they secrete ROS, TNF α , NO and Il-1 β . In contrast, patrolling monocytes mainly secrete Il-10. Additional activities originate from their inherent plasticity⁹⁸. C Jakubzick et al (2013) introduced the term 'tissue-resident monocytes' for monocytes that persist in their circulating phenotype within the tissue. They have the capacity to migrate and might transport antigen to the lymph nodes, but their functional classification still awaits definition.

Their ability of a dynamic and rapid recruitment qualifies them as an emergency squad that provides a transient supplement of pro-inflammatory or resolving activities¹⁰⁴.

1.2.3 Macrophages

Macrophages are distributed strategically throughout the body and are either tissue-resident or a mature differentiated form of monocytes that extravasated into tissue, consequently called monocyte-derived macrophages. Their main functions include phagocytosis, antigen processing, danger signal recognition and cytokine release¹⁰⁵. They orchestrate tissue development, homeostasis and inflammation and can be protective but also pathogenic by adopting a variety of activation phenotypes. Macrophages have a long half-life time.

Tissues resident macrophages do not form a homogenous group, but every tissue harbours its own type of macrophages with a unique, tissue-dependant ontogeny, morphology, and function like Kupffer cells in the liver (described in detail before) or microglia in the brain. Most of them originate from embryonic precursors that seed the tissues before birth, get locally imprinted and maintain themselves by self-renewal⁹⁸. Others like macrophages from the marginal splenic pool are replenished by definite hematopoiesis¹⁰⁶ or are of mixed origin. It is proposed that the tissue itself has major influence on balancing persistence versus recruitment¹⁰⁷ as well as the functionality¹⁰⁸. This was confirmed just recently by D R ckerl et al. (2017). Their results indicate that the tissue-specific functionality outweighs cellular plasticity¹⁰⁹. Under steady state conditions tissue-resident macrophages are mainly involved in programmed cell removal that works with "eat me" and "do not eat me" signalling pathways and immune inhibition as well as deactivation of auto-reactive T cells¹¹⁰. In addition to development and tissue homeostasis they are also important factors for the resolution of inflammation and wound repair. Under pathological conditions they can also induce inflammation and consequently the influx of inflammatory leukocytes¹¹¹.

Inflammatory signals recruit additional macrophages, monocyte-derived macrophages into the tissue that have a critical role as effector cells by either establishing a local inflammatory response or by orchestrating resolution of the latter. The respective orientation is controlled by the dynamic changes of tissue environment that influences the direction of programming, activation, and functionality. Phenotype and activity are 'tailored' according to the activating stimulus¹¹².

Over decades the classification of macrophages relied on the model of dichotomous states⁹⁹. The classical, M1 type is described as an effector cell that gets activated by IFN γ and TNF expressed by NK cells. Following activation, it also starts to produce proinflammatory cytokines like Il-1, Il-6 or Il-23 as well as inflammatory mediators like reactive oxygen species (ROS) and nitric oxide (NO). The alternatively activated, M2 type gets activated by PGE₂, Il-10 or apoptotic cells. It will start to produce TGF β or Il-10 and downregulate Il-12 production. Even though high levels of costimulatory molecules like CD80 or 86 have been found on its surface it is regarded as a regulatory cell¹¹³. Just research of the recent years started to describe more and more diverse phenotypes and functions^{114,115}.

1.2.4 Dendritic cells

Dendritic cells form a heterogenous cellular network of bone-marrow derived immune cells with a stellate morphology and endowed with specific functions, best known for their efficient antigen presentation and T cell priming. They capture, process and present antigens on their surface to T cells and thereby serves as the nexus between adaptive and innate immune responses. Furthermore, they are also involved in the fine tuning between tolerance and immunity¹¹⁶. Several subpopulations have been described whose classification is depending on origin, location and function. Their differentiation is dependent on cytokine signalling modulating transcription factor expression¹¹⁷. Dendritic cells were found in the circulation and residing in lymphoid and non-lymphoid tissues where they act as sentinels. Antigen presentation to T cells occurs locally or within the lymph nodes and its result is dependent on DC maturation state and subset as well as location and cytokine signature¹¹⁸.

Many subsets of DCs defined by their development and functionality have been reported, but the three main groups comprise plasmacytoid dendritic cells (pDCs) and conventional/classical dendritic cells type 1 and 2 (cDC1 and cDC2). Their migratory potential is pronounced and tightly regulated¹¹⁹. Migratory processes, mainly in the direction of the lymph nodes, induce the upregulation of MHCII. If the migration is induced by inflammation cytokine production and co-stimulatory molecules are also affected¹²⁰.

pDCs have smooth surfaces and are mainly found in primary or secondary lymphoid tissues (lymph nodes, spleen). They are defined by low expression of MHC class I and II along with poor antigen presentation potential, high expression of TLR7 and 9, B220, PDCA₁ and Siglec-h, as well as abundant expression of type I interferons (IFNs). They are engaged in antiviral and -bacterial responses – recognizing PAMPs and secreting large amounts of TNF α , Il-6 and type I IFNs¹²¹.

cDCs are mainly found in tissues where they sense antigens, transport it to the lymph nodes and induce either immunity or tolerance. cDCs are defined by their phenotype, the expression of CD11c, MHCII, CD135 (fms-like tyrosine kinase 3), c-kit and CCR7. Furthermore, their response to environmental stimuli is reflected in phenotypical changes which aggravates the classification of distinct subsets. The phenotypic plasticity of DCs especially manifests during inflammation¹²².

Non-lymphoid tissues harbour CD103⁺CD11b^{neg} and CD11b⁺cDCs. The CD103⁺cDCs account for about 30% of all cDCs and do not express typical macrophage markers like F4/80 or CD11b¹²³. CD11b⁺cDCs are a mixture of tissue cDCs and monocyte derived DCs. A clear

separation can only be achieved by ontological analysis, as their phenotype is tissue dependant¹²⁴. Lymphoid tissues harbour CD8⁺CD11b^{neg} and CD4⁺CD11b⁺cDCs. CD8⁺cDCs are phenotypical immature and express CD205, Clec9A and langerin¹²⁵. CD4⁺CD11b⁺cDCs display a more mature phenotype and produce more chemotactic cytokines like CCL17 or 22¹²⁶. Both subsets proliferate in situ.

CD103⁺cDCs from non-lymphoid tissues and CD8⁺cDCs from lymphoid tissues share the same functions and have been grouped as CD8 α ⁺ lineage¹²⁷ or cDC₁¹²². They sense pathogens and tissue damage and can activate naïve CD8⁺T cells especially via MHCI and Il-12 production. cDC₁s have a strong cross-presentation capability which explains their strong priming potential¹²⁸ and important role in the induction of adaptive immune responses. Furthermore, they are equipped with a unique immune checkpoint repertoire – Tim3^{hi}, PD-L1^{low} and lack of ILT2¹²⁹. The two CD11b⁺cDCs subsets are important sentinels of the non- CD8 α ⁺ lineage¹²⁷ or cDC₂ that activate CD8⁺ and CD4⁺T cells¹³⁰. Their cross-presentation capacity is not as pronounced, and they are rather relying on MCHII¹³¹ for antigen presentation. cDC₂s are well suited for activation of CD4⁺T cells and humoral immunity¹³². CD8⁺T cell activation involves the cooperation with CD4⁺T helper cells (T_H). CD4⁺T_Hcells activation induces their polarization towards an anti-inflammatory, immunoregulatory or proinflammatory phenotype. pDCs and cDCs are central players in the education of immune cells. Central and peripheral tolerance is achieved by the selection of developing lymphocytes and priming of T regulatory cells (T_{reg}) in the thymus and deletion of auto-reactive T cells in the periphery¹³³.

Inflammatory properties that are linked to activation and maturation manifest in phenotypical changes like upregulation of CD86, CD80 or CD40 and production of cytokines like Il-1, -6, -7, -12, -15, -18, TNF, TGF, M/GM-CSF. Regulatory properties are not so easy to grasp. For a while it seemed as if immune regulatory and tolerogenic functions were mainly linked to immature DCs which circulate in the blood or migrate into peripheral tissues searching for foreign antigens. No co-stimulatory signal 2 is present when antigen is presented to naïve T cells which results in T cell anergy and deletion¹³⁴. Recent studies however detected mature DCs involved in regulatory activities which suggested that regulatory properties are not restricted to one distinct phenotypical subset, but they rather belong to a distinct functional state¹³⁵.

Monocytes that differentiate into DCs upon inflammatory stimuli locally in the tissue or in lymph nodes are called inflammatory dendritic cells (iDCs) or monocyte-derived DCs (moDCs). They are inconspicuous under steady state conditions. moDCs are characterized by low CD11c and high MHCII, TNF α and iNOS expression and participate in direct anti-microbial defense as well as the induction of adaptive immunity¹³². Hitherto conflictive results have been reported ranging from high to no potential in induction of the adaptive immunity^{136,137}. Differences in TH polarization indicate that the potential might be depending on the type of inflammatory stimuli. Their transient appearance and phenotypical heterogeneity complicate a distinct classification. Recent research described a division of labor between moDCs and cDCs¹³⁸.

Other cells that also belong to the group of DCs but will not be described in more detail are epidermal Langerhans cells, semi-mature DCs, follicular DCs, Tip-DCs and NK-DCs¹¹⁷.

1.3 Intrahepatic myeloid cell aggregates for T cell population expansion (iMATE)

L Huang et al. (2013) were the first to discover intrahepatic myeloid cell aggregates for T cell population expansion (iMATEs). They are one example for how the hepatic tolerance can be overcome by specific stimuli. Furthermore, they are a unique anatomical structure as local T cell proliferation has been only described for T memory cells (T_{mem}) so far.

iMATEs are dense cocoon-like non-perfused structures that arise in the liver within 2 days after i.v. TLR9-L application (Fig.1). They develop in a dynamic way and gradually disappear within 6 to 8 days. iMATEs arise from inflammatory monocyte-derived cells that comprise $CD11b^+F4/80^+$ cells that are either $Ly6C^{\text{hi}}MHCII^{\text{neg}}$, $Ly6C^{\text{hi}}MHCII^+$ or $Ly6C^{\text{dim}}MHCII^+$. Kupffer cells, neutrophils, dendritic cells or NK cells do not have a prominent role in formation of these focal inflammatory structures. They are distinct from tertiary lymphoid structures as no collagen IV, smooth muscle actin, platelet derived growth factor receptor beta or lymphotoxin beta-receptor could be detected. Even though they are not demarcated from their surrounding tissue, iMATEs are distinct anatomical compartments. Experiments with mice deficient in recombinant-activating gene 2 ($RAG^{-/-}$) that are devoid of B and T cells did show that their formation does not rely on a crosstalk between myeloid cells and B or T cells. It was rather suggested that TNF signalling pushes iMATE formation via a local feed forward loop.

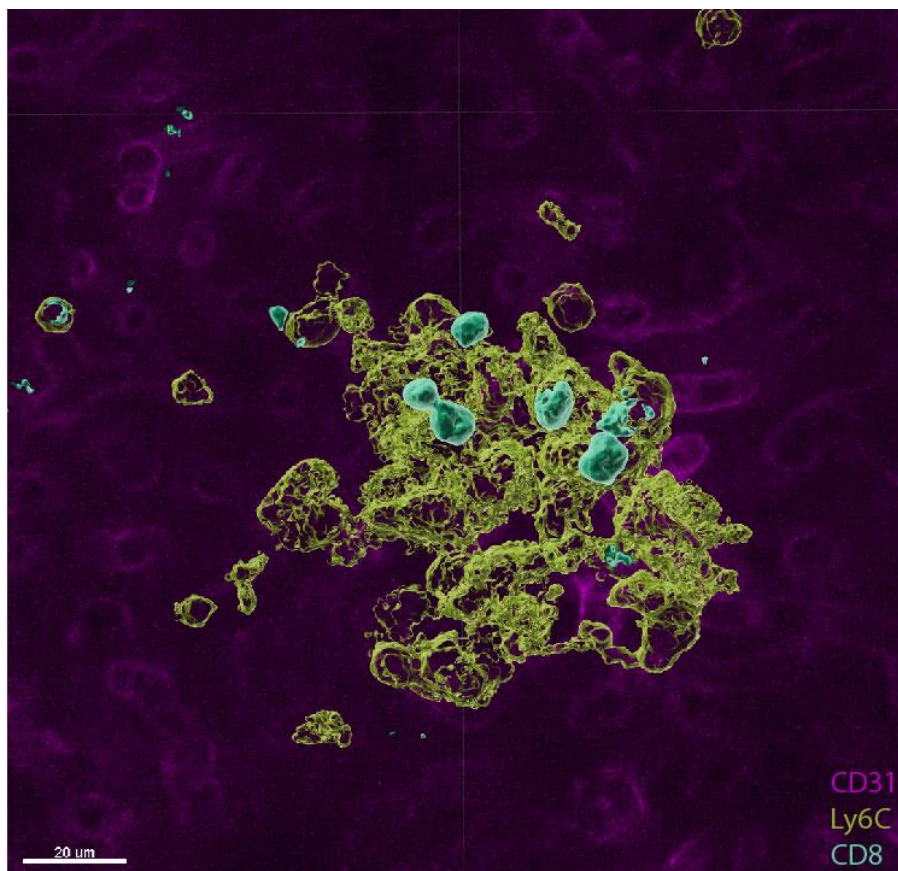


Figure 3: 3D image of an iMATE with T cells (pink: CD31 for vessels, yellow: Ly6C for inflammatory monocytes, turquoise: CD8 for T cells).

iMATEs exist in 3 different distinct structures: the condensed form with generally few proliferating cytotoxic T lymphocytes (CTLs) is found 24 to 48 hours after TLR9-L application;

the dispersed form harbors many proliferating CTLs and is found 72 hours after TLR9-L application; the diffuse form which has only few CTLs left can be observed after 4 days and will rapidly disperse with no trail left.

The results for CTL proliferation were obtained with adoptively transferred pre-activated T cells. Endogenous T cells did also undergo this second phase of expansion but not to the same extent. Even though the CTL population expansion detected was massive it did not come along with pronounced liver damage. This is probably owed to the fact that CTL proliferation is restricted to the iMATE structures. Experiments with splenectomy and or application of sphingosine 1-phosphate antagonist FTY720, which blocks the egress of lymphocytes from the lymph nodes could prove these data. Furthermore, no Ki67⁺ or BrdU⁺ hepatic T cells were found outside of the iMATEs and CTLs colocalized with CD11b⁺MHCII⁺ cells. The expansion was induced antigen independent as no MHC I restricted antigen recognition was observed. Instead, an important role for co-stimulatory molecules like OX40 was detected. Nevertheless, iMATEs can improve antigen-specific responses. In experiments with acute viral infection the viral clearance was facilitated when viral specific CTLs were transferred. It was also shown that acute viral infection alone could induce iMATEs. This induction was absent in chronic viral infections.

TLR9-L had earlier already been shown to overcome hepatic regulatory cues¹³⁹, but this was not accompanied by local T cell proliferation. Here the myeloid cells serve as nursing cells that form a shelter which protects T cells from the local inhibitory signals⁷⁴.

The formation of inflammatory foci has been known for a long time. T cells recruited to an infected site will secrete cytokines that induce other immune cell which in turn secrete chemokines for recruitment of further immune cells¹⁴⁰. Alternatively such a foci might be a sight of activation for naïve T cells by either hepatocytes, HSCs or LSECs^{43,141,142}. The iMATE concept is a radical new vision of these notorious structures¹⁴³. Nevertheless, it remains debateable whether iMATEs are a liver specific phenomenon that arises due to a strong artificial PAMP stimulus or whether they are used in many tissues to secure an appropriate supply of CD8 T cells. Recent research did not address this problem, but could show that MAPKAP kinase 2 prevents formation of iMATEs¹⁴⁴. Furthermore, iMATEs can be induced in a hepatic tumour microenvironment and are able to affect the tumor growth negatively¹⁴⁵.

2 Aim of the study

The liver is a lymphoid organ whose default is set to tolerance. The constant exposure to foreign antigens coming from the intestine would otherwise lead to continuous inflammatory processes, which could damage the liver and lead to constant systemic inflammation as well. Several liver resident immune and parenchymal cells secure the tolerogenic function of the liver. A certain threshold of inflammatory stimuli must be reached before tolerance turns to immunity. The application of TLR9-L did provide sufficient stimulation and enabled the formation of intrahepatic myeloid cell aggregates and the population expansion of cytotoxic T cells within those structures.

This study was aiming for a detailed phenotypic and functional characterization of the iMATE-forming myeloid cells to identify a biomarker for their identification and to understand how T cell activation within iMATEs is achieved.

3 Material and Methods

3.1 Material

3.1.1 Equipment

Equipment	Name	Supplier
Cell dissociation sieve		
Cell separator	autoMACS Pro Separator	Miltenyi Biotec B.V. & Co. KG, Bergisch-Gladbach, DE
cell sorter	SH6800S	SONY Biotechnology, Champaign, USA
Centrifuges	- Heraeus® Fresco 17 - Heraeus® Multifuge X3R	Thermo Fisher Scientific, Waltham, MA/USA
CO ₂ Incubator	HERAcell 150i	Thermo Fisher Scientific, Waltham, MA/USA
Counting chamber	Neubauer chamber	Karl Hecht GmbH, Sondheim, DE
Electrophoresis system	Mini-PROTEAN® Tetra Cell	BioRad, Hercules, USA
Freezer	-20°C Comfort No Frost	Liebherr, Bulle, DE
	-80°C	Thermo Fisher, Champaign, USA
fully automated IHC & ISH stainer	Bondmax Rx ^m	Leica Biosystems, Nussloch, DE
Flow cytometer; spectral cell analyzer	SA3800	SONY Biotechnology, Champaign, USA
	SP6800	
Fluorescence and absorbance plate reader	Infinite M1000 Pro	Tecan, Männedorf, CH
Flux-Analyzer	Seahorse XF ^e 96 Extracellular Flux Analyzer	Agilent Technologies, Santa Clara, CA/USA
Gel chamber		BioRad, Hercules, USA
Imaging-System	ChemiDoc™ XRS	Bio-Rad Laboratories, Feldkirchen, DE
Infrared lamp	IL21	Beurer, Ulm, DE
Microscope	DMi8	Leica, Wetzlar, DE
	Axio	Zeiss, Oberkochen, DE
Multiplexing Instrument	Luminex® Bio Plex 200	Bio-Rad Laboratories, Feldkirchen, DE
Paraffin Embedding System	Cool Unit TBS88	Medite GmbH, Burgdorf, DE

PCR-Cycler	ProFlex PCR System	Applied Biosystems, Foster City, CA/USA
Perfusion pump	Masterflex® L/S® Standard Drive	Digital Cole-Parmer, Vernon Hills, IL/USA
Perfusion pump	Masterflex® L/S® Standard Drive	Digital Cole-Parmer, Vernon Hills, IL/USA
pH-Meter	inoLab® pH 7110	WTW (Xylem Analytics), Weilheim, DE
Pipettes	Research plus 0,1 – 10 µL 2 – 20 µL 20 – 200 µL 100 - 1000µL	Eppendorf, Hamburg, DE
Power supply	PowerPac™ Basic	Bio-Rad Laboratories, Feldkirchen, DE
Precision scale	Analysenwaage ABS	Kern & Sohn, Balingen, DE
Refrigerator		Liebherr, Bulle, DE
RNA-Sequencing	NextSeq 500	Illumina, San Diego CA/USA
Rotary bath	Thermolab® 1092	GFL, Burgwedel, DE
Scale	S72 ABS - N	Kern, Balingen, DE
Slide-Scanner	Aperio AT2	Leica Biosystems, Nussloch, DE
Smart tissue processor	ASP300	Leica Biosystems, Nussloch, DE
Table centrifuge	Heraeus Pico 17	ThermoFisher, Champaign, USA
Thermomixer	compact	Eppendorf, Hamburg, DE
Thermomixer	MaxQ4000	Thermo Fisher Scientific, Waltham, USA
Vibratom	VT1000S	Leica Biosystems, Nussloch, DE
Waterbath	TW8	Julabo, Seelbach, DE

3.1.2 Consumables

Consumables	Name	Supplier
Cell culture plates	Microplate, 96-/ 24-/ 12-well F-Bottom, chimney-well:	Greiner Bio-One International, Kremsmünster, A

	- white, lumitrac	
	- μ -clear, black	
Cell culture bottles	TC bottle, T25 TC bottle, T75	Sarstedt, Nümbrecht, DE
Centrifugation tubes	Falcon™ tubes 50ml Falcon™ tubes 15ml	Greiner Bio-one, Solingen, DE
Insulin syringe	Omnican® Insulinspritzen	B.Braun, Melsungen, DE
Cannula (20G, 22G, 27G)	Sterican® Injektionskanülen	B.Braun, Melsungen, DE
Cannula	Supra	Misawa Medical, Kasama City, JPN
Microreactiontube	Eppi™ 0,5ml, 1,5ml, 2ml	Eppendorf, Hamburg, DE
Microscope slides	SüsseFrostPlus	Süsse, Stuttgart, DE
Pasteur pipette	Cellstar® (2mL, 5mL, 10mL, 25mL)	Greiner Bio-one, Solingen, DE
PCR Strip Tubes	Sapphire	Greiner Bio-one, Solingen, DE
Petri dish	PS, 94/16mm PS, 145/20mm	Greiner Bio-one, Solingen, DE
Scalpels	Feather® No.11	Feather, Osaka, Japan
Seahorse 96well Platte	XF96 cell culture microplates	Agilent Technologies, Santa Clara, CA/USA
Seahorse Cartridge	XF ⁹⁶ Extracellular Flux Assay Kit	Agilent Technologies, Santa Clara, CA/USA
Sterile filter	0.2 μ m Acrodisc®	Pall, Cornwall, UK
Syringes	5, 10, 20ml	B.Braun, Melsungen, DE
Tips	10 μ l 100 μ l 1000 μ l	Greiner Bio-one, Solingen, DE
Tissue molds	Tissue-Tek® Cryomolds	Sakura Finetek Europe B.V., Alphen aan den Rijn, NLD

3.1.3 Chemicals and Reagents

Chemical / Reagens	Supplier
0,9% NaCl (isotonische Kochsalzlösung)	Deltamedica, Reutlingen, DE
1,6-Diphenyl-1,3,5-hexatrien	Sigma-Aldrich, St. Louis, MO/USA
Agarose Ultrapure™	Invitrogen, Life Technologies, Carlsbad, USA
Antigenfix P0016	Diapath, Martinengo, BG
AntimycinA	Sigma-Aldrich, St. Louis, MO/USA
ATP (aus ATP Detektions-Kit)	Roche, Basel, CH
β-Mercaptoethanol	AppliChem, Darmstadt, DE
Bromphenoblu	Sigma-Aldrich, St. Louis, MO/USA
BSA	AppliChem, Darmstadt, DE
BSA (Fettsäure-frei)	Sigma-Aldrich, St. Louis, MO/USA
CaCl ₂ x 2 H ₂ O	Sigma-Aldrich, St. Louis, MO/USA
Carboxyfluorescein succinimidyl ester (CFSE)	ThermoFisher, Scientific, Waltham, MA/USA
Calibration beads (AlignCheck, 8-Peak, Automatic Setup)	SONY Biotechnology, Champaign, USA
CCCP	Sigma-Aldrich, St. Louis, MO/USA
CsCl	AppliChem, Darmstadt, DE
Cytochrom C	Sigma-Aldrich, St. Louis, MO/USA
DMEM	GIBCO, Life Technologies, Carlsbad, USA
DMSO	Sigma-Aldrich, St. Louis, MO/USA
DTT	AppliChem, Darmstadt, DE
EDTA	Sigma-Aldrich, St. Louis, MO/USA
EGTA	AppliChem, Darmstadt, DE
Essigsäure	Merck, Darmstadt, DE
Ethanol	AppliChem, Darmstadt, DE
FCS (fetal calf serum)	PAN-Biotech, Aidenbach, DE
H ₂ O (qPCR)	Roche, Basel, CH
H ₃ PO ₄ (Phosphat)	Sigma-Aldrich, St. Louis, MO/USA
HCl	AppliChem, Darmstadt, DE
Heparin	B.Braun, Melsungen, DE

HEPES	Carl Roth, Karlsruhe, DE
GBSS	PAN-Biotech, Aidenbach, DE
Glutamat (C ₅ H ₉ NO ₄)	Sigma Aldrich, St. Louis, USA
Glutamine (L-), (200 mM)	GIBCO, Life technologies, Carlsbad, USA
Glycin	Carl Roth, Karlsruhe, DE
HBSS	Sigma Aldrich, St. Louis, USA
Isofluran CP®	CP-Pharma, Burgdorf, DE
Isopropanol	AppliChem, Darmstadt, DE
KCl	AppliChem, Darmstadt, DE
KH ₂ PO ₄	AppliChem, Darmstadt, DE
KOH	Sigma-Aldrich, St. Louis, MO/USA
Methanol	Merck, Darmstadt, DE
MgCl ₂ x 6 H ₂ O	AppliChem, Darmstadt, DE
Na ₂ HPO ₄ x 2 H ₂ O	AppliChem, Darmstadt, DE
NaCl	AppliChem, Darmstadt, DE
NaOH	Merck, Darmstadt, DE
Natriumdeoxycholat	Sigma-Aldrich, St. Louis, MO/USA
Nigericin	Sigma-Aldrich, St. Louis, MO/USA
Normal mouse serum (NMS)	Thermo Fisher Scientific, Waltham, MA, USA
Oligomycin	Sigma-Aldrich, St. Louis, MO/USA
Paraformaldehyd (PFA)	AppliChem, Darmstadt, DE
Penicillin (10000 U/mL)/Streptomycin (10 mg/mL)	GIBCO, Life Technologies, Carlsbad, USA
Percoll™	GE Healthcare, Chalfont St. Giles, UK
poly-L-Lysin	Sigma-Aldrich, St. Louis, MO/USA
Ponceau S	AppliChem, Darmstadt, DE
Potassium chloride	Merck, Darmstadt, DE
Protease-Inhibitor (RIPA), cOmplete tablets mini	Roche, Basel, CH
Pyruvat	Sigma-Aldrich, St. Louis, MO/USA
Q-VD-OPh	Biomol, Hamburg, DE
RLT buffer	Qiagen, Hilden, DE

Rotenon	Sigma-Aldrich, St. Louis, MO/USA
RPMI GlutaMAXX	GIBCO, Life Technologies, Carlsbad, USA
SDS	AppliChem, Darmstadt, DE
Spectra™ Multicolor Broad Range Protein Ladder	Thermo Fisher Scientific, Waltham, MA/USA
Succinat	Sigma-Aldrich, St. Louis, MO/USA
Sucrose	AppliChem, Darmstadt, DE
TCL buffer	Qiagen, Hilden, DE
Tes	Carl Roth, Karlsruhe, DE
Tetraphenylphosphonium-Chlorid (TPP ⁺)	Sigma-Aldrich, St. Louis, MO/USA
Tissue-Tek® O.C.T.™ Compound	Sakura Finetek Europe B.V., Alphen aan den Rijn, NLD
Tris	Carl Roth, Karlsruhe, DE
Tween 20	Sigma-Aldrich, St. Louis, MO/USA
Williams Medium E	PAN-Biotech, Aidenbach, DE
XF Calibrant pH 7,4	Agilent Technologies, Santa Clara, CA/USA

3.1.4 Buffer and Media

Blocking buffer	Tris 0.1 M
	1% (w/v) BSA
	1% (m/v) GCWFS
	0.3% (v/v) Triton X-100
	distilled water
	0.1 mM L-Aspartic Acid
Calcium deprived buffer	0.2 mM L-Threonine
	0.3 mM L-Serine
	0.5 mM Glycine
	0.6 mM L-Alanine
	0.9 mM L-Glutamic Acid
	0.9 mM L-Glutamine
	20 mM D (+) Glucose

	20 mM Fructose
	197 mM Sucrose
	3 mM KCl, 0.7 mM NaH ₂ PO ₄ -H ₂ O
	0.5 mM MgCl ₂
	10 mM HEPES
	25 mM NaHCO ₃
	pH 7,4
	PBS
ELISA blocking buffer	0,1M Na ₂ HPO ₄
	pH 9
	PBS
ELISA washing buffer	0,05% Tween
ELISA stop buffer	2% H ₂ SO ₄ (0,1M)
	Distilled water
Erythrocyte Lysis buffer (Ammonium-chloride-Potassium, ACK)	0.15 M Ammonium chloride (NH ₄ Cl)
	10 mM Potassium bicarbonate (KHCO ₃)
	1 mM EDTA disodium salt
	pH 7.2
	PBS
FACS buffer	1% FCS
	0,01% sodium azide
	PBS
MACS buffer	1%FCS
	2mM EDTA
	137 mM NaCl
	2,7 mM KCl
Phosphate-buffered saline (PBS)	10 mM Na ₂ HPO ₄
	1,8 mM KH ₂ PO ₄
	pH 7,4
	Biochrom GmbH (Berlin)

P-buffer	100 ml distilled, sterile water 81 ml sterile 0.2 M Na ₂ HPO ₄ 19 ml sterile NaH ₂ PO ₄ pH 7.4
Sucrose, 30%	P-buffer 30% sucrose 20 mM Tris
TBST	137 mM NaCl pH 7,6 (mit HCl) 0,1 % (v/v) Tween 20 (apply freshly)
T cell medium	RPMI 1640 10%FCS 5ml L-Glutamine 5ml Penicillin-Streptomycin 10000 U/mL 500µl b-Mercaptoethanol
TE buffer	10 mM Tris-HCl (pH 8,0) 1 mM EDTA pH 8,0

3.1.5 Antibodies

Antigen	Conjugate	Usage	Application	Clone	Company
CCR2	BV421	1:200	FACS	SA203G11	Biologend
CD3	FITC	1:200	FACS	17A2	Thermo Fisher
CD4	eF450	1:200	FACS	RM4-5	Thermo Fisher
CD8a	PE	1:200	FACS	53-6.7	Thermo Fisher
CD8a	PE Cy7	1:200	FACS	53-6.7	Thermo Fisher
CD8a	BV510	1:300	IF	53-6.7	Biologend
CD11b	AF488	1:100	IF	M1/70	Thermo Fisher
CD11b	PE Cy5	1:200	FACS	M1/70	Thermo Fisher
CD11a	PE Cy7	1:200	FACS	M17/4	Thermo Fisher

Antigen	Conjugate	Usage	Application	Clone	Company
CD11c	eF450	1:200	FACS	N418	Thermo Fisher
CD11c	PE-Cy7	1:200	FACS	N418	Thermo Fisher
CD18	PE	1:200	FACS	M18/2	Thermo Fisher
CD19	FITC	1:200	FACS	eBio1D3	Thermo Fisher
CD24	APC Cy7	1:200	FACS	M1/69	Thermo Fisher
CD25	eF450	1:200	FACS	PC61.5	Thermo Fisher
CD25	PerCp/Cy5.5	1:200	FACS	PC61.5	Thermo Fisher
CD27	PE Cy7	1:200	FACS	O323	Thermo Fisher
CD30	AF647	1:200	FACS	Mec 13.3	Thermo Fisher
CD40	PE	1:200	FACS	1C10	Thermo Fisher
CD40	PerCp/Cy5.5	1:200	FACS	3/23	Thermo Fisher
CD40	AF647	1:200	FACS	HM40-3	Thermo Fisher
CD40L	PE	1:200	FACS	MR1	Thermo Fisher
CD44	APC	1:200	FACS	IM-7	Thermo Fisher
CD44	PerCp/Cy5.5	1:200	FACS	IM-7	Thermo Fisher
CD45.1	APC	1:200	FACS	A20	Thermo Fisher
CD45.1	PerCp/Cy5.5	1:200	FACS	A20	Thermo Fisher
CD58	PE	1:200	FACS	TS2/9	Thermo Fisher
CD64	BV711	1:200	FACS	X54-5/7.1	BioLegend
CD68	FITC	1:200	FACS	FA-11	Thermo Fisher
CD69	PE Cy7	1:200	FACS	H1.2F3	Thermo Fisher
CD80	PE	1:200	FACS	B7-1	Thermo Fisher
CD86	eF450	1:200	FACS	B7-2	Thermo Fisher
CD86	PE-Cy7	1:200	FACS	B7-2	Thermo Fisher
CD97	FITC	1:200	FACS	VIM3b	BioLegend
CD102	AF488	1:200	FACS	3C4	Thermo Fisher
CD107b	PerCp/Cy5.5	1:200	FACS	ABL-93	Thermo Fisher
CD115	PE Cy7	1:200	FACS	AFS98	Thermo Fisher
CD117	AF700	1:200	FACS	2B8	BioLegend

Antigen	Conjugate	Usage	Application	Clone	Company
CD120a	PE	1:200	FACS	HM104	Thermo Fisher
CD135	PE	1:200	FACS	A2F10	Thermo Fisher
CD137L	PE	1:200	FACS	TKS-1	Thermo Fisher
CD146	FITC	1:200	FACS	P1H12	Thermo Fisher
CD162	BV421	1:200	FACS	KPL-1	BioLegend
CD177	APC	1:200	FACS	MEM-166	BioLegend
CD184	PE	1:200	FACS	2B11	Thermo Fisher
CD194	PE Cy7	1:200	FACS	D8SEE	Thermo Fisher
CD195	PerCp/Cy5.5	1:200	FACS	HM-CCR5	BioLegend
CD206	PE	1:200	FACS	MR6F3	Thermo Fisher
CD244.2	FITC	1:200	FACS	2B4	Thermo Fisher
CD252	APC	1:200	FACS	RM134L	Thermo Fisher
CD273	PE	1:200	FACS	B7-DC	Thermo Fisher
CLEC4F	-	1:200	FACS	Polyclonal Goat IgG	R&D systems
CLEC4F	-	1:200	FACS/IHC	rat IgG2	R&D systems
CLEC4A	PE	1:200	FACS	9E8	BioLegend
CX3CR1	PE	1:200	FACS	SAO11F11	Biolegend
CX3CR1	PE Cy7	1:200	FACS	SAO11F11	Biolegend
CXCR6	BV421	1:200	FACS	SA051D1	BioLegend
GznB	PE	1:200	FACS	GB12	Thermo Fisher
F4/80	BV421	1:200	FACS	BM8	Biolegend
F4/80	PerCp/Cy5.5	1:200	FACS	BM8	BioLegend
F4/80	PE Cy7	1:200	FACS	BM8	BioLegend
IFNg	PE	1:200	FACS	XMG1.2	Thermo Fisher
IRF8	PE	1:200	FACS	<u>V3GYWCH</u>	Thermo Fisher
IRF8	APC	1:200	FACS	<u>V3GYWCH</u>	Thermo Fisher
Ly6A	PerCp/Cy5.5	1:200	FACS	D7	Thermo Fisher
Ly6A	FITC	1:200	FACS	D7	Thermo Fisher
Ly6A	PE Cy7	1:200	FACS	D7	Thermo Fisher

Antigen	Conjugate	Usage	Application	Clone	Company
Ly6A	AF700	1:200	FACS	D7	Thermo Fisher
Ly6C	FITC	1:200	FACS	RB6-8C5	Thermo Fisher
Ly6C	BV605	1:200	FACS	HK1.4	BioLegend
Ly6C	PE-Cy7	1:200	FACS	HK1.4	Thermo Fisher
Ly6C	AF700	1:200	FACS	HK1.4	Biolegend
Ly6C	APC eF780	1:200	FACS	HK1.4	BioLegend
Ly6G	FITC	1:200	FACS	RB6-8C5	Thermo Fisher
Ly6G	APC	1:200	FACS	RB6-8C5	Thermo Fisher
Ly6G	AF700	1:200	FACS	RB6-8C5	Thermo Fisher
MHCII	AF700	1:200	FACS	M5/114.15.2	Biolegend
MHCII	PE	1:200	FACS	M5/114.15.2	Biolegend
NK1.1	FITC	1:200	FACS	PK136	Thermo Fisher
Nkp46	FITC	1:200	FACS	29A1.4	Thermo Fisher
Rat IgG2a	PE	1:100	FACS	r2a-21B2	Thermo Fisher
TER119	FITC	1:200	FACS	TER-119	Thermo Fisher
TER119	PE eF610	1:200	FACS	TER-119	Thermo Fisher
Tim3	APC	1:200	FACS	<u>8B.2C12</u>	Thermo Fisher
Tim4	PerCp/eF710	1:200	FACS	RM-T4-54	Thermo Fisher
TNFa	PE Cy7	1:200	FACS	<u>MP6-XT22</u>	Thermo Fisher
VSIG4	FITC	1:200	FACS	NLA14	Thermo Fisher
XCR1	BV421	1:200	FACS	ZET	BioLegend
XCR1	PE	1:200	FACS	ZET	BioLegend
CD16/32	-	1:100	FACS block Anti-FcγRII+III	2.4G2	Own production

3.1.6 Kits

Kit

Supplier

2-NBDG Glucose uptake assay

Abcam, Cambridge, UK

ATP Bioluminescence Assay Kit CLS II	Roche, Basel, Schweiz
Bond Polymer Refine Detection	Leica, Wetzlar, DE
Bond Polymer Refine Red Detection	
Caspase-Glo® Assay (3/7 und 8)	Promega, Madison, WI/USA
eBioscience™ Foxp3 / Transcription Factor Staining Buffer Set	Thermo Fisher Scientific, Waltham, USA
eBioscience™ Intracellular Fixation & Permeabilization Buffer Set	Thermo Fisher Scientific, Waltham, USA
FITC BrdU Flow Kit	BD Bioscience, San Jose, CA, USA
Hexokinase Activity Assay	Abcam, Cambridge, UK
MitoProbe™ DiIC1(5)	Thermo Fisher Scientific, Waltham, USA
MitoTracker™ Green FM	Thermo Fisher Scientific, Waltham, USA
NucleoSpin® RNA	Macherey-Nagel, Düren
NucleoSpin® Tissue	Macherey-Nagel, Düren
ProcartaPlex™ Multiplex Immunoassay	Invitrogen, Waltham, USA
SensiFAST™ cDNA Synthesis Kit	Bioline Reagents, London, UK

3.1.7 Dextramer

MHC Allel	Fluorochrome	Concentration	Peptid	No.	Supplier
H-2Kb	PE	01:10	SIINFEKL	JD2163-PE	Immudex, Kopenhagen, DNK
H-2Kb	PE	01:10	SIYRYYGL	JD2164-PE	Immudex, Kopenhagen, DNK

3.1.8 Enzymes

Enzyme	Supplier
DNase I	Roche Diagnostics, Risch, CH
Trypsin	PAN Biotech, Aidenbach, DE
Kollagenase Type II	Worthington Biochemical Corporation, Lakewood, USA

Kollagenase NB 4G	SERVA Electrophoresis GmbH, Heidelberg, DE
-------------------	--

3.1.9 Recombinant cytokines and proteins

Name	No.	Supplier
Class B CpG ODN 1668 (200ug = 31.24nmol)	tlrl-1668-blk	InvivoGen, Toulouse, FR
IL-2	130-120-662	Miltenyi
ODN 1668 control	tlrl-1668c-5	InvivoGen, Toulouse, FR
Lipopolysaccharid (LPS) - E.coli O111:B4	L2630	Sigma-Aldrich, St. Louis, USA
Polyinosinic acid potassium salt (Poly-I)	P4154	Sigma Aldrich, St.Louis, MO, USA
Polyinosinic: polycytidylic acid (Poly-I:C)	P9582	Sigma Aldrich, St.Louis, MO, USA
Ovalbumin	A5503	Sigma-Aldrich, St. Louis, USA
Ova257-264 (SIINFEKL)	6-7015-901	Iba Lifesciences, Göttingen, DE
Tumor necrosis factor (TNF)	PMC3013	ThermoFisher Scientific, Waltham, MA, USA

3.1.10 Beads

Name	No.	Supplier
CD8 (TIL) MicroBeads, mouse	130-116-478	Miltenyi Biotec, Bergisch-Gladbach, DE
CD11b MicroBeads, mouse	130-049-601	Miltenyi Biotec, Bergisch-Gladbach, DE
CountBright™ Absolute Counting Beads	C36995	ThermoFisher Scientific, Waltham, MA, USA
Dynabeads™ Mouse T-activator CD3/CD28 for T-cell expansion and activation	11453D	ThermoFisher Scientific, Waltham, MA, USA

3.1.11 Mice

strain	description	origin
C57BL/6J	wildtype mice	Janvier labs

CD40 ^{-/-}	cells lack the expression of CD40	C Weber
CD40L ^{-/-}	cells lack the expression of CD40L	C Weber
OT-I	transgenic CD8 ⁺ T cells with a TCR (V α 2V β 5.1) specific for SIINFEKL peptide derived from hen egg ovalbumin	The Jackson Laboratory
OT-1 x CD45.1	OT-I genotype with additional specific variant of the CD45 molecule that is not present in wildtype C57Bl/6 mice	Own breeding
RAG ^{-/-}	no production of mature B or T cells – “non-leaky” immune deficiency	The Jackson Laboratory

3.1.12 Software

Software	Supplier
Adobe Illustrator	Adobe, San José, CA, USA
FlowJo	Tree star, Ashland, OR, USA
Image Lab	Bio-Rad Laboratories, Inc., CA, USA
i-control 2.0	Tecan Group, Männedorf, CH
LivingImage 4.3.1	Caliper Lifesciences, Waltham, MA, USA
Magellan	Tecan, Männedorf, CH
Mendeley	Mendeley Ltd., DE
Microsoft Office	Microsoft, Redmond, VA, USA
Prism for Mac	GraphPad, La Jolla, CA, USA
R Studio	
SeaHorse XF Software	SeaHorse, MA, USA

3.2 Methods

3.2.1 Injections

Intravenous injections were applied into the tail vein of mice after gentle warming under an infrared lamp. Mice were immobilized in special restrainers during injection. If not stated otherwise, all injections were carried out in a volume of 100 μ l for intravenous (i.v.) injections

3.2.2 Preparation of murine tissue

Mice were euthanized with spinal dislocation, disinfected using 70 % ethanol and dissected under the laminar flow. The organs of interest were harvested under sterile conditions: spleen, lung, kidney and lymph nodes were removed and kept in PBS on ice until further use.

3.2.3 Single cell isolation from tissues

3.2.3.1 Hepatic non-parenchymal cells

The mice were euthanized, and the abdomen opened. The liver was perfused via the portal vein with 5ml pre-warmed (37°C) 0.05% Collagenase IA / Ca⁺-deprived medium with a 0.4 x 20mm syringe and a perfusion pump. After excision, the liver was transferred into a PBS filled Falco tube and put on ice. The liver was put into a petri dish and minced into small parts using scissor blades. The parts were transferred to a 50ml tube together with 5ml of 0.04% Collagenase IA / GBSS. The tube was incubated in a rotary water bath with shaking speed of 250rpm for 18min at 37°C. Afterwards the cell suspension was passed through a metal mesh (250µm) using the plunger of a 2ml syringe. The mesh and old tube were washed trough with pre-warmed GBSS. The suspension was centrifuged at 50g and 4°C for 2min. The supernatant was transferred to a new 50ml tube and centrifuged at 800g and 4°C for 10min, the pellet was discarded. The cells were washed with ice-cold PBS and pelleted down by repeating the previous centrifugation step. After removing the supernatant cells were resuspended in 20ml of ice-cold PBS. With a 10ml syringe and 0.9 x 120mm long needle a layer of 6ml 25% Percoll and 5ml 80% Percoll were added under the cell suspension. The gradient was performed at 1369g and 4°C for 30min. The acceleration speed was put to 5 and the deceleration speed to 1. The non-parenchymal cells were collected at the interface between the two Percoll concentrations and transferred to a new 50ml tube. The tube was filled up to 50ml with ice-cold PBS and centrifuged at 1600rpm for 6min. The cells were filtered through a 100µm nylon mesh and washed once again. Cells then could be used for staining or further experiments.

3.2.3.2 Non-parenchymal cells from spleen, lung, kidney and lymph node

A plunger of a 2ml syringe was used to is pass the organ through a metal mesh (250µm) into a 50ml tube. The mesh was washed with ice-cold PBS and the cells were pelleted down by centrifugation – 1600rpm, 6min. The cells were resuspended in 2ml of AcK lysis buffer and incubated for 2min. The cells were washed with ice-cold PBS and filtered through a 100µm nylon mesh before the final washing step. Cells now could be used for staining or further experiments.

3.2.3.3 Blood myeloid cells

Blood was withdrawn by puncture of the central hepatic vein with a syringe that contained a small volume of heparin. Blood was transferred to a 15ml Falcon™ tube and filled up with PBS up to 10ml. 3ml of Pancoll are layered under the blood – PBS – Mix. Centrifugation of the Pancoll gradient was carried out at 2200rpm and 4°C for 20 min with reduced acceleration (7 of 10) and no brake. The interface between the upper PBS and the lower Pancoll layer was collected with the help of a Pasteur pipet, washed with MACS buffer and stained for flow cytometric analysis or fluorescent-activated cell sorting.

3.2.3.4 Isolation of OT-I T cells and adoptive T cell transfer

OT-I transgenic mice were sacrificed by cervical dislocation and spleen and lymph nodes were harvested in sterile 1x PBS. The organs were dissociated by grinding through metal cell

dissociation sieves with 1x PBS and cells were collected by centrifugation at 800 g for 10 min. Erythrocyte lysis was performed in 1x ACK buffer for 3 min and after washing with 1x PBS and filtration through nylon gauze, CD8⁺ T cells were isolated by MACS (CD8⁺ T cell isolation kit, mouse) according to manufacturer's instructions. 10 000 OT-I T cells were transferred in 1x PBS intravenously.

3.2.4 Surface marker staining and FACS analysis

The surface marker staining for FACS analysis was performed with cells isolated from liver, blood and spleen. The antibodies were used as indicated in 3.1.5 and diluted in FACS buffer. Up to 5×10^6 Cells were stained in 50 μ l FACS buffer in 96-well plates with different combinations of antibodies for at least 15 min or overnight at 4°C and washed with FACS buffer. Anti-CD16/32 antibody was added at 10 μ g/ml for Fc-receptor blocking. Dextramer staining was performed in 20 μ l 1x PBS with the addition of 4 μ l Dextramer and 40 μ g/ml anti-CD16/32 antibody for 10 min at room temperature before 50 μ l FACS buffer supplemented with desired antibodies was added and further incubated for 15 min at 4°C.

A known number of fluorescent counting beads were added directly before acquisition of the sample if a determination of absolute cell numbers was required. Flow cytometric measurement was performed with SP6800 and SA3600 and data analysis was carried out with the help of FlowJo software. Absolute cell numbers were calculated with the help of the number of counting beads acquired.

3.2.5 Granzyme B staining

The surface staining for other markers was performed before the GzmB staining. Cells were washed with FACS buffer and resuspended in 100 μ l of freshly prepared Foxp3 Fixation/Permeabilization solution (1xFoxp3 Fixation/Perm concentrate + 3x Foxp3 Fixation/Perm diluent). The cells were incubated for 30-60min at 2-8°C before they were washed with 200 μ l of 1xPerm/Wash buffer. Each sample was divided into two wells to perform additional isotype control. The antibody and the isotype control were prepared in Perm/Wash buffer at a concentration of 1:100. Each sample was resuspended in 50 μ l of either antibody or isotype control and incubated for 2hours at 2-8°C. The cells were washed with Perm/Wash buffer and resuspended in 200 μ l FACS buffer for FACS analysis.

3.2.6 Intracellular staining

Before intracellular staining, the cell surface staining is performed (3.2.4). The cells were fixed with fixation buffer in the dark for 20min at room temperature. The cells were centrifuged at 350 x g for 5 minutes, the supernatant was discarded. For permeabilization the cells were resuspended in 200 μ l Permeabilization Wash buffer and centrifuged at 350g for 5-10min twice. The intracellular antibodies were diluted (as indicated in 3.1.5) in Permeabilization Wash buffer. The staining was performed in the dark at RT for 20min. Cells were washed twice with Permeabilization Wash buffer and resuspended in FACS buffer for subsequent FACS analysis.

3.2.7 CFSE staining

Isolated T cells were resuspended in PBS – $5-10 \times 10^6$ cells / ml – and 1 μ M CFSE was added. Cells were incubated at room temperature (RT) for 10min in the dark. The labelling was stopped by adding medium and storage at 4°C for 5min. Afterwards the cells were washed three times with medium and plated on a 96 Well plate that had been coated with anti-CD3/CD28 (5 μ g/ml) on the day before. Two to three days later the proliferation was measured with the SP6800.

3.2.8 Cell Sorting

The surface marker staining was performed as described in 3.2.4. The SH6800S was used for cell sorting. The cells were sorted into medium or RLT buffer in case of the RNA sequencing probes.

3.2.9 RNA-sequencing and bioinformatic analysis

The cell populations I wanted to analyze were sorted directly into TCL buffer and stored at -80°C. The whole RNA-sequencing process was performed by Dr. Rupert Öllinger (2. Medizinische Klinik, Klinikum rechts der Isar, Munich). The bioinformatic analysis was performed by Dr. Sainitin Donakonda (Institut für Molekulare Immunologie, Klinikum rechts der Isar, Munich).

3.2.9.1 RNA sequencing

Isolated cells were subjected to single-cell RNA sequencing analysis using the Chromium System (10x Genomics, California, USA). Per sample, 1000 cells were used with a recovery rate of about 60%. Sequencing was performed on Illumina NextSeq 550 (paired-ends, 2×75bp), resulting in 60000 reads per cell and $\sim 4 \times 10^8$ total reads per Illumina chip.

Library preparation for bulk 3'-sequencing of poly(A)-RNA was done as described previously¹⁴⁶. Briefly, the barcoded cDNA of each sample was generated with a Maxima RT polymerase (Thermo Fisher) using oligo-dT primer containing barcodes, unique molecular identifiers (UMIs) and an adapter. 5' ends of the cDNAs were prolonged by a template switch oligo (TSO) and after combining of all samples full-length cDNA was augmented with primers binding to the TSO-site and the adapter. cDNA was augmented with the Nextera XT kit (Illumina) and 3'-end-fragments finally amplified using primers with Illumina P5 and P7 overhangs. The library was sequenced on a NextSeq 500 (Illumina) with 75 cycles for the cDNA in read1 and 16 cycles for the barcodes and UMIs in read2. The sample and gene wise UMI tables were analyzed using Drop-seq pipeline (<https://github.com/broadinstitute/Drop-seq>). GRCm38 reference genome was used for the alignment. ENSEMBL annotation release 75 was used for Transcript and gene definitions. DESeq2 R package¹⁴⁷ was used to process the read count table and to identify the differentially expressed genes (DEGs, Fold change 2 and adjusted p-value (padj) ≤ 0.05). To calculate the transcript abundance, the mean Transcripts per million (TPM) values were computed from sequence read counts. Principal component analysis (PCA) was performed using 'prcomp' function in R and 2D PCA plot was visualized using ggplot2 R package. The Euclidean distance between the samples was calculated and clustered using the heatmap.2 function in R.

3.2.9.2 Construction of gene co-expression modules, validation and identification of hub genes

We constructed gene co-expression modules of DEGs in (CD40 vs KC) using the Weighted co-expression network analysis (WGCNA R-package)¹⁴⁸. Correlations between all pairs of genes across the samples were converted into an adjacency matrix by taking their absolute value and fostering them to the power β . The Power β is translated as a soft-threshold of the correlation matrix, which was set at 20. The TOM matrix was made and topological overlap (TO) based dissimilarity was used to perform average linkage hierarchical clustering. The following parameters was used to build co-expression modules: The dynamic deep split:2, minimum module size 30 and merge height: 0.03. To assess the co-expression modules, we used the *modulePreservation* function in the WGCNA R package. We randomly permuted the gene

labels 500 times and computed the log p-values and the Z-scores for module quality statistics such as module membership and connectivity. The Z-score and p-value suggest how significant the modules are related to a random module. Z-summary ≥ 2 and a p-summary of ≤ 0.05 were used to identify the statistically significant gene co-expression modules in comparison to random module¹⁴⁹. Module Eigengene (ME) was calculated for each gene as described previously¹⁴⁹. This module membership also specifies the intramodular connectivity (kME) of genes in the module. In our signed gene co-expression modules, we expect positive kME values and we considered the top 10% of kME as hub genes in the gene co-expression modules. For clarity, only the hub gene connections are visualized using Cytoscape v3.7.1¹⁵⁰.

3.2.9.3 Transcription factor analysis

To predict the transcription factors (TFs) regulate (CD40 vs KC) DEGs, we used Binding Analysis for Regulation of Transcription (BART) prediction tool 2.0¹⁵¹ with default settings. We overlapped the Mouse transcription factor atlas¹⁵² and differentially expressed genes to identify TFs regulated by CD40. The transcription network was constructed using RTN R package¹⁵³ centered on TFs which are differentially expressed in CD40 by predicting the target genes using the mutual information. We predicted the top TF regulated by computing the number of targets (Degree) using the igraph R package (<https://igraph.org/>).

3.2.9.4 Gene set enrichment and pathway analyses

We performed Gene Set enrichment Analysis (GSEA) using following gene sets: Interferon (alpha, beta and gamma) from Molecular signature database (MsigDB) (<http://software.broadinstitute.org/gsea/msigdb/index.jsp>), TNF alpha pathway gene set was extracted from Wikipathways (<https://www.wikipathways.org/index.php/Pathway:WP231>) and gene set related to Cell surface protein atlas (CSPA) was downloaded from (<http://wlab.ethz.ch/cspa/>). Human gene symbols were converted to mouse homologs using custom Biomart R script. Gene set enrichment was performed using GSEA v3.0¹⁵⁴ using the DEGs (CD40 vs KC) which were ranked according to the \log_2 foldchanges provided by DESeq2. The PreRanked tool from GSEA was used to compute the normalized enrichment score (NES) and FDR $q \leq 0.25$ is measured as a statistically significant NES. The co-expression modules were subjected to Kyoto Encyclopedia of Genes and Genomes (KEGG) pathways was using Metascape (<http://metascape.org/gp/index.html#/main/step1>)¹⁵⁵. We considered pathways as statistically significant at a $P \leq 0.05$.

3.2.10 ELISA

On the day prior to the ELISA a 96-Well plate with F-bottom was coated with the primary antibody – 1:100 in Elisa-coating buffer, 50 μ l per well, 4°C. On the following day the primary antibody was discarded and replaced by 100 μ l 1%BSA in PBS. The plate was incubated for one hour at 4°C and washed with ELISA washing buffer. The standard series with recombinant IL-2 (40, 20, 10, 5, 2,5, 1,25 and 0ng/ml) was prepared in medium and incubated for 2h at RT. The supernatant of the cell culture that was supposed to be analyzed was put on the plate at the same time. Afterwards the plate was washed twice before adding the secondary antibody (1:200 in medium), 100 μ l per well, 30min at 37°C. The plate was washed three times before peroxidase (1:1000 in PBS) was added and incubated for 30min at 37°C. The plate was washed four to five times and 50 μ l 3,3',5,5'-Tetramethylbenzidin (TMB) were added for 5-10min until the wells reached a darker blue tint. The reaction was stopped with 50 μ l of ELISA stop buffer and the plate was analyzed with the Tecan reader (absorption: 450nm, measuring time: 3s)

3.2.11 BrdU pulse chase

One mg / mouse of BrdU was injected i.v. one and twelve hours prior to sacrificing the mice. The blood, splenic and hepatic cells were isolated as described () and surface staining was performed (). The cells were washed with FACS buffer and afterwards resuspended in 100µl BD Cytofix / Cytoperm buffer and incubated for 30min on ice. For the permeabilization cells were washed with 100µl Perm / Wash buffer. Afterwards they were resuspended in 100µl Cytoperm Plus Buffer and incubated 10min on ice. The cells were washed with 100µl BD Perm / Wash buffer and resuspended in 100 µl BD Cytoperm / Cytofix buffer and incubated 5min on ice. After that they were washed again, resuspended with 100 µl DNase (300 µg/ml in PBS) and incubated for one hour at 37°C. Cells were washed with 200 µl Perm / Wash buffer, resuspended with 50 µl FITC-BrdU in 1x BD Perm / Wash buffer (1:75) and incubated for 20min at RT. After that the cells were washed twice and resuspended in 200 µl FACS buffer before analyzing them with the SP6800.

3.2.12 DiIC₁(5)

Prior to the experiment the vials of DiIC₁(5) and CCCP were equilibrated to room temperature. For each sample, the cells were suspended in 1 mL warm medium at approximately 1×10^6 cells/ml. For the control tube, 1 µL of 50 mM CCCP (50 µM final concentration) were added and incubated at 37°C for 5 minutes. 5 µL of 10 µM DiIC₁(5) (50 nM final concentration) were added to the other cells and incubated at 37°C, 5% CO₂, for 15 to 30 minutes. Cells were washed with warm medium and resuspended in 500 µL PBS. The analysis was performed with the SP6800.

3.2.13 MitoTracker® Green

The MitoTracker® was diluted to the final working concentration (25-500nM) in RPMI medium and 200 µL were added to each well. The cells were incubated for 15-45min at 37°C and washed in pre-warmed medium. Pre-warmed medium with 2–4% formaldehyde was used to fix the cells at 37°C for 15 minutes. After fixation cells were washed several times with buffer and analyzed with the SP6800.

3.2.14 Cross-presentation assay

Myeloid cells were sorted with the SH6800S according to the cell populations that should be analyzed. They were seeded onto a 96-well plate – 1×10^5 cells per well and loaded with 200µg OVA /ml. Cells were incubated at 37°C for 60min. OT-I CD8 T cells were isolated from the spleen of OT-mice. Splenic leukocytes were isolated as described (), incubated with anti-CD8 beads and subjected to the AutoMACS. Freshly isolated CD8 T cells were put on top of the OVA-loaded myeloid cells- 2×10^5 / well. The plate was incubated overnight. The supernatant was subjected to an IL-2 ELISA the next day. As a negative control I used either single myeloid or single CD8 T cells. As a positive control I added SIINFEKEL to either a coinubation or a pure T cell well.

3.2.15 T cell coinubation assay

For the T cell coinubation assay I used the SH6800S to sort the hepatic myeloid populations I wanted to analyze. I used the spleen to isolate CD8 T cells as described (3.2.3.2) and stained them with CFSE as described (3.2.7). The T cells needed some low dose prior activation, so I added 10U of IL-2 and 1:2 CD3/CD28 dynabeads (2µl contain 8×10^4 beads). I seeded 4×10^4 T cells per well in 96 U bottom plates and put the same number of myeloid cells on top. The plate was incubated at 37°C for 3 days. At day 3 T cells were subjected to FACS analysis to analyze

markers like CD25, CD44 and CD69 as well as the CFSE labeling to determine the proliferation rate.

3.2.16 Hexokinase assay

About 1×10^6 cells are resuspended in 200 μL of assay buffer and centrifuged for 5min at 4°C and 12000rpm. The supernatant is collected and 50 μL of the reaction mix (68% assay buffer, 4% enzyme mix, 4% developer, 4% coenzyme, 20% hexokinase substrate) are added. Additional wells were prepared with the standard (preparation described in the supplier's manual) and for sample background and positive control and also topped with reaction mix. The plate was incubated for 20-60min at room temperature and afterwards measured with the Tecan reader (OD 450nm).

3.2.17 Measurement of the extracellular acidification rate (ECAR)

The extracellular acidification rate of the myeloid cells was measured with a flux analyzer (Seahorse XF⁹⁶ Extracellular Flux Analyzer). The measuring fluorophores were incubated in XF calibrant at 37°C overnight. The myeloid cells were adjusted to 1×10^6 / well in 20 μL MAS buffer. Before starting the measuring the cells were centrifuged at 1600rpm for 2min to get them down to the bottom of the plate and 160 μL of MAS buffer were added on top. The four ports of the plate were filled with oligomycin 2 μM (port A), CCCP 0,8 μM (port B), deoxy-glucose 50mM (port C) and calibrant (port D). The ports were injected at this same order into the wells during the analysis. The respiration was measured after each injection for 3 cycles and the oxygen concentration was regenerated each time after wards. The whole measuring was performed at 37°C .

Operation	time [min]	repetitions
Kalibration		
Wait	3	
Mix	1,75	3
Measure	3	
Inject port A		
Mix	2	2
Measure	2	
Inject port B		
Mix	2	2
Measure	2	
Inject port C		
Mix	2	2
Measure	2	

Inject port D

Mix	2	2
Measure	2	

3.2.18 2-NBDG assay

The cells were suspended in 100 μ L Williams E medium with additional 2-NBDG (1:1000) and incubated for 30min at 37°C. The cells were washed twice with ice-cold PBS and resuspended in 100 μ L PBS for subsequent FACS analysis.

3.2.19 ProcartaPlex™ multiplex Immunoassay

The assay was started with the preparation of the antigen standard (preparation described in the supplier's manual) and the pre-wetting of the plate with reading buffer. In the following the antibody magnetic beads were prepared and added to each well. The supernatant of myeloid cells incubated overnight with different stimulants was added on the top and incubated for 60-120min at RT, in the dark and continuously shaking. The detection antibody was added and incubated for 30min at RT in the dark. After washing for 3 times Streptavidin-PE was added and incubated for 30min at RT in the dark, continuously shaking. The plate was washed three more times and reading buffer was added. The plate then was submitted to the Luminex instrument for analysis.

3.2.20 Immunohistochemistry of liver sections

The histochemistry was performed together with the Institute of Pathology (Technical University Munich) headed by Dr. Katja Steiger and with the help of Anne Jacob. Parts of hepatic lobes were fixed for 48 hours in 4% paraformaldehyde (PFA) and subsequently transferred to PBS. The tissue samples were dehydrated before they were embedded into paraffin. 2 μ m thin liver sections were deparaffinated before they were submitted to the staining process. The staining was executed by a BondMax Rx™ and primary antibodies against Clec4F, CD11b and Ly6C were used. DAB or Fast Red were used as secondary antibodies. Hematoxylin was used to do counterstains of the sections.

3.2.21 Immunofluorescence of liver tissue

Cryo- or vibratom-sections were needed for the immunofluorescent staining of hepatic sections. Thus, livers were perfused with Antigen Fix and incubated in AntigenFix at 4°C overnight. Another incubation of 24hours in 30% sucrose-solution was needed to dehydrate the tissue.

For the cryosections the tissue was transferred to tissue molds, embedded in embedding medium (Tissue-Tek® O.C.T.) and transferred to -80°C for at least 4 hours. A cryostat was used to generate 30 μ m thick sections at -20°C which were then transferred to microscopy slides. The sections were dried at RT for about 20min and stored at -80°C for long-term storage. Stainings were performed directly on the slide. The sections were rehydrated with 0.1M TRIS in H₂O for 10min at RT and after that circled with a PAP pen. They were covered with 300 μ l of blocking buffer and incubated for 2h at RT in a wet chamber. The primary staining was performed in 300 μ l blocking buffer overnight at RT. The slides were washed with 0.1M TRIS three times, the last wash incubated for 10min. If secondary staining was necessary, it was

performed in 300µl of blocking buffer and incubated for 6-8hours at RT. The washing step was repeated. The sections were mounted with 50µl Mowiol and left drying for at least 2 hours before they were analyzed by microscopy.

For the vibratom-sections the tissue was fixed on the cutting table with superglue and 300µm sections were generated. They were transferred to a 24 well plate filled with PBS + 0,02% sodium azide. The sections were incubated in blocking buffer overnight. Stainings were performed in 24 well plates in blocking buffer. The primary staining was incubated for at least 48h, the secondary for at least 24h, both at 4°C. For the staining I used Ly6C (APC), CD8 (BV421), CCR2 (BV421) and MHCII (BV510) (see). The sections were mounted using iSpacers to create a mold that was filled with 200-300µl of Mowiol and left drying for at least 12 hours. The sections were visualized with the microscope.

3.2.22 Statistical Analyses

Data was analyzed with the help of Excel 2011 and Prism 5 for Mac. If not indicated otherwise, data of one representative experiment out of at least two is shown. Bar graphs and scatter dot plots show mean values and standard deviation (SD) for the given group size (n). For statistical analyses of data comparing two groups with normal distribution, a two-tailed student's t-test was used. For statistical analyses of data comparing 3 or more groups, a One-way ANOVA analysis and a subsequent Tukey's Multiple Comparison test as a post-test was used. Significances are indicated by star symbols where * = $p \leq 0.05$, ** = $p \leq 0.01$, *** = $p \leq 0.001$ and ns = not significant.

4 Results

4.1 Dynamics of myeloid cell composition after TLR9-L application

iMATE formation is characterized by a rapid influx of myeloid cells. This study was designed for phenotypic, functional and metabolic characterization of these cells.

4.1.1 Transient disappearance of Kupffer cells and increase influx of CD11b⁺ cells

iMATEs were described to appear within 24 hours after TLR9-L application and to disappear completely within 6 days⁷⁴. Therefore, the myeloid cell population of the liver was analyzed 1 to 6 days after the application of TLR9-L. All hepatic non-parenchymal leukocytes were isolated and analyzed by multicolor flow cytometric. T cells (CD3, 4, 8), B cells (CD19) and NK cells (Nk46, Nk1.1) were excluded from the analysis (**Fig. 4A**) as well as erythrocytes using TER119 to decrease noise/background signals. The analysis of the remaining cells led to the discovery that CD11b⁺Clec4F⁺Ly6C^{neg} Kupffer cells disappeared within 24 hours after the application of TLR9-L (**Fig. 4B,C**). This was also confirmed by immunohistochemistry with anti-Clec4F staining (**Fig.1D**). Kupffer cells did not reappear before 72 hours after TLR9-L application and did not return to steady state conditions until the end of the analysis at day 6 (**Fig. 4B,C**).

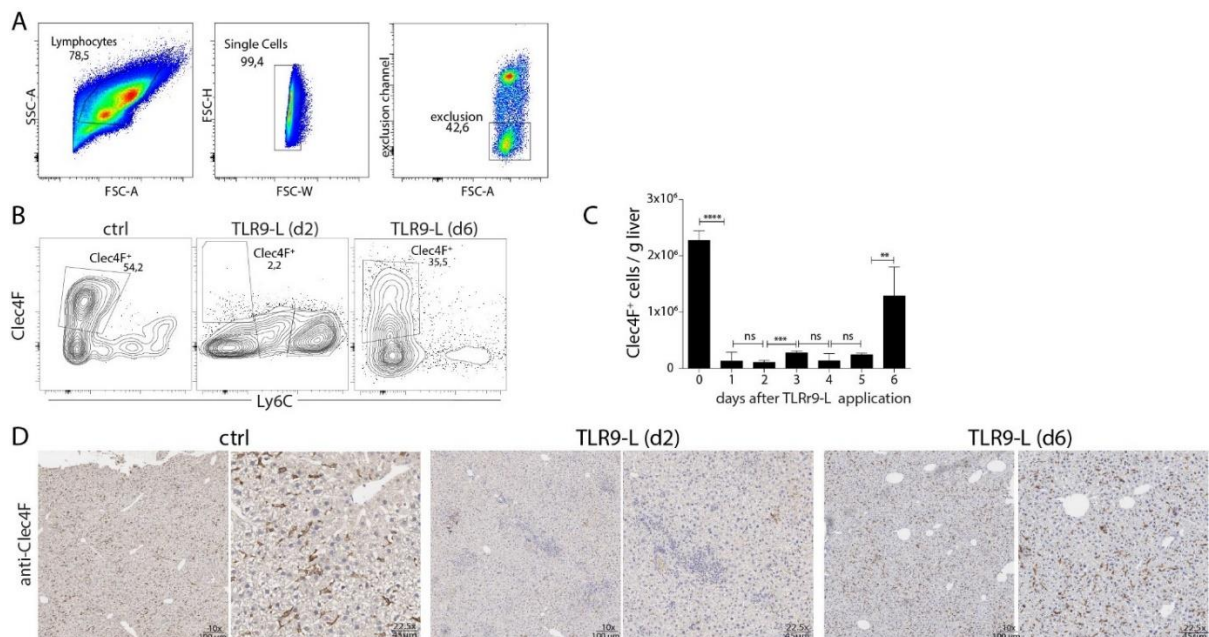


Figure 4: (A-D) Hepatic myeloid cells after the application of TLR9-L. (A) Gating strategy for the analysis of hepatic myeloid cells. Data are representative for $n \geq 3$ experiments. (B) FACS analysis of Clec4F Kupffer cell before and after the application of TLR9-L. Data are representative for $n \geq 3$ experiments. (C) Quantification of (A). Pooled data from 3 experiments ($n=4$). Mann-Whitney t test. *** $p < 0.001$ (D) Anti-Clec4F immunohistochemistry of the liver. Representative data for 5 independent experiments.

Whereas the Kupffer cells disappeared due to the application of TLR9, a strong increase in numbers of the CD11b⁺Ly6C⁺ inflammatory cells was detectable (**Fig. 5A**). Within 48 hours after TLR9-L application a dramatic increase in numbers of CD11b⁺Ly6C⁺ inflammatory cells was observed. The numbers had increased 10-fold. Immunohistochemical staining with anti-CD11b confirmed the rapid influx of CD11b⁺ cells (**Fig. 5B**). The CD11b⁺ cells formed cocoon-like clusters termed iMATEs before⁷⁴. iMATEs were distributed throughout the entire liver tissue (**Fig. 5B**).

Further staining using anti-Ly6C antibody did show the same cocoon-like structures as anti-CD11b staining, indicating that most of the CD11b⁺ cells within the iMATEs co-express Ly6C (Fig. 5C). 72 hours after the application of TLR9-L the numbers of CD11b⁺ cells did decrease drastically and returned to a basal level. No further increase was detectable until the last time point analyzed at day 6. The CD11b⁺Ly6C^{neg} monocytes presented themselves with a similar pattern – a strong increase in numbers between day 1 and 2 after TLR9-L application and a sudden drop in numbers between day 2 and 3 (Fig. 5A).

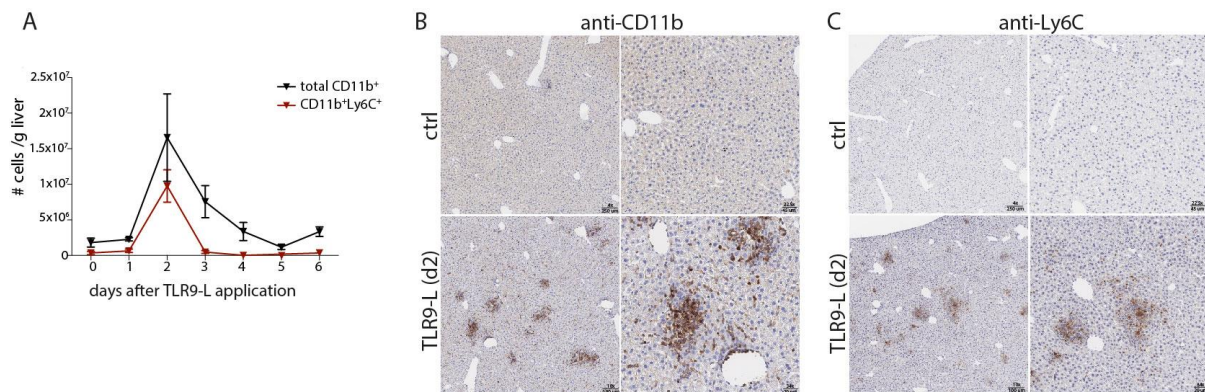


Figure 5: (A-C) Analysis of CD11b⁺ cells after the application of TLR9-L. (A) Quantification of CD11b⁺ cell numbers after the application of TLR9-L. Pooled data from 2-3 experiments (n=4). (B) Anti-CD11b immunohistochemistry displays densely packed iMATE structures two days after the application of TLR9-L. (C) Anti-Ly6C immunohistochemistry displays densely packed iMATE structures two days after the application of TLR9-L. (B,C) Data are representative for n≥3 independent experiments.

These data show that the application of TLR9-L induces the transient disappearance of Kupffer cells and simultaneously a transient influx of inflammatory myeloid cells (Fig. 6).

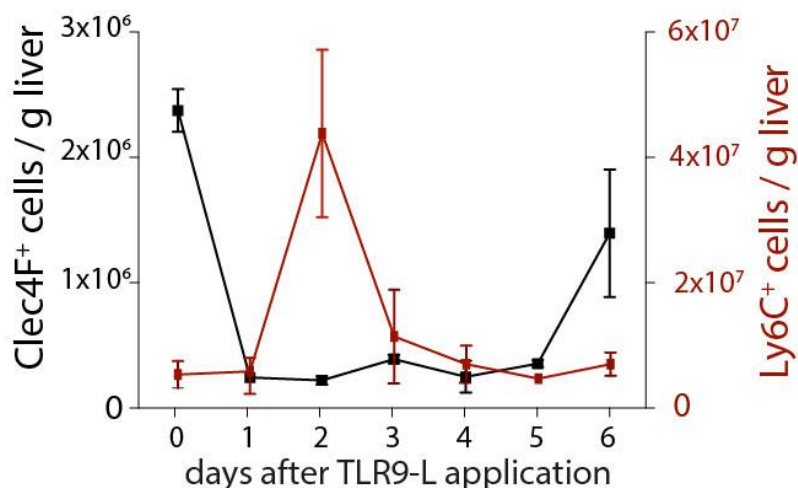


Figure 6: The immunogenic window. Cell numbers of Clec4F⁺ Kupffer cells and liver Ly6C⁺ myeloid cells. Pooled data from n≥3 independent experiments (n=4).

4.1.2 TLR9-L application does affect other lymphoid organs as well

In order to analyze the effect of TLR9-L application on other lymphoid organs¹⁵⁶, splenic myeloid cells were purified, although iMATEs have not been detected in the spleen yet⁷⁴. Furthermore,

comparing splenic and hepatic myeloid cells was supposed to help identify iMATE-specific myeloid cells. In the spleen the number of CD11b⁺Ly6C^{neg} monocytes already started increasing around 24 hours after the TLR9-L application (Fig. 7A). The peak was reached at day 2 with an about 3,5-fold increase. Numbers started to decrease at day 3 after TLR9-L application but did not return to the prevailing conditions within the analyzed time period. The development of CD11b⁺Ly6C⁺ inflammatory cells in the spleen did resemble the hepatic one. An about 10-fold increase from day 1 after TLR9-L application to day 2 was observed. The numbers strongly decreased between day 2 and day 3.

As it was hypothesized that most of the myeloid cells found in the liver at day 2 were recruited from the circulation, blood myeloid cells were included into the analysis. The effect of TLR9-L application did not influence the population size of CD11b⁺Ly6C⁺ cells in the blood. CD11b⁺ cells however displayed a strong increase in cell numbers two days after the application of TLR9-L. Those numbers started decreasing at day 3, hit a plateau at day 4 and returned to steady state conditions during day 5 and 6 (Fig. 7B).

In addition to spleen and blood the kidneys and the liver draining lymph nodes were analyzed before and after the application of TLR9-L. The kidneys were not affected by the application of TLR9-L. A slight increase in CD11b⁺Ly6C^{neg} monocytes was detected but it was not significant. The numbers of CD11b⁺Ly6C⁺ inflammatory cells did not change (Fig.4C). In the lymph nodes a significant increase of both cell populations was observed, but this can be explained by the hepatic recruitment of myeloid cells from the circulation (Fig. 7C).

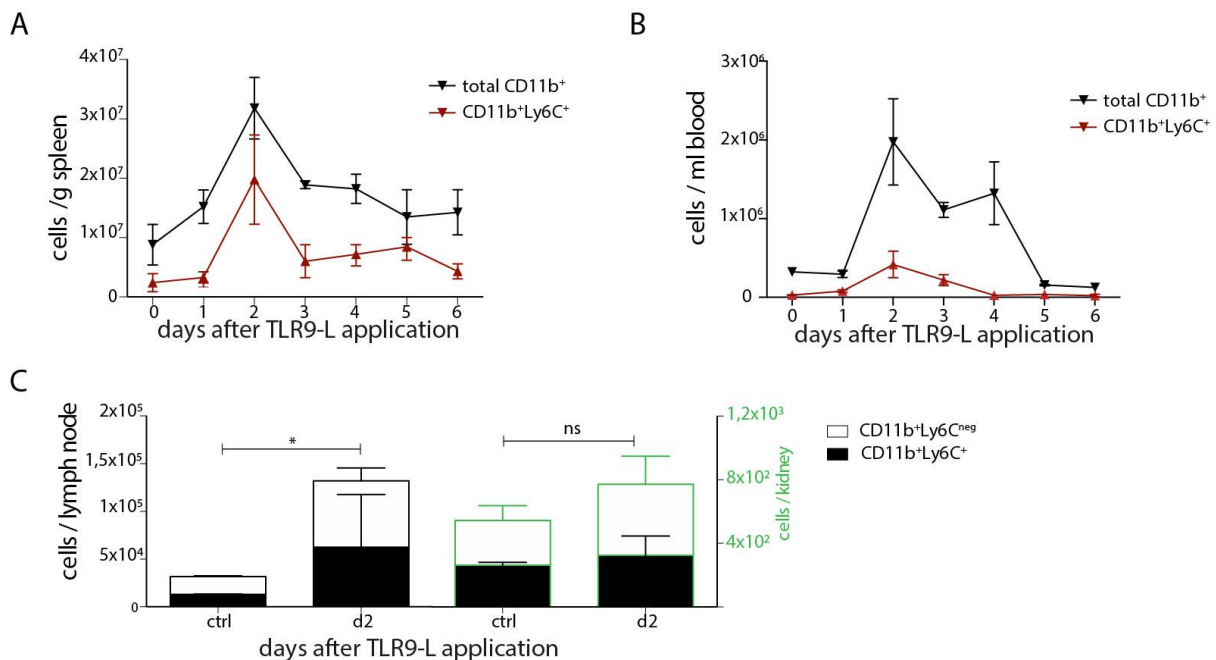


Figure 7: (A-C) Influence of TLR9-L on myeloid cells in blood, spleen, kidney and lymph nodes. (A) Quantification of splenic myeloid cells after the application of TLR9-L. (B) Quantification of blood myeloid cells after the application of TLR9-L. (C) CD11b⁺Ly6C^{+/neg} cells in lymph nodes and kidney before and after the application of TLR9-L. (A-C) Pooled data from 3 independent experiments (n=4). Mann-Whitney t test. *p < 0.001**

In conclusion these data show that the application of TLR9-L application affects the myeloid population in other organs as well and induces an elevated availability. Nevertheless, the drastic increase in myeloid cell numbers was only observed within the liver.

4.2 The disappearance of CD11b⁺Clec4F⁺Ly6C^{neg} Kupffer cells is not a prerequisite for iMATE formation

The application of TLR9-L induces a quick disappearance of Kupffer cells and appearance of CD11b⁺Ly6C⁺ myeloid cells (**Fig. 4**). This led to the hypothesis that the disappearance of the Kupffer cells created a niche that enables the strong influx of CD11b⁺Ly6C⁺myeloid cells. Furthermore, the niche might not only create an opportunity but might be indispensable for the iMATE formation. In order to test this hypothesis, poly-inosinic acid (poly-I), a ligand for scavenger receptor A¹⁵⁷ was used to block the uptake of TLR9-L into Kupffer cells. This blockade should prevent the disappearance of Kupffer cells. Poly-I was applied 5min before the application of TLR9-L and the effects were analyzed 24, 48 and 72 hours later.

The additional application of poly-I did counteract the effect of TLR9-L. One third less Kupffer cells disappeared within the first 24 hours after the application of the two substances (**Fig. 8A,B**). This effect was not permanent as about half of the remaining Kupffer cells did disappear within the next 24 hours. The repopulation of the Kupffer cell niche did start around the same time in both experimental setups. Even though only a portion of the Kupffer cells was rescued, the influx of CD11b⁺Ly6C⁺ myeloid cells was considerably retarded. It first started around day 3 after the application of TLR9-L and poly-I, and further analysis is needed to monitor the development. Anti-CD11b immunohistochemistry did show iMATE structures within the poly-I treated animals (**Fig. 8C**) as well as anti-Clec4F staining Clec4F⁺Kupffer cells at day 2 after TLR9-L application. The Kupffer cells were not located within iMATEs but in their environment (**Fig. 8C**).

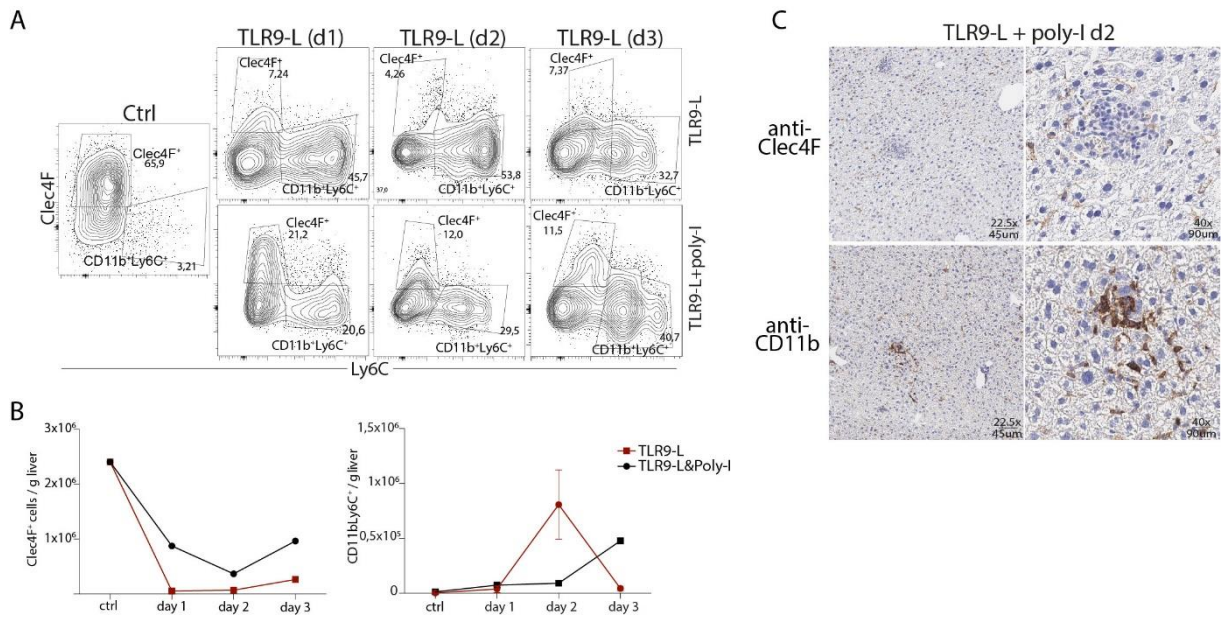


Figure 8: (A-C) Kupffer cell disappearance is slowed down by additional poly-I treatment. (A) Kupffer cell populations after the application of TLR9-L w/o poly-I. Data are representative for 2-3 experiments. (B) Quantification of (A). Pooled data from 2-3 experiments (n=3). Mann-Whitney t test. ***p < 0.001 (C) Anti-Clec4F and anti-CD11b immunohistochemistry. Data are representative for 2-3 independent experiments.

The detection of iMATE structures in the histological sections did raise the question whether iMATEs in Poly-I treated animals had the potential to expand hepatic CTLs. Therefore, the number of endogenous CD8⁺ T cells at 72 hours after the application of both poly-I and TLR9-L were analyzed. Elevated numbers of CD8⁺ T cell (Fig. 9A) were detected but like the disappearance of Kupffer cells and the appearance of inflammatory myeloid cells, the expansion of endogenous CD8⁺ T cells in the liver was reduced due to the application of poly-I.

The effect of poly-I was tested also in blood and spleen as well. A stronger increase in splenic cell numbers within all CD11b⁺ populations compared to TLR9-L application alone was detected, which indicates that poly-I does also impact the splenic environment (Fig. 9B). Blood myeloid cells were not affected at all (Fig. 9B).

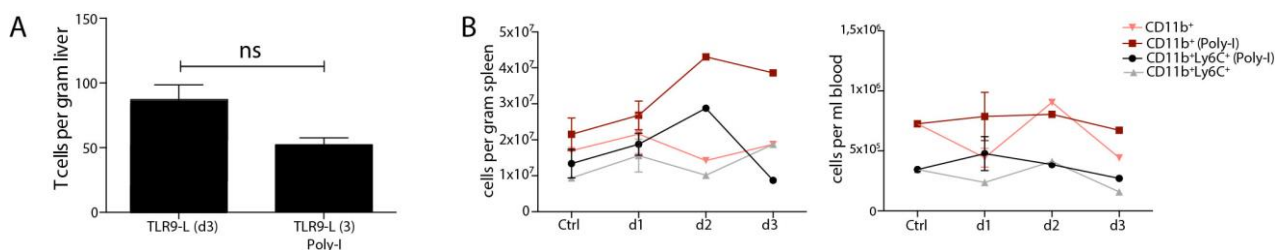


Figure 9: (A-B) Effect of poly-I application on myeloid cells in spleen and blood. (A) T cell population expansion after the application of TLR9-L w/o poly-I. (B) Quantification of CD11b⁺ cells in spleen and blood after the application of TLR9-L w/o poly-I. (A,B) Pooled data from 3 independent experiments. Mann-Whitney t test. ***p < 0.001

Altogether, these data suggest that poly-I prevented TLR9-L binding to TLR9 and thereby had multiple effects. Even though the immigration of myeloid cells was retarded functional iMATEs did form and induced intrahepatic T cell population expansion.

4.3 iMATE formation is only induced by TLR9-L

TLR9 belongs to a family of microbial-sensing proteins that can initiate adaptive or innate immune responses (TRL1-9). The effects of further TLR-ligands like TLR3 (poly(I:C)) or TLR4 (LPS) on T cell expansion have already been described elsewhere⁷⁴. The ligand for TLR3 poly-inosinic poly-cytidylic acid (poly(I:C)) is described to induce inflammation¹⁵⁸ and uses TRIF for its signaling cascade. The ligand for TLR4 lipopolysaccharide (LPS) is known to impair liver homeostasis and metabolism¹⁵⁹ and uses TRIF and MyD88. So far it has never been investigated whether they can induce iMATEs. In order to answer this question, mice were treated with 10µg LPS or 30µg poly(I:C) and analyzed 48 hours later.

Both ligands induced Clec4F⁺Kupffer cell disappearance as observed with TLR9-L (**Fig. 10A,B**). This was also confirmed by liver immunohistochemistry with anti-Clec4F (**Fig. 10C**). An increase in CD11b⁺Ly6C⁺cells, however, was only observed in animals treated with LPS (**Fig. 10D**) but no myeloid cell clusters in the liver were detected (**Fig. 10C**). Nevertheless, endogenous CD8⁺T cells expansion was detectable although to a lesser degree than after TLR9-L (**Fig. 10E**). The treatment with poly (I:C) did not increase the numbers of hepatic CD11b⁺Ly6C⁺cells and consequently also neither caused formation of iMATEs nor CD8⁺T cell expansion (**Fig. 10E**).

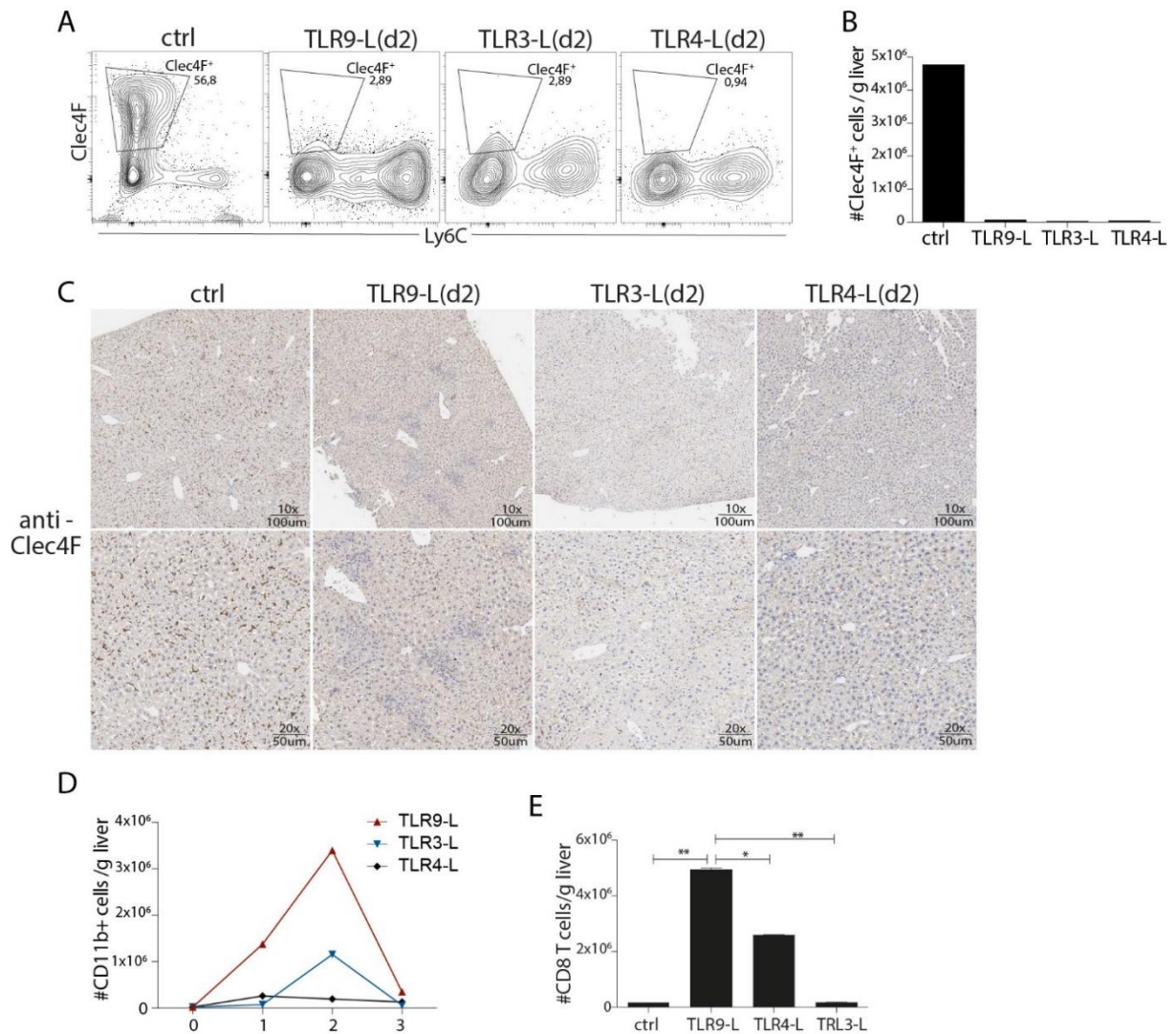


Figure 10: (A-E) Analysis of myeloid cells after the application of different TLR ligands. **(A)** FACS analysis of Clec4F⁺Kupffer cells after the application of TLR ligands. Data are representative for $n \geq 3$ experiments. **(B)** Quantification of **(A)**. Pooled data from $n \geq 3$ experiments. **(C)** Anti-Clec4F immunohistochemistry after the application of TLR ligands. Data are representative for $n \geq 3$ experiments. **(D)** Quantification of CD11b⁺ cells after the application of TLR ligands. Pooled data from 4 independent experiments. **(E)** Quantification of T cell expansion after the application of TLR ligands. Pooled data from 3 experiments. Mann-Whitney *t* test. *** $p < 0.001$

These data show that the recruitment of inflammatory myeloid cells into the liver and the disappearance of Kupffer cells were not only induced by the application of TLR9-L. Nevertheless, the formation of iMATEs is exclusive to the application of TLR9-L whereas the increase in the CD8 T cell population is not. It was not analyzed however whether the increasing numbers of T cells in the LPS treated animals are due to local proliferation or immigration. Referring to the results of the previous section the data show that the hepatic recruitment of myeloid cells is dependent on the disappearance of Kupffer cells, but not the formation of iMATEs.

4.4 iMATE forming myeloid cells originate from the circulation

The myeloid cells found in the liver at steady state conditions, apart from yolk sac derived Kupffer cells, originate from circulating monocytes in the blood⁴⁷. The strong increase in

numbers within a short time frame after the application of TLR9-L raised the question whether local proliferation within the liver might be involved in this rapid increase in cell numbers. To address this question, pulse-chase experiments with bromodeoxyuridine (BrdU) were performed. Mice injected with TLR9-L received BrdU 12 for 1 or 12hrs before cell isolation was performed. Very few BrdU⁺ cells were found after both pulses, indicating that the strong increase in numbers of CD11b⁺ cells is due to recruitment from the circulation and not to local proliferation (Fig. 11).

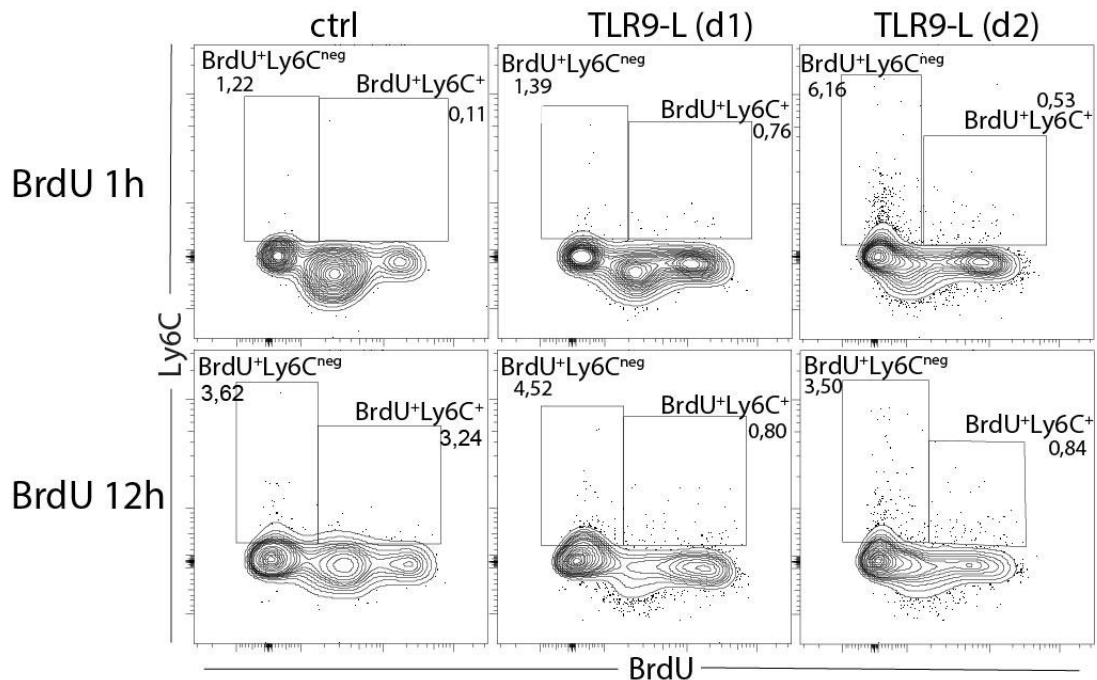


Figure 11: FACS analysis of one and 12h pulse chase experiment with BrdU and TLR9-L. Data are representative for 4 independent experiments.

The data indicate that the myeloid cells found in the liver after the application of TLR9-L originate from the circulation and accordingly from the bone marrow and were not derived from local proliferation within the liver.

4.5 TLR9L induces a specific cytokine expression profile not only in the liver.

According to Huang et al (2013)⁷⁴ iMATE formation is driven by TNF α signaling. The analysis of liver, spleen, kidney tissue and blood after the application of TLR9L was aimed to determine which additional signaling molecules are involved. In the liver TNF α , IL6 and MIP1 α expression increased by more than 3 log levels within 1 hour. The other cytokines were barely affected. Whereas MIP1 α displayed a sustained expression until 72 hours, IL6 levels were gradually reduced. TNF α levels did decrease, increase and decrease again. The second increase was accompanied by raising IFN γ levels, that continued rising until having reached its highest point after 72 hours. It then fell back to basal levels together with TNF α . Within the spleen MIP1 α was the only cytokine that displayed elevated levels. In the blood TNF α , IL6, MCP1 and MIP1 α expression increased more than 3 log levels within 1 hour before returning to about basal levels

within the next 3 hours. Like in the liver IFN γ levels did raise more slowly in the blood. They did reach their limit after 48 hours and did not induce another increase in TNF α levels. In the kidney little to no difference in cytokine levels were detectable (**Fig.12A**). The level of TNF α in liver cells was analyzed additionally by flow cytometry. CD11b⁺ cells at day 2 after the application of TLR9L expressed TNF α , but this expression was not higher than that in Kupffer cells. The same results were achieved for the expression of iNOS. Whereas Kupffer cells expressed ROS only little expression was found in CD11b⁺ cells at day 2, indicating that TLR9L did not trigger oxidative stress.

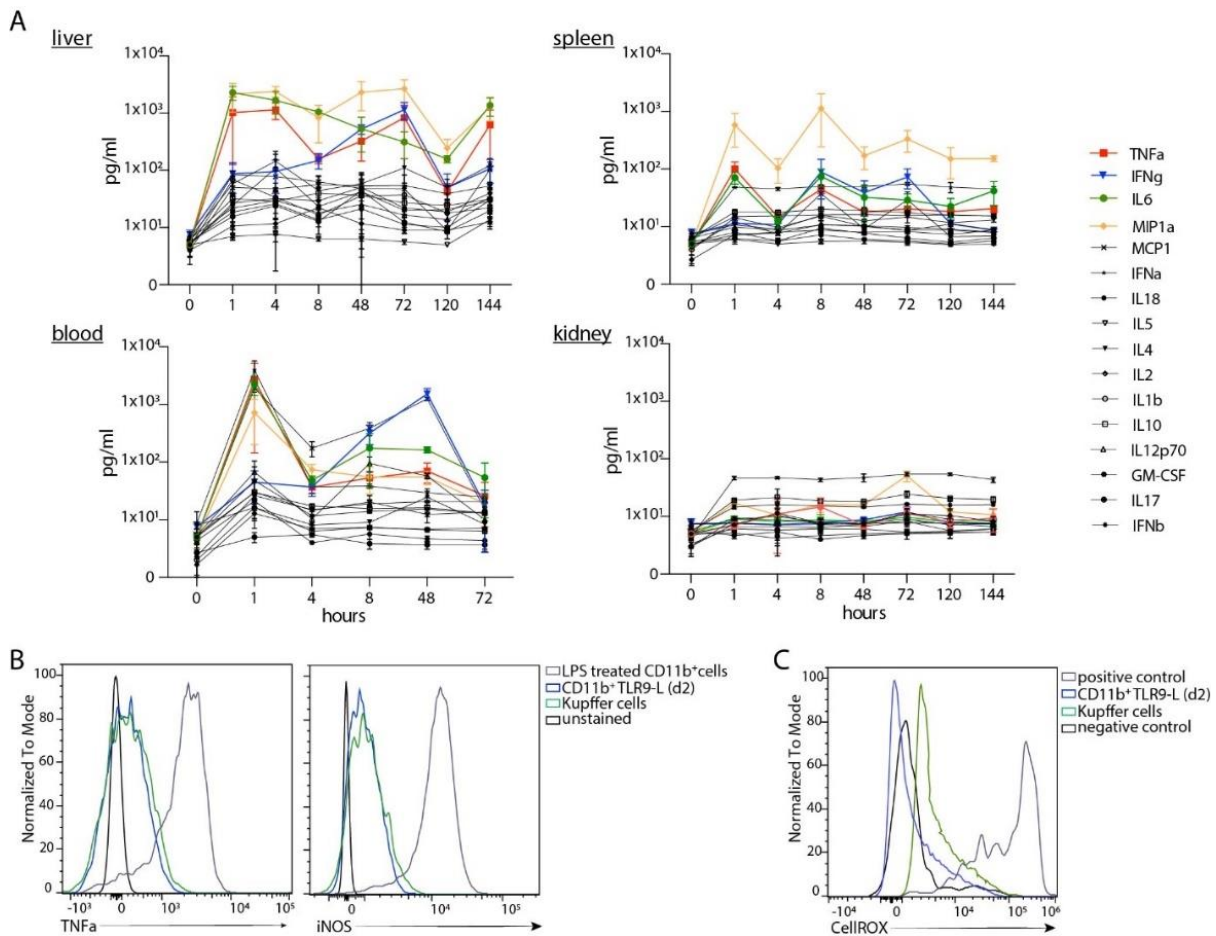


Figure 12: (A-C) Cytokine expression in different organs after the application of TLR9L at day 2. **(A)** Cytokine expression profile of CD11b⁺ cells of different organs. Pooled data from 3 experiments. **(B)** Expression of TNF α and iNOS by Kupffer cells and CD11b⁺ cells after the application of TLR9L. Data are representative for 4 experiments. **(C)** Expression of ROS by Kupffer cells and CD11b⁺ cells after the application of TLR9L. Data are representative for 4 independent experiments.

The results show that TLR9L signaling induces a tightly regulated cytokine response mainly in the myeloid cells of liver and blood without triggering excessive oxidative stress.

4.6 Phenotypical plasticity observed after the application of TLR9-L in the liver

The study was aiming to characterize iMATE-forming myeloid cells. Therefore, a detailed phenotypic analysis was performed.

4.6.1 Four markers display the heterogeneous nature of myeloid cells

F4/80, CX₃CR1, CCR2 and MHCII were chosen for the first phenotypical screening. F4/80 also known as EGF-like module-containing mucin-like hormone receptor-like 1 and a member of the adhesion G-protein coupled receptors (GPCRs) is a marker that is widely used for murine macrophage populations¹⁶⁰. CX₃CR1 the fractalkine receptor of GP(C) R13 is expressed on most leukocytes and can mediate their chemotaxis. It was described in the context of tissue homeostasis and promotion of cell survival¹⁶¹. CX₃CR1⁺ cells are involved in either pro- or anti-inflammatory responses¹⁶² qualifying CX₃CR1 as mononuclear phagocyte marker¹⁶³. CCR2 the C-C chemokine receptor type 2 is the receptor for monocytes chemoattractant protein 1. It is involved in monocyte infiltration and mediates chemotaxis^{164,165}. MHCII a class of major histocompatibility (MHC) molecules are commonly expressed on antigen presenting cells where they present antigenic fragments to the immune system¹⁶⁶.

The inflammatory myeloid cells (CD11b⁺Ly6C⁺) under steady state conditions did not express MHCII and only few of them F4/80. About 50% of them were positive for CX₃CR1 and two thirds of those co-expressed CCR2. The monocytes (CD11b⁺Ly6C^{neg}) were more versatile. There was only little CX₃CR1 and CCR2 found but F4/80 and MHCII were expressed together and alone on more than two thirds of the cells (Fig. 7A). Invading CD11b⁺Ly6C⁺ inflammatory cells analyzed at day 2 after TLR9-L application were mainly positive for CCR2 (**Fig. 13A**), a marker needed for monocyte and macrophage recruitment¹⁶⁵. They were partially double positive for CX₃CR1. About 20% of them were positive for F4/80 whereas MHCII expression was barely found. The CD11b⁺Ly6C^{neg} monocytes found at day 2 did not express MHCII or F4/80 and only very few were found to be positive for CCR2. Expression of CX₃CR1 was found on about 30% of the cells, pointing towards a naïve type of myeloid cell (**Fig. 13A**).

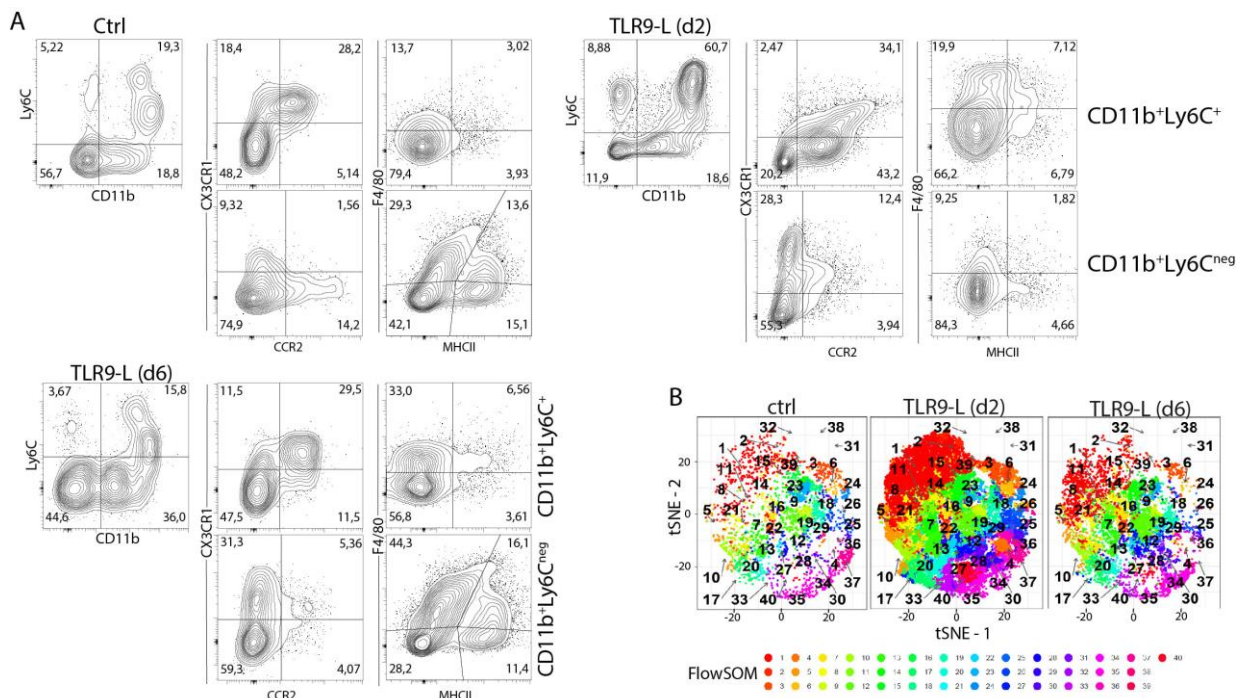


Figure 13: (A,B) Phenotypic analysis of myeloid cells at steady state and two and six days after TLR9-L application. (A) FACS analysis of Ly6C, CCR2, CX3CR1, MHCII, F4/80 expression on CD11b⁺ cells. Data are representative for n≥3 experiments. (B) FlowSOM analysis of (A) (analysis was performed in collaboration with Sainitin Donakonda). Pooled data are from 4 independent experiments.

The phenotype of both the CD11b⁺Ly6C⁺ and CD11b⁺Ly6C^{neg} cells found at day 6 strongly resembled the myeloid cells detected under the steady state conditions (Fig. 10A). The fluent dynamic in surface marker expression during the analyzed time course was displayed with FlowSOM analysis (Fig. 13B). This algorithm uses self-organizing maps together with two-level clustering and can visualize the data in several ways like star or pie charts as well as grid or tree structures. It gives an overview about the entire marker on all cells and is able to detect subsets that might be missed otherwise.

The data display the plasticity of myeloid cells and the transient nature of their surface marker expression further diversified by the application of TLR9-L.

4.6.2 Additional phenotypical characterization did not result in an iMATE-specific marker

Conventional phenotyping approaches for myeloid cells used markers such as CD11c, CD11b, major histocompatibility complex (MHC)-II or CD68. This reduced selection is not suited to fully reflect the heterogeneity of these cells due to the lack of proper lineage markers and the high cellular plasticity².

The surface markers used so far had already illustrated the heterogeneity of the hepatic myeloid cells. Further screening was used to target a suitable biomarker for iMATE-forming myeloid cells. The focus was put on the myeloid cells 2 days after TLR9-L application compared to steady state.

4.6.2.1 Co-stimulatory surface molecules

The work of Huang et al.⁷⁴ showed that cytotoxic CD8⁺ T cells (CTLs) undergo a second round of proliferation within the iMATEs. It has not been described yet how the iMATE forming myeloid cells induce this T cell expansion. One possible explanation could be the activation of T cells via co-stimulatory surface molecules. Therefore, several of known costimulatory molecules were analyzed on liver myeloid cells.

The protein B7-2 or CD86 is expressed on antigen presenting cells and provides co-stimulatory signals that are needed for T cell activation and survival¹⁶⁷. The application of TLR9L induced increased expression on the myeloid cells especially on Ly6C⁺ cells. CD86 works in tandem with CD80 also known as B7-1¹⁶⁸. The expression level of CD80 did not change on Ly6C⁺ cells due to the application of TLR9L. However, a slight increase was detectable on Ly6C^{neg} cells. The T Cell immunoglobulin and mucin domain containing 4 (Tim4) is a phosphatidyl-serine receptor that is involved in regulating T cell proliferation and lymphotoxin signaling^{169,170}. A strong expression of Tim4 was detected on Kupffer cells like it had been described by van de Laar et al. (2016)¹⁷¹. Less expression of Tim4 on Ly6C^{neg} cells was found on Ly6C^{neg} cells after the TLR9L application mainly due to the loss of Kupffer cells. No changes were found in the group of Ly6C⁺ cells. The TNF superfamily member 4, also known as OX40L mediates interactions of T cells and APCs and co-stimulates T cell proliferation and cytokine production^{172,173}. Its low expression on Ly6C⁺ /

neg was not affected by the application of TLR9L. CD58 also known as lymphocyte function-associated antigen 3 that is a ligand for CD2 on T cells and is involved in adhesion and activation of T lymphocytes¹⁷⁴. TLR9L application induces the downregulation on Ly6C neg cells. Low to no expression was detected on Ly6C+ cells and was not affected. Tim3, a phosphatidyl-serine receptor that has been described to modulate innate and adaptive immune responses rather in a regulatory manner¹⁷⁵ by activating the T_H1 response that leads to induction of peripheral tolerance¹⁷⁶. Tim3 is mainly found on Ly6C+ cells and was slightly downregulated. A small increase in expression levels was detectable on the Ly6Cneg cells. CD195 also known as CCR5 is one of the receptors that bind RANTES, a proinflammatory CC-chemokine that induces the production of proinflammatory cytokines¹⁷⁷. A little reduction in expression levels were detectable on both Ly6C+/neg cells (**Fig.14**).

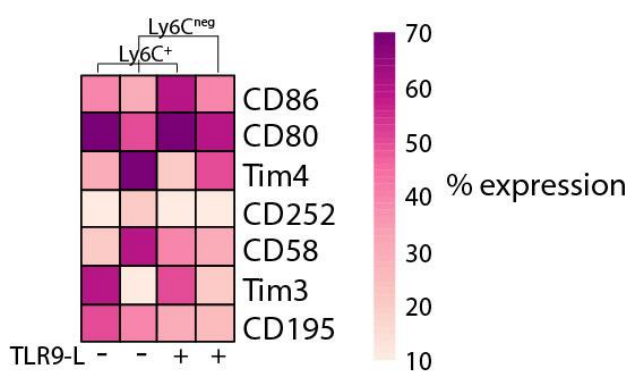


Figure 14: Quantification of marker expression at steady state and two days after the application of TLR9-L in CD11b⁺ cells. (CD11b⁺Ly6C^{neg} cells at steady state correspond to Clec4F⁺ Kupffer cells). Pooled data are from 4 independent experiments.

None of the analyzed marker is strongly affected by TLR9-L application and could explain the exclusive local proliferation of T cells (**Fig. 14**). Accordingly, local expansion of T cells could not be explained by these results and led me to look for other so far unknown mechanisms.

4.6.2.2 Surface molecules for intercellular adhesion

The iMATEs are dense cocoon-like non-perfused structures. Their cohesion could not be explained by a fibrous ring or fibrocytes surrounding the iMATE⁷⁴. An up-regulated expression of adhesion molecules might be a possible explanation for this phenomenon.

Intercellular adhesion molecule 1 (ICAM1, CD54) is an integrin continuously expressed in low concentrations by cells of the immune system, whose expression is increased by cytokine stimulation leading to transmigration into tissues¹⁷⁸. The expression of CD54 did not change due to the application of TLR9L. The β 2 integrin subunit α L CD11a combines with the subunit β 2 (CD18) to form the integrin lymphocyte function-associated antigen 1 (LFA-1) that plays an important role in intercellular adhesion by interacting with ICAMs like CD11b²⁶ and is involved in the regulation in the key aspects of immune cell function¹⁸⁰. The expression of CD11a and CD18 did not change in the group of Ly6C+ cells, but it got upregulated on Ly6Cneg cells. CD162 also known as selectin P ligand is a glycoprotein that serves as a high affinity counter receptor for cell adhesion molecules on myeloid cells and plays an important role in leukocyte trafficking during inflammation¹⁸¹. CD162 was highly expressed on both Ly6C+/neg cells and no changes

in the expression levels were detected. Macrophage, a surface protein and member of the LAMP (lysosome associated membrane protein) proteins, is a cell adhesion molecule highly expressed by members of the monocyte lineage, by phagocytes and tissue resident macrophages¹⁸² whose function remains unknown. Only little expression was found in the steady state. This was reduced on the Ly6Cneg cells and slightly increased on the Ly6C+ cells. The integrin subunit α 2 or CD49b mediates the adhesion to the extracellular matrix¹⁸³. The expression of CD49b was at basal levels in the steady state and did not much increase due to the application of TLR9L. Integrin α X, also known as CD11c, is a type I transmembrane protein expressed on monocytes, granulocytes and macrophages that is commonly described as a marker for dendritic cells¹⁸⁴. The population of Ly6CnegCD11c+ cells did not change whereas the Ly6C+ cells started upregulating CD11c. The lysosomal associated membrane protein 2 (LAMP2) or CD107b is involved in the protection, maintenance and adhesion of lysosomes^{185,186} as well as cell-cell adhesion¹⁸⁷ and was not affected by the application of TLR9L. Nevertheless, its expression was markedly elevated on the Ly6C+ cells. Intercellular adhesion molecule 2 (ICAM2), also known as CD102 is a type I transmembrane glycoprotein that amongst others plays a role in lymphocyte recirculation and adhesive interactions¹⁸⁸. The expression of CD102 got downregulated in both the Ly6C+ and Ly6Cneg cells (**Fig. 15**).

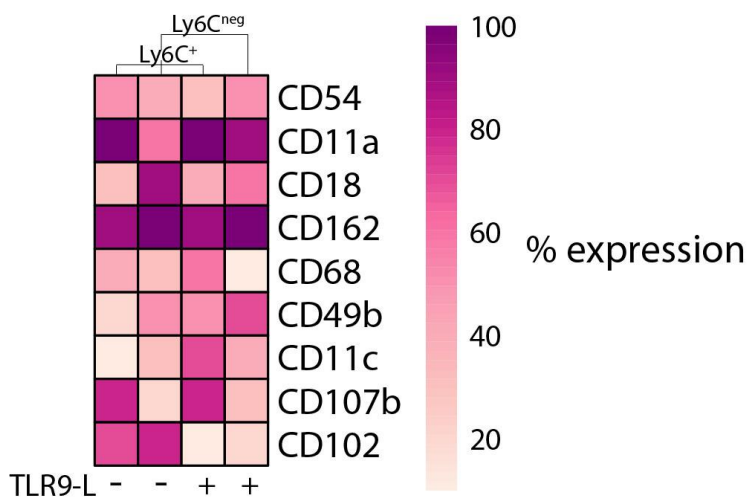


Figure 15: Quantification of marker expression at steady state and two days after the application of TLR9-L in CD11b+ cells. (CD11b+Ly6Cneg cells at steady state correspond to Clec4F+ Kupffer cells). Pooled data are from 4 independent experiments.

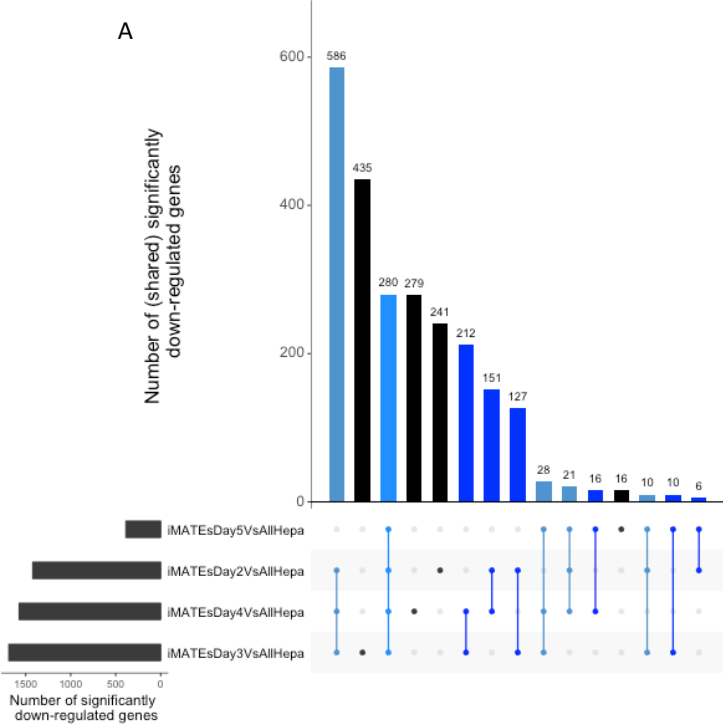
Even though several markers were affected by the application of TLR9-L none of them was suited to be used as biomarker. The most pronounced changes were detected in the expression of CD11c, but as a marker for dendritic cells it is not exclusively found in iMATE-forming cells. (**Fig. 15**).

4.7 Genetic profiling of iMATE tissue identifies CD40 as a potential biomarker

The extensive phenotypic characterization of myeloid cells found in the liver after TLR9-L application did show a diverse composition, but none of the analyzed marker was found to be exclusive. Furthermore, for the analysis of the iMATE-forming cells all hepatic myeloid cells were isolated impeding the classification of iMATE specific marker. This obstacle was bypassed

by laser-capture microdissection of single iMATEs that were subjected to micro-array analysis that was used to create a genetic profile of iMATE forming cells. Areas without iMATEs were used as a tissue control. RAG^{-/-} mice lacking B and T cells were used to determine myeloid cell specific genes. The tissue sections used for this experiment are displayed in Suppl. Table 1. The genetic profile of iMATE-forming cells was used to detect molecular mechanisms involved in and quantitative biomarkers for iMATE formation.

The overall numbers of differentially expressed genes are displayed in suppl. table 2. The numbers of (shared) significantly up- and down-regulated genes are displayed in **Fig. 16A,B**. Throughout d2, 3 and 4 a big proportion of the same genes was downregulated. 47% stay downregulated until day 5. This strong consistence was not observable in the group of upregulated genes. Only few genes stay upregulated until day 5 and only 21% more are upregulated at day 2, 3 and 4. Whereas day 3 and day 4 share a significant number of upregulated genes, these genes can be no longer found at day 5. iMATE sections from day 3 displayed the highest number of up- and downregulated genes (**Fig. 16A,B**).



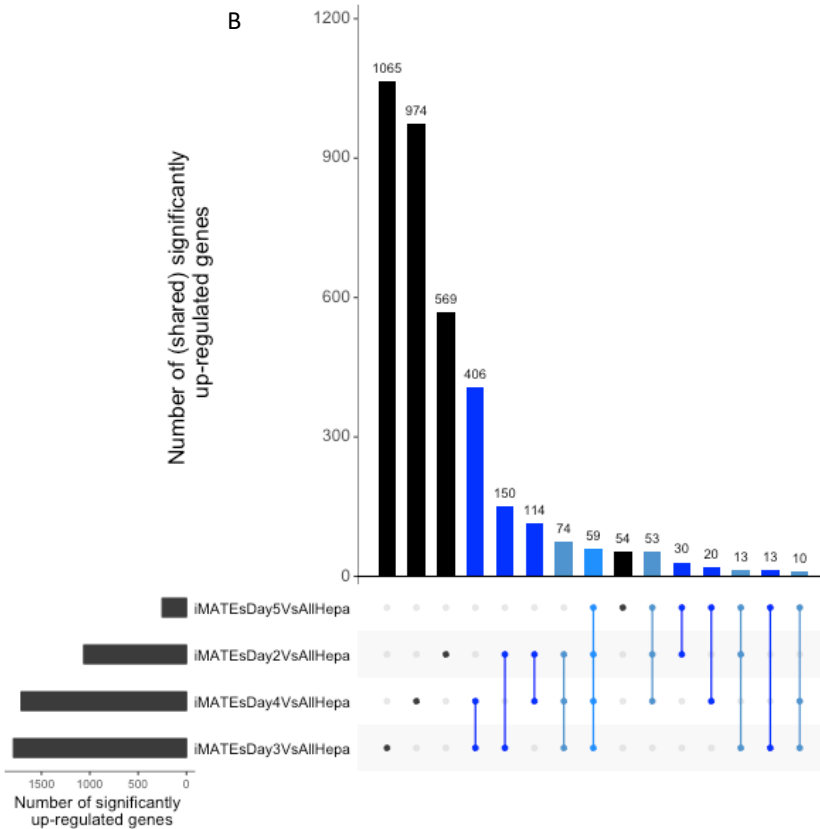


Figure 16: (A-B) Visualization of the overlap of the significantly up-regulated genes by iMATEs day2 vs hepatocytes, iMATEs day 3 vs hepatocytes, iMATEs day4 vs hepatocytes and iMATEs day5 vs hepatocytes (A) Number of (shared) significantly down-regulated genes. (B) Number of (shared) significantly up-regulated genes. Data are pooled from 4 independent experiments.

These data show the plasticity of myeloid cells once again. Each day has a special set of myeloid cells with a different gene expression profile.

4.7.1 Potential iMATE specific markers

The markers that were grouped under the term iMATE specific marker by the collaboration partner were collected from the analysis of day 2 and 3. They were differentially expressed both in C57BL/6J and RAG^{-/-} mice, indicating the specificity for myeloid cells. The discovered genes are involved in inflammatory processes (IFN γ ¹⁸⁹, Cybb¹⁹⁰, GzmB^{191,192}, Cst7^{193,194}, IRF8, Clec4e¹⁹⁵⁻¹⁹⁷, Traf1^{198,199}), co-stimulation & T cell activation (CD40²⁰⁰, MHCII¹⁶), lymphoid lineage (Ly6i^{201,202}, Ly6A^{203,204}), regulatory processes (Il1rn²⁰⁵⁻²⁰⁷, Irg1²⁰⁸, Ifit2^{209,210}), chemotaxis & cell recruitment (CCRL2^{211,212}, CXCL10^{213,214}, Ms4a4c^{215,216}) and metabolic processes (Sl2a6²¹⁷⁻²²⁰) (Fig. 17).

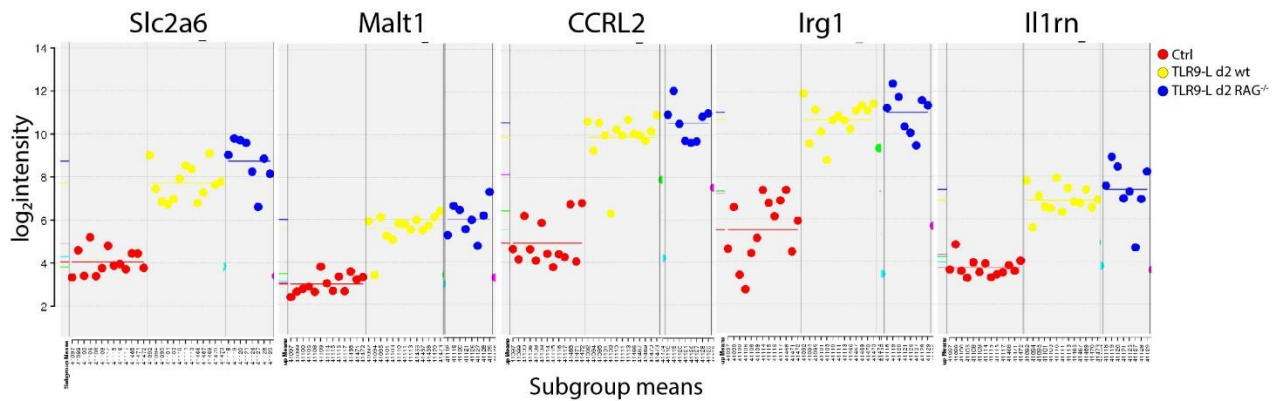


Figure 17: Genetic expression profiles of hepatic cells. Representative plots for upregulated iMATE specific genes in hepatic cells of B16 and RAG^{-/-} mice treated with either TLR9-L or non-TLR9-L.

Expression of the surface markers CD40, MCHII and Ly6A was analyzed by flow cytometry and immunohistochemistry to confirm the data of the microarray.

The Tumor Necrosis Factor Receptor Superfamily Member 5 CD40 is a costimulatory receptor on antigen-presenting cells. It has a pivotal role in initiation and progression of immune and inflammatory responses of the innate and adaptive immune system^{221,222}. Its ligand CD40L (CD154) is transiently expressed on T cells and other non-immune cells²²³. A 4-fold upregulated expression of CD40 in the iMATE sections compared to iMATE-free liver tissue both in C57BL/6J and RAG^{-/-} mice (**Fig. 18A**) was detected. This result was also proven with flow cytometric analysis. Only few CD40⁺ cells were detected in the steady state liver. The number of CD40⁺ cells increased 10-fold within 48 hours after TLR9-L application (**Fig. 18B**) especially on CD11b⁺Ly6C⁺ inflammatory cells. CD40 was not found on CD11b⁺Clec4F⁺Ly6C^{neg} Kupffer cells and only few CD11b⁺Ly6C^{neg} monocytes did stain positive. It was not possible to show CD40 expression with immunohistological staining.

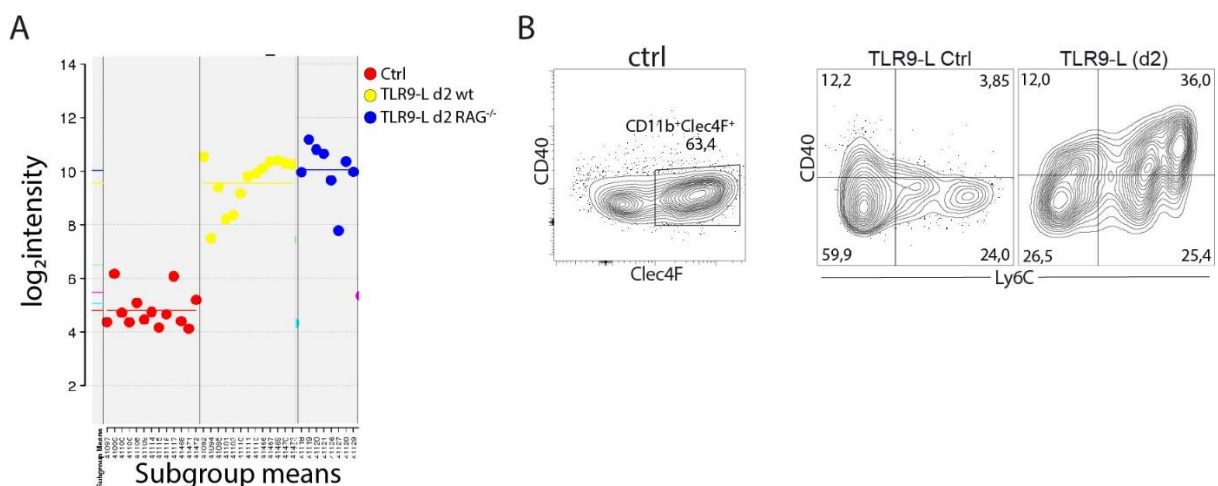


Figure 18:(A,B) Upregulated CD40 expression after the application of TLR9-L. **(A)** CD40 expression in control hepatic tissue, iMATEs of wildtype and RAG^{-/-} mice. **(B)** CD40, Clec4F and Ly6C expression on CD11b⁺ cells. Data are representative for n≥3 independent experiments.

The lymphocyte antigen 6A (Ly6A) also known as stem cell antigen-1 (Sca-1) is a member of the family of Ly6-alloantigens that were described to be involved in T cell activation²⁰³. Ly6A is a

GPI-anchored cell surface protein that is developmentally regulated. It is suggested to be involved in several biological processes like T cell signaling, cell adhesion, immune-responsiveness and promotion of T cell maturation²⁰⁴. Ly6A expression was found to be upregulated about 2,6-fold in the iMATE sections of both C57BL/6J and RAG^{-/-} mice (**Fig. 19A**). The expression of Ly6A was found on most CD11b⁺Clec4F⁺Ly6C^{neg} Kupffer cells, as well as CD11b⁺Ly6C^{neg} monocytes and CD11b⁺Ly6C⁺ inflammatory cells (**Fig. 19B**). Anti-Ly6A immunohistochemical staining located Ly6A in iMATE-like structures (**Fig. 19C**).

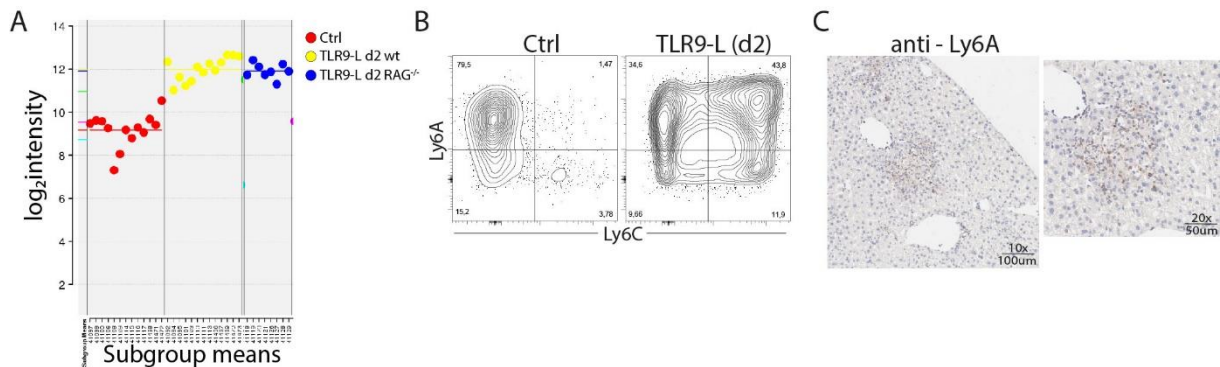


Figure 19: (A-C) Upregulated Ly6A expression after the application of TLR9-L. (A) Ly6A expression in control hepatic tissue, iMATEs of wildtype and RAG^{-/-} mice. (B) Ly6A and Ly6C expression on CD11b⁺ cells. (C) Anti-Ly6A immunohistochemistry. (B,C) Data are representative for n≥3 independent experiments.

The major histocompatibility complex class II (MHCII) is expressed on antigen presenting cells and presents peptides from lysosomal antigen degradation processes to CD4⁺T cells^{224,225}. Within the iMATE sections more MHCII was detected and the results from the RAG^{-/-} mice confirmed that this result was specific for myeloid cells (**Fig. 20A**). The FACS analysis failed to confirm the microarray data, but it can only detect the MHCII molecules that are expressed at the surface (**Fig. 20B**). Therefore, additional intracellular staining would need to be performed to verify the microarray data.

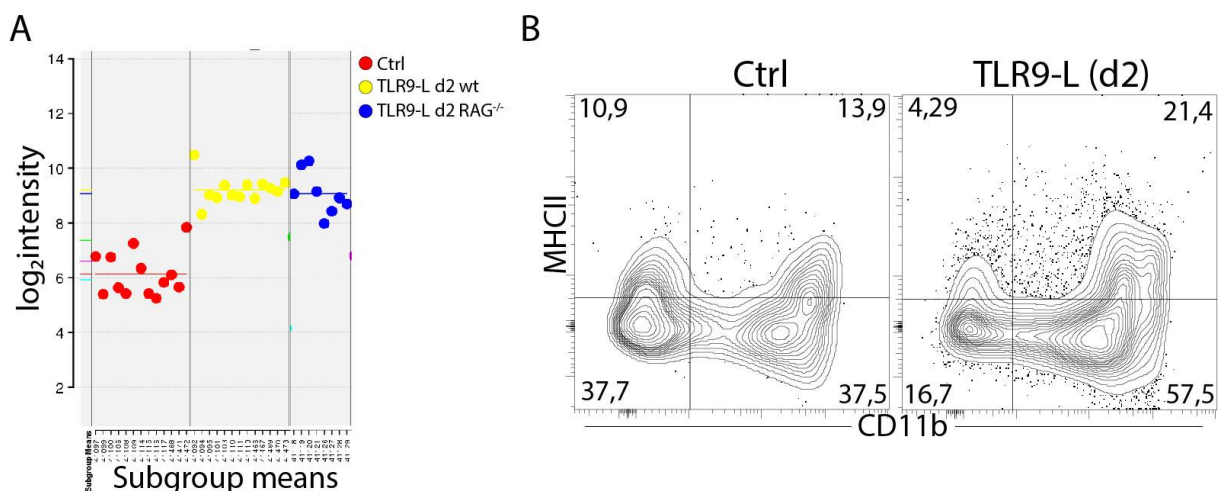


Figure 20: (A,B) Upregulated MHCII expression after the application of TLR9-L. (A) MHCII expression in control hepatic tissue, iMATEs of wildtype and RAG^{-/-} mice. (B) MHCII and CD11b expression on hepatic cells. Data are representative for n≥3 independent experiments.

Based on the results of the iMATE - specific marker set and subsequent FACS analysis, CD40 represented a promising candidate for a quantitative biomarker. This assumption was challenged in the following section (4.8).

4.7.2 Overall differentially expressed genes

Principal component analysis of the differentially expressed genes of time points and cell types demonstrates a clear separation of liver and iMATE-specific genes at day 2. The distance of this separation gradually got smaller with time (Fig. 21).

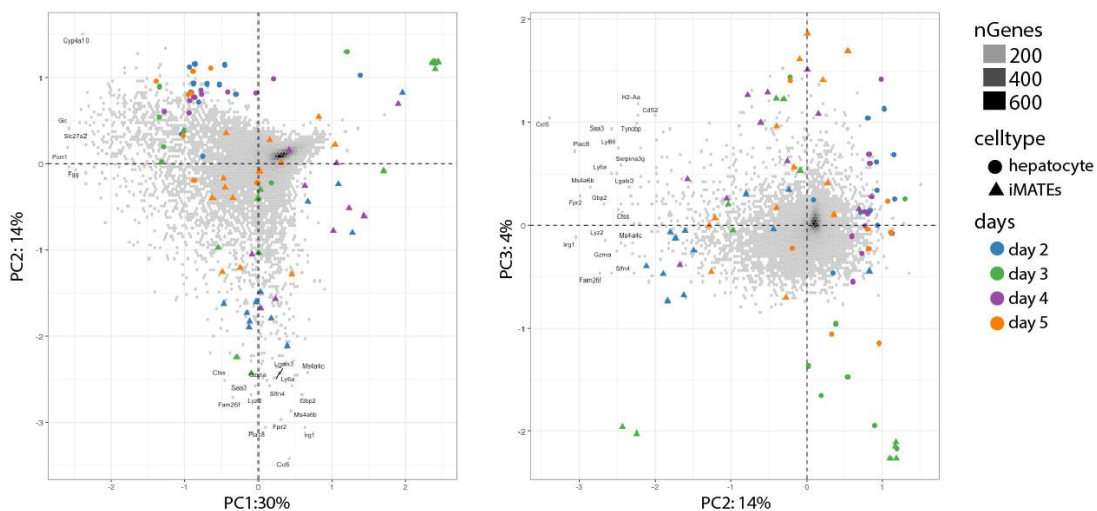


Figure 21: Principal component analysis in 3 dimensions, colored by time and shaped by cell type.

The analysis of the differential expression of genes at the analyzed time points in iMATEs and hepatocytes (Fig. 22) display a large number of differentially up- and downregulated genes. Genes for migration and chemoattraction (CCL5, Vim), metabolic activity (Ms4a4, aa467197, Slc2a6), antiviral activity / inflammation (Ifit1 / 2, Gbp2, Chil3), costimulation (CD40, Rsad2) and cell proliferation and differentiation (Slfn4, CCnd2, Pyhin1, S100a4) belong to the top upregulated. CD40 also belongs to the group of top upregulated genes indicating an important role during iMATE formation. Genes for the glucocorticoid transport (serpina6), the carbohydrate and lipid metabolism (Gpd1) and for steroid and lipid synthesis (cyp4a10) belong to the top downregulated.

These data illustrate the plasticity of myeloid cells and the dynamic changes that are induced by the application of TLR9L within the liver. Immigrating myeloid cells that form the iMATEs display a specific genetic profile that changes throughout the time period analyzed.

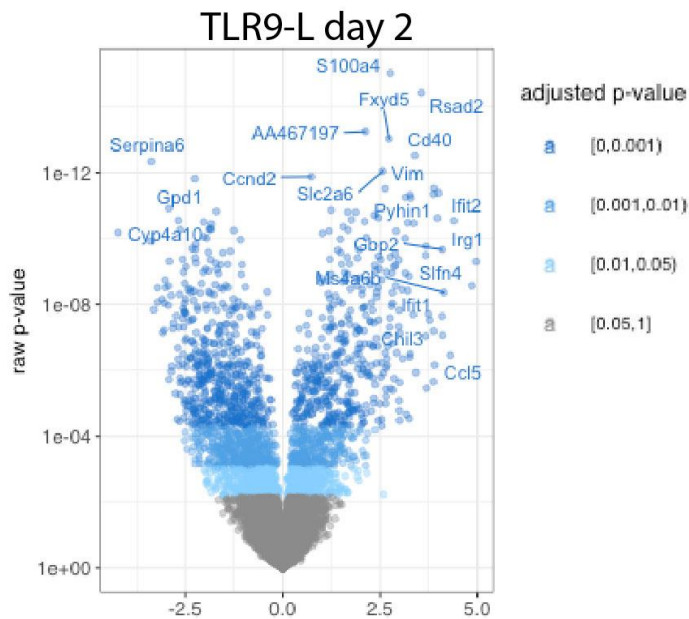


Figure 22: Volcano plot of the gene differential expression effects between iMATEs versus Hepatocytes per Time point for day 2 after TLR9L application. Data pooled from 4 independent experiments. Genes with significant effect (p -value < 0.05) are colored in blue and non-significant genes in grey. The top 20 genes with highest significance and/or highest fold change are highlighted.

4.8 Validation of the potential role of CD40 as a biomarker

The TNF receptor CD40 was one of the markers that were classified as an iMATE specific marker by gene array analysis. First explorative flow cytometric analysis confirmed this. There was only little expression found in the steady state and elevated expression after application of TLR9-L on CD11b⁺Ly6C⁺ inflammatory cells (**Fig.18**). CD40 appeared to be a potential biomarker. In order to investigate this hypothesis, it was challenged in different settings.

4.8.1 Transient expression of CD40 on hepatic CD11b⁺Ly6C⁺ cells after TLR9-L application

Monitoring of CD40 expression was performed over the iMATE time course, meaning day 0 until day 6. As described before only few cells expressed CD40 under steady state conditions and 24 hours after the application of TLR9-L. 48 hours after the application the expression had risen significantly together with the strong influx of CD11b⁺Ly6C⁺ cells. CD40 expression was primarily detected on those cells. At day 3 after the application no more CD40 expression was detectable and numbers of CD11b⁺Ly6C⁺ cells were clearly reduced. Until the end of the analysis at day 6 CD40 expression remained low or undetectable on CD11b⁺Ly6C⁺ cells (**Fig. 23A,B**). A small population of CD11b⁺Ly6C^{neg}CD40⁺ cells was found throughout the whole analysis. These results so far supported the biomarker hypothesis.

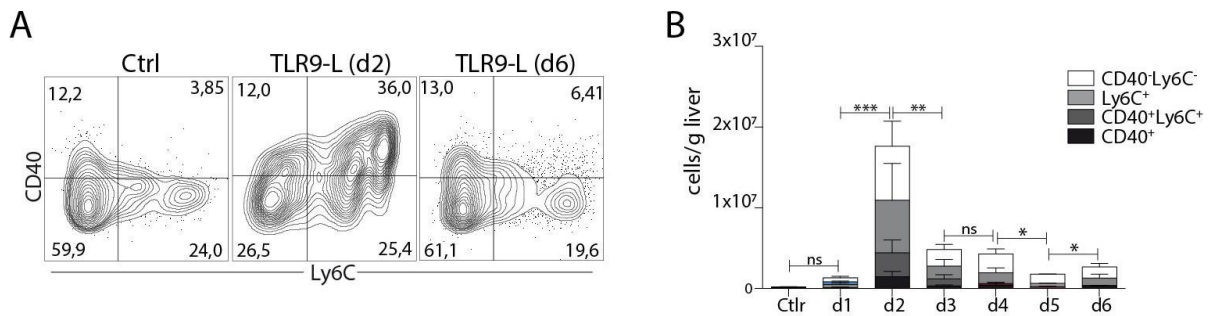


Figure 23: (A-B) Transient expression of CD40 on hepatic CD11b⁺Ly6C⁺ cells after TLR9-L application. (A) FACS analysis of the expression of CD40 and Ly6C on CD11b⁺ cells. Data are representative for n \geq 3 independent experiments (B) Quantification of (A). Pooled data from 3 independent experiments (n=4); Mann-Whitney t test. ***p < 0.001.

The data show, that CD40 expressing Ly6C⁺ myeloid cells only transiently appear after the application of TLR9L.

4.8.2 CD40 expression on Ly6C⁺ cells is only found in the liver

In the next step it was investigated whether the transient CD40 expression was also occurring in other organs. Myeloid cells of spleen and blood at steady state, two and six days after the application of TLR9-L were analyzed. Under steady state conditions, no CD40 expression was observed in blood or spleen. This did not change within the analyzed time course (Fig. 24). This indicates that the CD40 expression induced by TLR9-L application was liver specific.

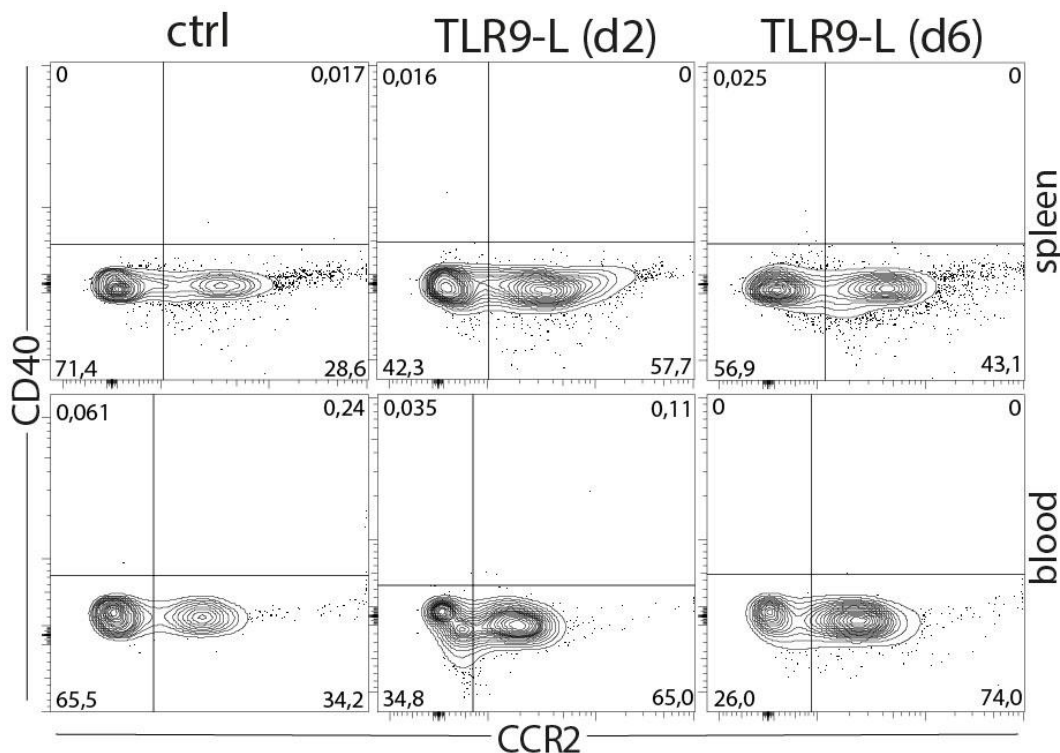


Figure 24: Expression of CD40 and Ly6C on CD11b⁺ cells in spleen and blood. Data are representative for n \geq 3 independent experiments.

The data show that the appearance of CD11b⁺Ly6C⁺CD40⁺ cells is restricted to the liver.

4.8.3 CD40 is the only TNF receptor that is significantly upregulated due to the application of TLR9-L

Signaling via TNF is causing the iMATE formation⁷⁴ and the CD40 as member of the TNF receptor superfamily appears transiently after application of TLR9-L. This coincidence raised the question whether other TNF receptors might also be involved in iMATE formation. To address this question, multicolor flow cytometry was applied to search for other TNFRs that might have been also affected by the application of TLR9-L. For the first explorative analysis untreated and mice 48 hours after the application of TLR9-L were used.

CD137 is the TNF receptor superfamily member 9. This receptor induces proliferation of peripheral monocytes, enhances T cell apoptosis, promotes Th1 cell response and contributes to clonal expansion, survival and development of T cells. Even though CD137 has been described to be especially expressed on T cells, expression on myeloid cells has also been confirmed²²⁶. The results showed that CD137 was not expressed on any of the analyzed cell populations (**Fig. 25**).

CD27 the Tumor Necrosis Factor Receptor Superfamily, Member 7 is exclusively expressed on B and T cells and required for generation and long-term maintenance of T cell immunity²²⁷. The results showed no CD27 expressed at all in CD11b⁺ cells in the liver at steady state or after the application of TLR9-L (**Fig. 25**).

CD30 the Tumor Necrosis Factor Receptor Superfamily, Member 8 is expressed by lymphocytes and highly expressed in thymus and spleen. It was described to direct cytokine secretion and production by T cells²²⁸. Whereas CD30 expression could not be detected after the application of TLR9-L, a substantial population of cells was expressing CD30 under steady state conditions (**Fig. 25**). This indicates that CD30 could be expressed on the Kupffer cells and therefore be involved in the primary TNF signaling events induced by the application of TLR9-L that disappear within the following 24 hours.

The TNF Receptor Superfamily Member 1A, also known as CD120a is found both membrane-bound and as a soluble form. It can interact with membrane bound and soluble TNF. This interaction has influence on cell survival, apoptosis and inflammation. The cross-linking of CD120a and b activates the mitogen-activated protein kinase (MAPK) cascade^{229–231}. This receptor could not be found on neither of the analyzed populations (**Fig. 25**).

The results showed that TNF signaling via specific TNF receptors is involved in the formation of iMATEs – CD30 in the beginning, then followed by CD40.

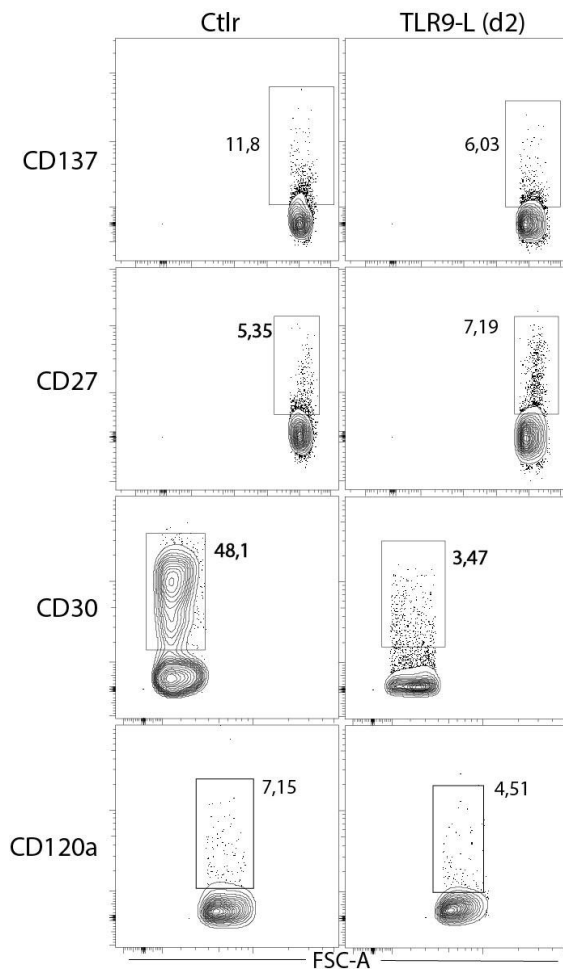


Figure 25: Expression of TNF receptors under steady state conditions and after the application of TLR9-L on CD11b⁺Ly6C⁺ cells. Data are representative for 3 independent experiments.

4.8.4 CD11b⁺Ly6C⁺CD40⁺ cells form a rather homogenous cell population

Previous in-depth phenotypical screening of hepatic myeloid cells by me and other groups²³² found that they separate into very diverse subpopulations. The transient appearance of the CD40 expression led to the hypothesis that the CD11b⁺Ly6C⁺CD40⁺ cells might form one group of myeloid cells with unique phenotypic properties. This hypothesis was characterized with multicolor flow cytometric analysis of CD11b⁺Ly6C⁺CD40⁺ cells.

Most of the CD11b⁺Ly6C⁺CD40⁺ cells were positive for CCR2 and CX₃CR₁. About half of the cells were expressing CX₃CR₁. The expression of MHCII was not very prominent and only found on around one fifth of the cells. The majority of them co-expressed Ly6A and F4/80 (**Fig. 26A**).

Out of the large number of additionally analyzed markers especially markers that are involved in co-stimulation (CD273, CD86), differentiation & cell growth (CD135), immunoregulation (CD68) and adhesion & migration (CD102, CD97) were found on CD11b⁺Ly6C⁺CD40⁺ cells and rendered them a rather homogenous cell population (**Fig. 26B**).

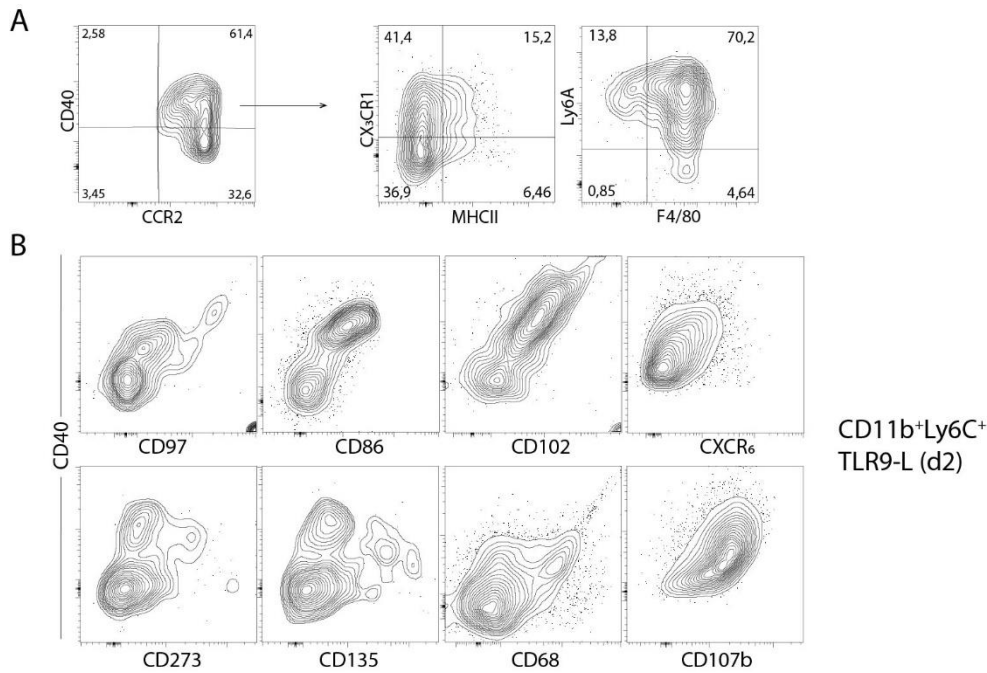


Figure 26: (A,B) FACS analysis of co-expressing markers on CD11b⁺Ly6C⁺ cells. (A) Phenotypic analysis of CD11b⁺Ly6C⁺CD40⁺CCR2⁺ cells. (B) Co-expression of different marker with CD40 on CD11b⁺Ly6C⁺ cells. Data are representative for n≥3 independent experiments.

The data illustrate a homogeneity in the group of CD11b⁺Ly6C⁺CD40⁺ cells that demarcates them from the very heterogenous group of the other immigrating myeloid cells.

4.8.5 CD11b⁺Ly6C⁺CD40⁺ cells are not found in the liver after the treatment with other TLR ligands

Even though it already had been described (4.3) that the ligands for TLR3 and 4 do not induce iMATE formation, it hadn't been analyzed so far whether they are able to induce CD40 expression. Therefore, mice were treated with TLR3 and 4 ligands as described above. The expression of CD40 on CD11b⁺Ly6C⁺ cells was analyzed with flow cytometry. Neither the ligand for TLR3 nor for TLR4 induced CD40 expression on Ly6C⁺CD11b⁺ cells in the liver (Fig. 27A,B). These results indicated that CD40 might be a suitable surrogate marker for iMATE-forming inflammatory myeloid cells.

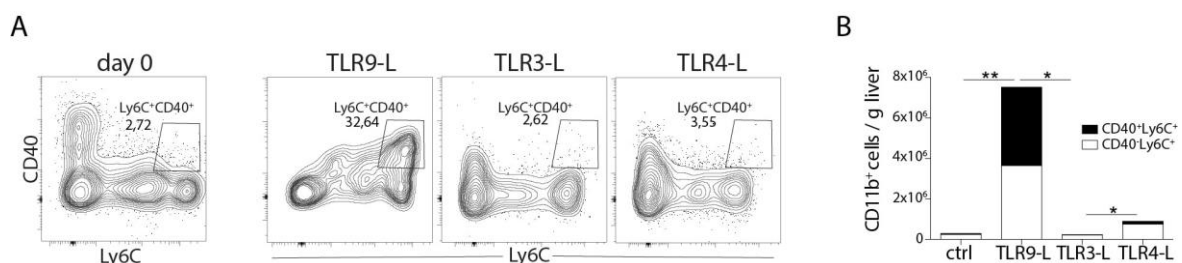


Figure 27: (A-B) CD40 expression after the application of different TLR-L. (A) FACS analysis of CD40 and Ly6C expression after the application of TLR ligands. Data are representative for n≥3 experiments. (B) Quantification of (A). Pooled data from 3 independent experiments (n=4); Mann-Whitney t test. ***p < 0.001.

The appearance of CD11b⁺Ly6C⁺CD40⁺ cells within the liver is restricted to the application of TLR9L.

4.8.6 No elevated expression of CD40L was detected in the liver after application of TLR9-L

The elevated expression of CD40 after TLR9L application coincides with several publications describing the essential role of CD40 in immunity^{200,233,234}. For this role the ligand of CD40 - CD154 – is needed. Consequently, the expression of CD40L was analyzed on several different cell types. No expression was detectable on CD11b⁺Cy6C⁺CD40^{neg} cells and only few CD11b⁺Ly6C⁺CD40⁺ monocytes did express CD154 (**Fig. 28A**), undermining the hypothesis of a self-amplifying cascade. No expression of CD40L was detectable on CD8⁺ or CD4⁺ T cells (**Fig. 28B**).

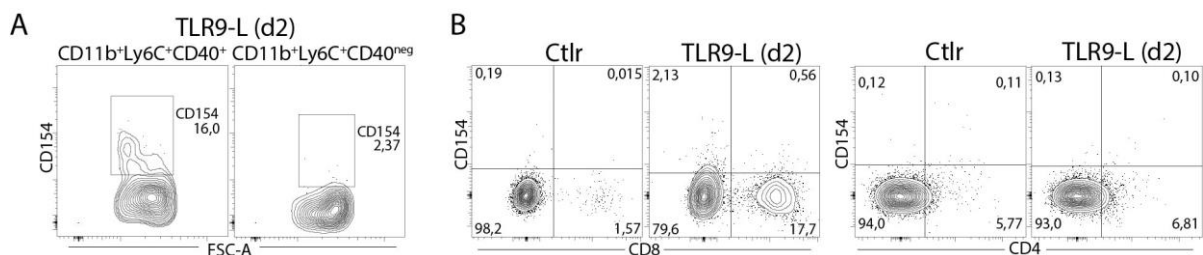


Figure 28: Expression of CD154 on hepatic myeloid (A) and T cells (B). Data are representative for n≥3 independent experiments.

No elevated levels of CD40L were detectable in the liver after the application of TLR9L indicating an alternative signaling mechanism for CD40.

4.8.7 CD11b⁺Ly6C⁺CD40⁺ cells have a specific cytokine expression profile

In order to determine the functionality of CD11b⁺Ly6C⁺CD40⁺ monocytes *ex vivo* FACSsorted hepatic CD11b⁺ cells were subjected to TLR9-L or TLR3-L stimulation followed by bead-array based detection of secreted cytokines. Clec4F⁺ Kupffer cells, CD11b⁺Ly6C⁺CD40^{neg} and CD11b⁺Ly6C⁺CD40⁺ monocytes showed different response patterns to TLR9-L and TLR3-L stimulation. The cellular response of Clec4F⁺ Kupffer induced by TLR9-L or TLR3-L stimulation was not as pronounced as the one of hepatic CD11b⁺Ly6C⁺ cells (**Figure 29**). Nevertheless, a more prominent secretion of Gro α and IL-6, and a weak IL-2 expression was detected. This is in line with their role in antigen-presentation to CD8 T cells²³⁵. No major differences between hepatic CD11b⁺Ly6C⁺CD40^{neg} compared to CD11b⁺Ly6C⁺CD40⁺ monocytes were detected. However, hepatic showed a pronounced expression of IL-6, TNF, M-CSF, type I IFN and IFN γ was detected in CD11b⁺Ly6C⁺CD40^{neg} monocytes. CD11b⁺Ly6C⁺CD40⁺ monocytes in contrary had higher levels of IL-22 and IL-15 (**Figure 29**). This illustrates functional differences between liver resident Clec4F⁺ Kupffer cells and CD11b⁺Ly6C⁺ monocytes recruited to the liver. Furthermore, CD11b⁺Ly6C⁺CD40⁺ cells may support the iMATE restricted T cell expansion rather by the expression of T cell stimulatory cytokines like IL-15 than by pro-inflammatory cytokines.

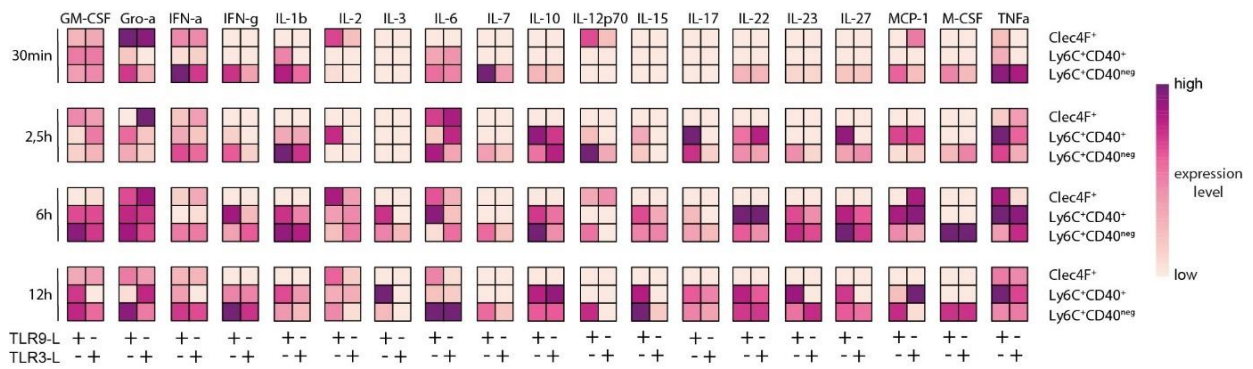


Figure 29: Cytokine expression profile of FACSsorted Clec4F+ Kupffer cells or hepatic Ly6C+CD40+ compared to Ly6C+CD40neg cells after TLR-L stimulation ex vivo. Data are pooled from 3 independent experiments.

The analysis of the bead array showed a distinct cytokine expression profile of CD11b+Ly6C+CD40+ cells that differed from the one of Kupffer cells.

4.8.8 CD40 expression is not necessary for iMATE formation and CD8+T cell expansion

The results gathered so far were strongly suggesting a potential role of CD40 expression on CD11b+Ly6C+ inflammatory cells as a biomarker for iMATE-forming myeloid cells. CD40+ cells were only detected in the liver, only after TLR9L application and the expression was transient as were the iMATEs. In order to analyze the role of CD40 expressing cells in iMATE formation and T cell expansion CD40^{-/-} and CD40L^{-/-} mice were used.

The influx of inflammatory CD11b+Ly6C+ cells after TLR9L was not significantly influenced in neither of the knockouts (**Fig. 30A**). The recruitment of CD11b+ cells after application of TLR9-L was not significantly affected in CD40L^{-/-} mice. This was confirmed by anti-CD11b histochemistry that did not show any impairment in the formation and structure of iMATEs (**Fig. 30B**). A significant difference in the recruitment was detected in the CD40^{-/-} mice, but the number of CD11b+ cells still reached high levels. Immunohistochemical analysis showed reduced iMATE formation and a less as densely packed structure. Nevertheless, the expansion of T cells was not impaired. In CD40L^{-/-} mice a significant difference in CD8 T cells expansion was detected but the T cells did expand even though not at such a high number. In both CD40^{-/-} and CD40L^{-/-} mice iMATE structures were detectable by anti-CD11b immunohistochemistry (**Fig. 30C**).

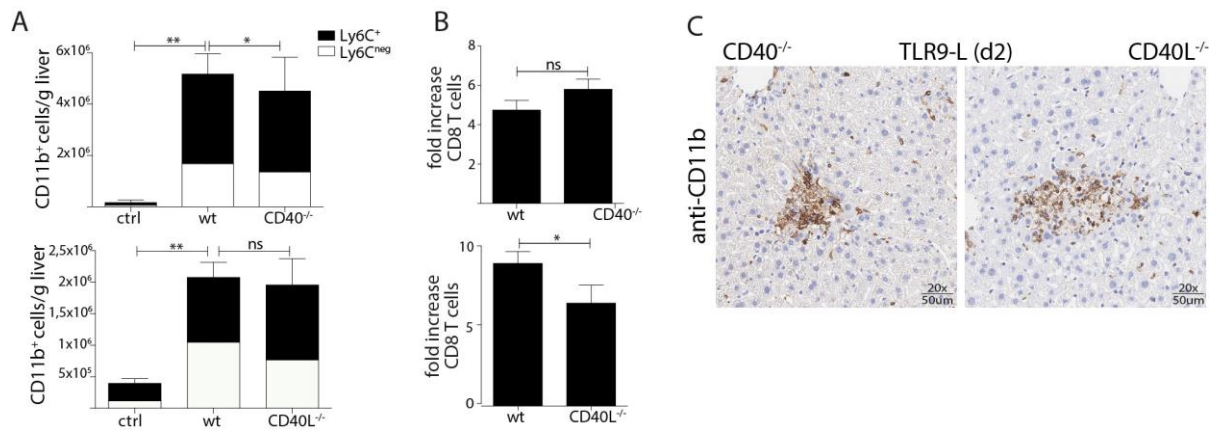


Figure 30: (A-C) Effect of TLR9-L on hepatic myeloid cells of CD40^{-/-} and CD40L^{-/-} mice. (A) Quantification of CD11b⁺ cells before and after TLR9-L application in CD40^{-/-} and CD40L^{-/-} mice. (B) Quantification of T cell expansion after the application of TLR9-L in CD40^{-/-} and CD40L^{-/-} mice. (A,B) Pooled data from 3 independent experiments (n=4); Mann-Whitney t test. *p < 0.001. (C) Anti-CD11b immunohistochemistry in CD40^{-/-} and CD40L^{-/-} mice. Data are representative for 3 independent experiments.**

These results indicate that CD40 was not a co-stimulatory molecule involved in T cell expansion. Furthermore, CD40 cannot be used as a bio- but a surrogate marker.

4.9 mRNA sequencing identifies a unique set of genes that is differentially expressed by CD11b⁺Ly6C⁺CD40⁺ cells

Notwithstanding that CD40 was not causally involved in T cell expansion after TLR9-L, CD40 expressing cells in the liver were still unique to the application of TLR9-L. Further characterization was performed in contrast to Kupffer cells and CD40^{neg} inflammatory monocytes. These cell populations were sorted and subjected to RNA-sequencing. The bioinformatic analysis was performed as outlined in Fig. 31.

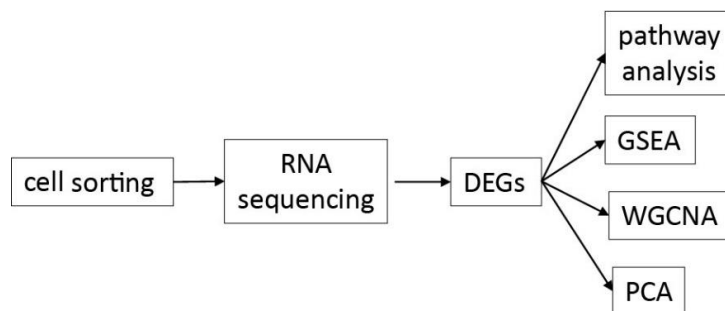


Figure 31: Workflow of bioinformatic analysis. (analysis was performed in collaboration with Sainitin Donakonda)

4.9.1 Comparing Ly6C⁺CD40⁺ myeloid cells to Clec4F⁺Kupffer cells identifies fundamental differences

The principal component analysis (PCA) that was used as a first overview, demonstrated that the 3 analyzed cell populations could be distinguished from each other (Fig.32A). Both CD11b⁺Clec4F⁺Ly6C^{neg} Kupffer cells and CD11b⁺Ly6C⁺CD40⁺ cells were clustering closely together, indicating rather homogenous populations. They were nicely separated from each other forming distinct populations. The CD11b⁺Ly6C⁺CD40^{neg} cells presented themselves as

widely separated demonstrating a rather heterologous composition that had been already reflected by the diversity of phenotypic characteristics analyzed before.

The analysis of the differentially expressed genes did confirm the difference between Kupffer cells and CD40 expressing cells that had been observed before (Fig.32A). At a p-value $\leq 0,01$ more than 3000 genes (> 0.66 -fold log2) were differentially expressed when comparing CD11b⁺Ly6C⁺CD40⁺ cells to Clec4F⁺ Kupffer cells (Fig. 32B). This result illustrated profound differences in the cellular profiles of these two groups. Further analysis was aiming to analyze these differences in detail.

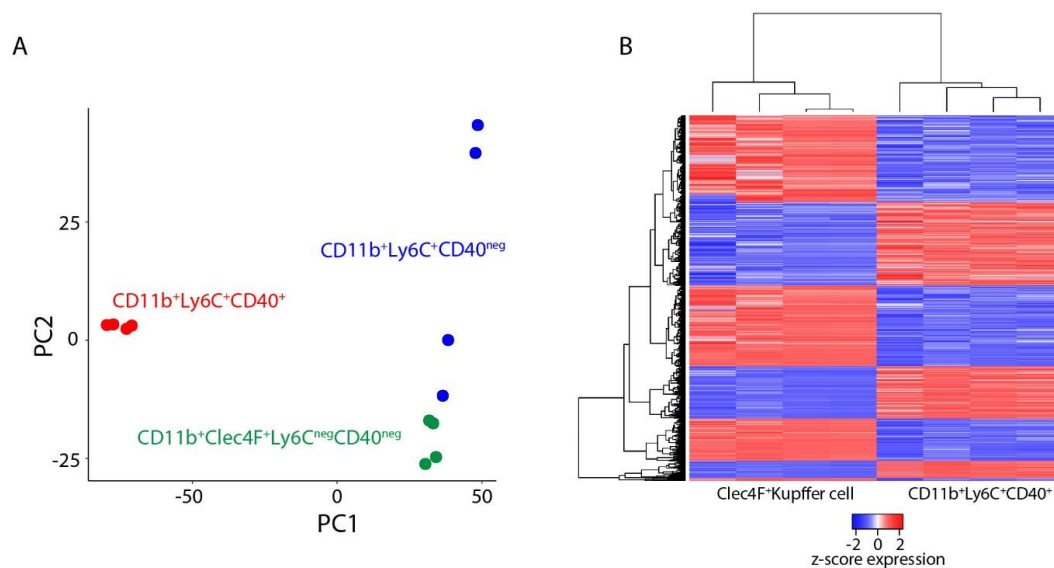


Figure 32: (A-B) Bioinformatic analysis of gene expression data of CD11b⁺Ly6C⁺CD40^{neg} and Clec4F⁺ Kupffer cells. (A) Principal component analysis (PCA) of hepatic myeloid cells after the application of TLR9-L. (B) Comparison of RNA sequencing data from FACSsorted hepatic CD11b⁺Ly6C⁺CD40⁺ cells two days after TLR9-L application with Clec4F⁺ Kupffer cells at steady state. Pooled data from 4 independent experiments. (analysis was performed in collaboration with Sainitin Donakonda)

Around one third (1407) of all differentially regulated genes when comparing CD11b⁺Ly6C⁺CD40⁺ cells to Clec4F⁺ Kupffer cells were upregulated (the complete list of sequencing experiments is found in suppl. Table 3). The list of the 20 most affected genes is displayed in suppl. Table 4. The processes those genes are involved in ranged from apoptosis (Bcl2l14) to cell proliferation (IL12 β). They could not be attributed to one specific function.

The peptide hormone secretin has mainly been investigated in the gastrointestinal system^{236,237}. F4/80 has been described to be homologous to the secretin receptor family²³⁸. Just recently the expression of secretin in the cholangiocytes and its role in hepatic fibrosis was investigated²³⁹. S Afroze et al.²⁴⁰ describe it as a neuroendocrine hormone with pleiotropic effects on several organ systems. Until today the expression of secretin by members of the myeloid system has not been described. Therefore, it could only be hypothesized which role secretin might play in iMATE formation and T cell expansion. One possible direction was given by K.Sato et al. who described the role of secretin in the inflammatory cell-cell communication of cells treated with LPS²⁴¹.

The apoptosis regulator *Bcl-G* is a pro-apoptotic intracellular protein that has been identified just a couple of years ago²⁴². Even though recent research by M Giam et al.²⁴³ suggested that *Bcl-G* is rather involved in protein trafficking inside the cell instead of functioning in the classical stress-induced apoptosis pathway, there are a few factors that strongly support the pro-apoptotic functionality. Not only could I detect an up-regulation of the ubiquitin-like protein MNSF β that covalently binds to intracellular *Bcl-G*²⁴⁴, but additionally I saw an up-regulation of *Ptgs2os2*. This gene is downregulating *Cox-2* in macrophages. The down-regulation of *Cox-2* in macrophages has been described as enhancer of the pro-apoptotic effect of the MNSF β -*Bcl-G* interaction²⁴⁵. With this pro-apoptotic effect *Bcl-G* is a potential driver of the iMATE degradation that started between day 2 and 3 after the application of TLR9L.

Around two thirds (2056) of all differentially regulated genes were downregulated. The list of the 20 most affected genes is displayed in suppl. Table 5. Most of those genes are involved in differentiation and proliferation processes of cells. This could indicate that most of the CD11b⁺Ly6C⁺CD40⁺ cells are fully differentiated. This assumption is in line with the rapid disappearance of the CD11b⁺Ly6C⁺CD40⁺ cells that starts between day 2 and 3 after TLR9L application. The genes downregulated in CD11b⁺Ly6C⁺CD40⁺ cells are upregulated in Clec4F⁺Kupffer cells. None of those genes stood out.

Apart from the genes that were strongly up- or downregulated, several further genes did sharpen the genetic profile of the CD11b⁺Ly6C⁺CD40⁺ cells. The list of chemokines upregulated in CD11b⁺Ly6C⁺CD40⁺ cells (**suppl. Table 6**) was headed by *Ccl12*. *Ccl12*, the monocyte chemotactic protein 5 (MCP-5), is a chemokine that attracts eosinophils, monocytes and lymphocytes in this case to the liver. Even though MCP-5 is predominantly found in lymph nodes and the thymus, its expression can strongly be induced in macrophages^{246,247}. The data indicate that *Ccl12* is the main driver of monocyte recruitment to the liver after TLR9-L application. Same as *Ccl12*, *Ccl5* is also involved in chemotaxis as a potent chemoattractant for immune cells²⁴⁸. Its receptors CCR5 and CCR1 are upregulated on the CD11b⁺Ly6C⁺CD40⁺ cells indicating that *Ccl5* cooperates with *Ccl12* in recruiting. Furthermore, *Ccl5* is also a potent T-cell recruiter²⁴⁸ and might be involved in the T cell expansion within iMATEs. The list of chemokine receptors was led by CCR7 and CCR2. The more important receptor, not only due to its lower p-value, was CCR2. The expression of this receptor had been verified prior by FACS analysis. As well as CCR5, CCR2 directs leukocytes to sites of inflammation, forming the primary chemokine axis for recruitment of monocytes and macrophages together with its ligand *Ccl2*²⁴⁹. *Cxcl12* and *13* are the most prominent downregulated chemokine genes. The binding of *Cxcl12* to its receptor *Cxcr4* initiates signals that are related to cell survival and/or proliferation and gene transcription²⁵⁰ which might be involved in the self-renewing program of Kupffer cells. *Cxcl13* is known as a B-lymphocyte chemoattractant. It supports the co-migration of T cells and T_H cells into B follicles²⁵¹. These results confirmed the hypothesis, that the strong increase in numbers of CD11b⁺Ly6C⁺ cells detected two days after the application of TLR9-L was due to the recruitment from the circulation.

The list of differentially regulated surface markers when comparing CD11b⁺Ly6C⁺CD40⁺ cells to Clec4F⁺Kupffer cells includes mainly co-stimulatory and activating molecules (**suppl. Table 7**). Some are involved in adhesion processes and antigen scavenging as well as presentation. The leader of the list the lymphocyte antigen 75 (*Ly75*) is a scavenging receptor for CpG the ligand for TLR9²⁵². Another gene that is directly regulated by TLR9-L signaling is *Tarm1*, an activating receptor on myeloid cells that enhances TLR-mediated signaling²⁵³. *CD53* and *CD52* gene upregulation was highly significant. The role of CD52 is unknown so far whereas CD53 is a member of the transmembrane 4 superfamily and transduces signals that are involved in development, activation and motility²⁵⁴. A marker of great interest was CD134 (OX40; TNFRSF4) that had already been described as a molecule of great importance for the CTL population expansion in iMATEs⁷⁴. *CD134* was significantly upregulated compared to Kupffer cells. The list of surface markers that were downregulated in CD11b⁺Ly6C⁺CD40⁺ cells and therefore upregulated in Clec4F⁺Kupffer cells consisted mainly of molecules involved in adhesion, scavenging and apoptosis inhibition. The strong downregulation of *Clec4F* and *Vsig4* further confirmed that CD11b⁺Ly6C⁺CD40⁺ cells did not arise from Clec4F⁺Kupffer cells.

TLR9-L application also affected interleukins and their receptors (**suppl. Table 8**). Most of the upregulated cytokine genes had pro-inflammatory or co-stimulatory functions for T cells. Especially *Il12b* acts as a growth factor for T cells. The cytokines that are upregulated in the Clec4F⁺Kupffer cells are rather involved in proliferation or survival as well as the induction of a T_H2 immune response.

It was hypothesized that a strong expression of different adhesion molecules might be the reason why iMATE-forming cells cluster together. The data for differentially expressed genes could not confirm this hypothesis. Most of the molecules involved in intercellular adhesion could not be found in CD11b⁺Ly6C⁺CD40⁺ cells. Especially not the signature adhesion molecules of the liver: *siglec-9* and *10*, *VAP-1*, *VLA4*, *VCAM-1*²⁵⁵. The ones found were mostly downregulated. Nevertheless, the first molecule found in the list, glycoprotein VI, is highly upregulated. GPVI has been described as a platelet collagen receptor, the central receptor for platelet-collagen interaction. GPVI couples to FcR γ and induces intracellular signaling molecules²⁵⁶. GPVI expression on myeloid cells hasn't been described so far. It could be possible that platelets have been sticking to the cells during the sorting process, but this would have happened to the Kupffer cells as well and they are even bigger. On the other hand, GPVI could be involved in the coherence of the iMATEs, as several FcR γ chains are also upregulated. Most of the other upregulated adhesion molecules belong to the family of integrins. These molecules are important for the trans-endothelial migration. They often work in concert with each other. ItgaX for example combines with Itgb2 and the so formed receptor is not only involved in adhesion but also phagocytosis of complement-coated particles. Itgb2 can also combine with ItgaL to form the lymphocyte function-associated antigen 1 (LFA-1). The combination with ItgaM forms the macrophage-1 antigen (Mac-1), a complement receptor. These data cannot explain the clustering of the iMATE-forming cells but support the hypothesis that most of them are recruited from the circulation.

The analysis of the differentially expressed genes comparing CD11b⁺Ly6C⁺CD40⁺ cells to Clef4F⁺ Kupffer cells demonstrated significant differences within their expression profiles that could not be dedicated to one specific function or signaling but are more complex.

4.9.2 Data generated by RNA sequencing are partially found in the gene array

The results of the RNA sequencing analysis were compared to the results of the gene microarray at day 2 in order to detect any similarities. Even though the starting setup was a little bit different both times a transcriptome profiling was performed and the correlation between gene expression profiles that have been generated by either of this platforms has been described as high²⁵⁷. With the microarray whole iMATEs were analyzed, including lymphocytes and other hepatic cells as well. The RNA sequencing was focused on the CD11b⁺Ly6C⁺CD40⁺ cells. Comparing the results of these two analyses was supposed to give an idea whether CD11b⁺Ly6C⁺CD40⁺ cells could be located within the iMATEs. About one fifth of the genes from the microarray were also found to differentially regulated in the RNA seq data. Giving the fact that the microarray included all cells that are found within an iMATE it can be concluded that CD11b⁺Ly6C⁺CD40^{neg} cells are located within the iMATE structure.

In more detail about 70% of the top 20 most affected genes that were detected in the analysis of the microarray data were also found in the data of the RNA seq analysis (**Table 1**).

Symbol	logFC	adj.P.Val	RNA Seq
Pyhin1	4.0	6.0 ⁻⁰⁹	-
Ms4a6d	3.9	6.0 ⁻⁰⁹	x
Vim	3.9	4.9 ⁻⁰⁹	x
Rsad2	3.6	3.3 ⁻¹¹	x
Cd40	3.4	1.0 ⁻⁰⁹	x
Gsn	3.3	6.4 ⁻⁰⁹	x
Ifit1bl1	3.3	6.0 ⁻⁰⁹	x
Slamf7	3.2	6.4 ⁻⁰⁹	x
S100a4	2.8	1.7 ⁻¹¹	x
Fxyd5	2.7	4.1 ⁻¹⁰	x
Upp1	2.6	4.9 ⁻⁰⁹	x
Slc2a6	2.6	2.3 ⁻⁰⁹	x
AA467197	2.1	3.3 ⁻¹⁰	-
Ptpro	1.7	1.3 ⁻⁰⁸	x
Mxd1	1.2	1.3 ⁻⁰⁸	x
Ccnd2	0.7	2.9 ⁻⁰⁹	-
Tst	-1.7	1.3 ⁻⁰⁸	-
Gpd1	-2.3	3.0 ⁻⁰⁹	-
Retsat	-2.9	1.3 ⁻⁰⁸	x
Serpina6	-3.4	1.3 ⁻⁰⁹	-

Table 1: The 20 most affected genes of the microarray at day 2; data were compared to the differentially expressed genes comparing CD11b⁺Ly6C⁺CD40⁺ cells at day 2 with Clec4F⁺ KCs. (analysis was performed in collaboration with Sainitin Donakonda)

The gene microarray was also performed for samples isolated at day 3, 4 and 5 after TLR9-L application. Data from day 3, 4 and 5 were additionally included in order to monitor, which genes stay up- or downregulated over a longer period of time. Around 60% of the 20 most strongly affected genes at day 3 after TLR9L application, all of them downregulated, were also detected as downregulated in the in the RNA seq analysis (**suppl. Table: 9**). The microarray data of the iMATEs was compared to the microarray data of iMATE-free liver tissue. So, it was even more surprising that many genes were found in both analyses, indicating a strong regulation that was restricted to the CD11b⁺Ly6C⁺CD40⁺cells. The number of genes downregulated in both analyses started to decline at day 4 (**suppl. Table 10**). At day 5 after the application of TLR9-L still half a dozen genes were differentially regulated in both data sets. At day 5 CD11b⁺Ly6C⁺CD40⁺cells are no longer present in the hepatic tissue indicating that those genes are also differentially regulated in CD11b⁺Ly6C⁺CD40^{neg} cells (**suppl. Table 11**).

These data indicated that the cells sorted from liver tissue are also present in iMATEs as they display a comparable gene expression profile as the iMATE cells isolated by laser capture microdissection.

4.9.3 Pathway and gene set enrichment analysis illustrated the pro-inflammatory nature of CD11b⁺Ly6C⁺CD40⁺cells

The data so far showed that CD11b⁺Ly6C⁺CD40⁺cells have a specific gene expression profile. Further analyses were supposed to elucidate where those genes are involved in. Therefore, the differentially expressed genes in CD11b⁺Ly6C⁺CD40⁺cells were submitted to KEGG pathway analysis. This analysis is used to analyze high-level functions and utilities of the biological system. The pathways that were detected include inflammatory responses, cytokine signaling and T cell activation (**Fig. 33A**). Additionally, gene set enrichment analysis verified the cytokine signaling profile (**Fig. 33B**). This analysis was used to look for the cytokines that were affected by the upregulation of genes involved in regulation of cytokine production. A result found earlier in the KEGG pathway analysis. The expression of type I interferons is significantly

enriched. These data support the hypothesis that CD11b⁺Ly6C⁺CD40⁺ cells play a major role in iMATE formation and induction of T cell activation and expansion.

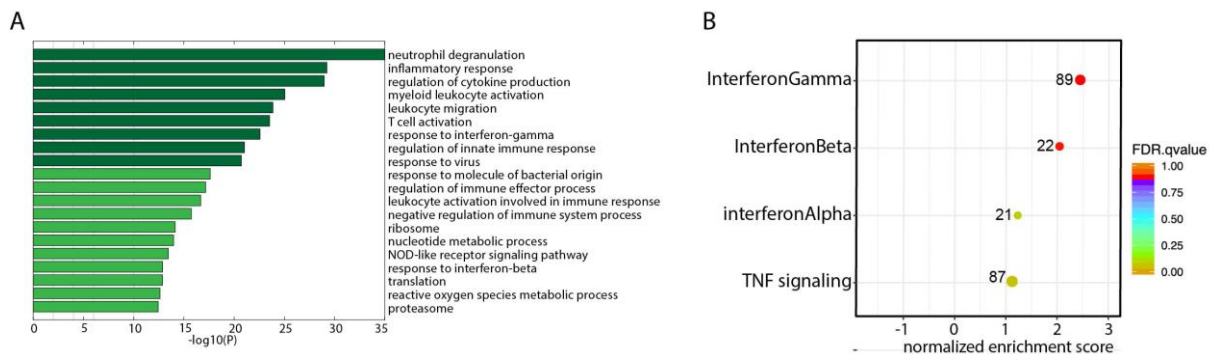


Figure 33: (A,B) Additional analysis of gene expression data of CD11b⁺Ly6C⁺CD40⁺ cells compared to Clec4F⁺Kupffer cells.

(A) KEGG pathway analysis of genes differentially expressed in CD11b⁺Ly6C⁺CD40⁺ cells compared to Clec4F⁺ Kupffer cells. (B) Gene set enrichment for genes involved in cytokine signaling. (analysis was performed in collaboration with Sainitin Donakonda)

The performed pathway analysis followed by gene set enrichment attributed strong inflammatory and stimulatory properties to the CD11b⁺Ly6C⁺CD40⁺ cells.

4.9.4 Transcription factor analysis detects an IRF8 core signature

The RNA sequencing showed that many genes in CD11b⁺Ly6C⁺CD40⁺ cells are differentially regulated in comparison to Clec4F⁺ cells. The regulation of gene expression is performed by transcription factors. Therefore, the identification of the transcription factors that induced the changes was important to understand the regulatory network that had been affected by TLR9L. Transcription factor analysis without significance cut-off resulted in many transcription factors that either regulate CD11b⁺ Ly6C⁺CD40⁺ cells or are regulated by them. This numbers were reduced when tested for their significance (Table 2).

	No. of differentially regulated TFs	No. of significantly (p-value ≤ 0,01) up- regulated TFs	No. of significantly (p-value ≤ 0,01) down-regulated TFs
TFs regulating CD11b ⁺ Ly6C ⁺ CD40 ⁺ cells	567	50	44
TFs regulated by CD11b ⁺ Ly6C ⁺ CD40 ⁺ cells	174	38	60

Table 2: Differentially regulated transcription factors (TF) expressed in in CD11b⁺Ly6C⁺CD40⁺ cells compared to Clec4F⁺ Kupffer cells. (analysis was performed in collaboration with Sainitin Donakonda)

The analysis suggested that interferon-regulating factor 8 (IRF8) was one of the main drivers of gene expression in Ly6C⁺ monocytes (**Fig. 34A**). A gene set enrichment analysis confirmed the IRF8 core signature of CD11b⁺Ly6C⁺CD40⁺ cells (**Fig. 34B**).

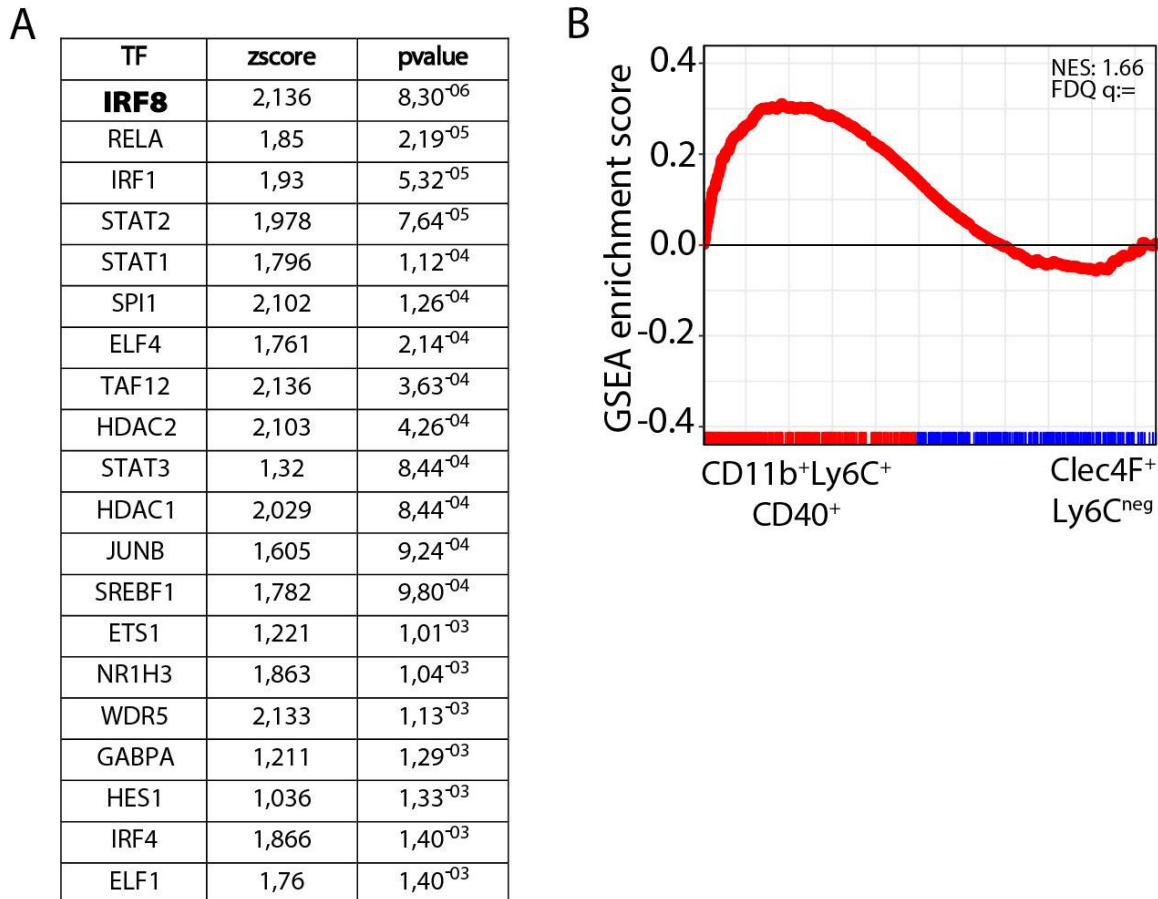


Figure 34: (A-B) Transcription factor analysis of data from CD11b⁺Ly6C⁺CD40⁺ cells compared to Clec4F⁺Kupffer cells.

(A) Transcription factors (TF) involved in the differentiation of CD11b⁺Ly6C⁺CD40⁺ cells (z-score: number of target genes). **(B)** Gene set enrichment analysis for IRF8 signaling. (analysis was performed in collaboration with Sainitin Donakonda)

Noticeably IRF8 was also detected in the list of transcription factors that were up- or downregulated (**suppl. Table 12**) due to the BatF3-dependant autoactivation²⁵⁸. The number one of the list C/EBP β is a transcription factor involved in immune and inflammatory responses. It is activated in response to IFN γ ²⁵⁹ and can act as a nuclear factor for IL-6²⁶⁰, a cytokine whose expression was also upregulated.

The IRF8 target signature (**suppl. Table 13**) included many of the genes that are highly upregulated in CD11b⁺Ly6C⁺CD40⁺ cells, indicating that IRF8 might be one of the main drivers in the polarization and differentiation process. Most importantly CD40 expression is regulated by IRF8. The other genes include the Bcl family that can be either pro- or antiapoptotic²⁴³, the Slc family who is involved mainly involved in the glucose transport²⁶¹, several transcription factors

(SpiB, IRF5, IRF7) and surface molecules involved in intercellular communication (XCR1, CD274, CD69, CD52, CD74).

These data indicate an important role of IRF8 during iMATE formation and for its functionality.

4.9.5 An elevated glycolytic capacity in CD11b⁺Ly6C⁺CD40⁺ cells is detected by weighted gene correlation analysis (WGCNA)

Weighted gene correlation analysis was performed to further refine the profile of CD11b⁺Ly6C⁺CD40⁺ cells. It is a data mining method that allows studying biological networks and detecting their correlation patterns. Genes do not work alone but interact with each other in networks. Identifying specific networks allows to predict functions and detect the genes with key roles in the respective network¹⁴⁸. WGCNA not only detects the networks but assigns them to modules highlighting the respective central genes – hub genes. This allows a detailed characterization of the cells. The analysis identified 4 different modules within the differentially expressed genes. Two modules (one and two) represented genes that were upregulated, the other two (three and four) genes that were downregulated. Most of the upregulated genes were clustered in module one (Fig. 35A,B). Most of the downregulated genes were clustered in module 3. Their difference was pronounced with a low standard deviation. This was different in module 2 and 4. Both displayed a high standard deviation probably due to the low number of included genes. Gene ontology analysis of the modules one and two identified cytokine signaling and metabolic pathways. Module three and four are involved in the lipoprotein metabolism and mitotic cell cycle (Fig. 35C).

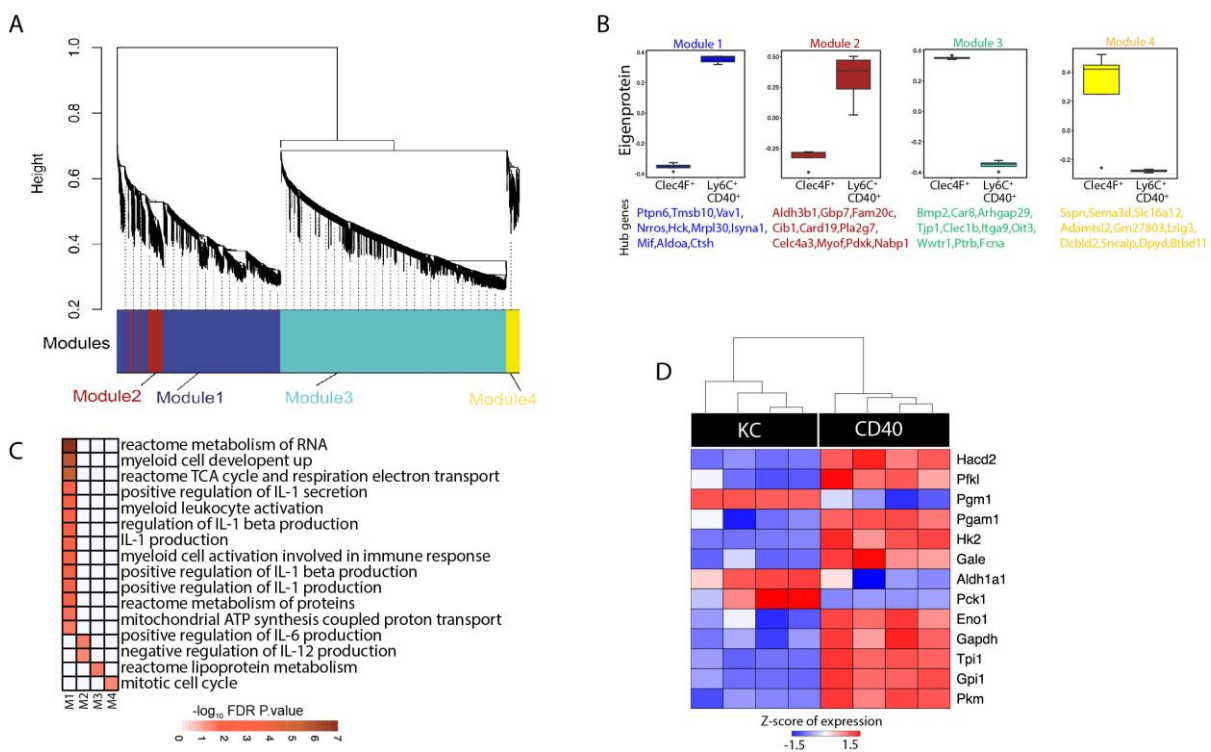


Figure 35: (A-D) Gene co-regulation analysis of genes differentially expressed in CD11b⁺Ly6C⁺CD40⁺ cells compared to Clec4F⁺ Kupffer cells.

(A) Dendrogram of the module clustering. (B) Eigenprotein analysis within the 4 modules and identification of the main hub genes for the individual modules. (C) Gene ontology analysis of four modules of differentially expressed genes in Clec4F⁺Kupffer cells compared to CD11b⁺Ly6C⁺CD40⁺ cells that were identified by WGCNA. (D) Differential expression of genes involved in glycolysis in Clec4F⁺Kupffer cells compared to CD11b⁺Ly6C⁺CD40⁺ cells. (analysis was performed in collaboration with Sainitin Donakonda)

The results of the WGCNA initiated the screening for genes that are involved in metabolic pathways. The most prominent finding was the upregulation of most of the genes that are involved in glycolysis. Among those were also glycolysis rate-limiting enzymes like *hexokinase* and *phosphofructokinase* (Fig. 35D). In addition, the upregulation of IKKε, a serine/threonine kinase that has recently been described to be essential for the increase of glycolysis induced by TLR²⁶² was detected. Many Glucose transporters were also found to be differentially regulated but the ratio of up- and downregulation was balanced (suppl. Table 14).

Taken together the results confirmed the proinflammatory potential of CD11b⁺Ly6C⁺CD40⁺ cells and the anti-inflammatory functions of Clec4F⁺ cells. The cells were substantially different from each other contradicting the hypothesis that Kupffer cells might have re-differentiated and integrated into the pool of iMATE-forming cells.

4.9.6 The strong differences in gene expression cannot be found when compared to other cell types.

The profound differences found when comparing CD11b⁺Ly6C⁺CD40⁺ to Clec4F⁺ Kupffer cells could not be detected when comparing CD11b⁺Ly6C⁺CD40⁺ to CD11b⁺Ly6C⁺CD40^{neg} cells and Clec4F⁺ Kupffer cells to CD11b⁺Ly6C⁺CD40^{neg} cells (Table 3). At a p-value ≤ 0,01 only 299 genes were differentially expressed in the first comparison and with 13 genes in the second one even less. These striking differences in the number of differentially expressed genes can be explained by the heterologous nature of the CD11b⁺Ly6C⁺CD40^{neg} cells that is already displayed in the PCA and the very strict cut of at a p- value of ≤ 0,01 used for bioinformatic analysis.

	differentially expressed genes p≤0,01	up-regulated genes	down-regulated genes
Ly6C ⁺ CD40 ⁺ vs Clec4F ⁺ Ly6C ^{neg}	3463	1407	2056
Ly6C ⁺ CD40 ⁺ vs Ly6C ⁺ CD40 ^{neg}	299	129	170
Ly6C ⁺ CD40 ^{neg} vs Clec4F ⁺ Ly6C ^{neg}	13	13	0

Table 3: Number of differentially expressed genes in the different combinations.

Despite the low number of differentially regulated genes when comparing CD11b⁺Ly6C⁺CD40⁺ to CD11b⁺Ly6C⁺CD40^{neg} cells, there is still a reasonable number of gene that are specific for either population (suppl. Table) and genes that differentiate CD11b⁺Ly6C⁺CD40⁺ cells from both CD11b⁺Ly6C⁺CD40^{neg} and Clec4F⁺ Kupffer cells (Table 4).

Genes	log2FC	padj
<i>Ii12b</i>	4,90636001	6,43224 ⁻²⁰
<i>Ccl8</i>	3,38793891	3,01505 ⁻⁰³
<i>Xcr1</i>	3,37718302	6,97532 ⁻⁰⁴
<i>Ii4i1</i>	3,21746021	3,89354 ⁻⁰³
<i>Ccl12</i>	2,50936528	2,01E ⁻⁰⁶
<i>Vcam1</i>	1,98390113	2,88564 ⁻⁰³
<i>Nos2</i>	1,95589505	1,0795 ⁻⁰⁴
<i>Cd86</i>	1,68474352	2,43E ⁻¹⁰
<i>Cd63</i>	1,61803695	8,8835 ⁻⁰⁴
<i>Spic</i>	1,42292155	4,8917 ⁻⁰⁴
<i>Cd74</i>	1,42156348	2,85293 ⁻⁰³
<i>Batf3</i>	1,21551006	1,26E ⁻⁰⁵
<i>Ly6i</i>	1,12984549	3,56805 ⁻⁰³
<i>Ly6a</i>	1,10635665	4,4699 ⁻⁰⁴
<i>Irf7</i>	1,05456283	6,25481 ⁻⁰³

Table 4: Genes specific for CD11b⁺Ly6C⁺CD40⁺ cells – upregulated in the analysis against Clec4F⁺ Kupffer cells and CD11b⁺Ly6C⁺CD40^{neg} cells.

The small differences in gene expression between Clec4F⁺ Kupffer cells and CD11b⁺Ly6C⁺CD40^{neg} cells are on the one hand due to high cut off p-value of $\leq 0,01$. The elevation to a p-value of $\leq 0,05$ resulted in 14134 significantly regulated genes. On the other hand, the Clec4F⁺ Kupffer cells are also a more heterogenous population, which was already displayed in the PCA (Fig. 33).

The gene array analysis illustrated a unique transcriptomic profile that shapes the pro-immunogenic metabolic phenotype of the CD11b⁺Ly6C⁺CD40⁺ cells. This profile is especially pronounced when compared to Clec4F⁺ Kupffer cells whereas the differences towards other CD11b⁺Ly6C⁺ cells are not as prominent.

4.10 CD11b⁺Ly6C⁺CD40⁺ cells display a glycolytic phenotype and an increased capacity to induce CD8⁺T cell proliferation

Following up on the results from the RNA sequencing, several assays to analyze the metabolic and functional properties of the CD11b⁺Ly6C⁺CD40⁺ cells were performed. Clec4F⁺ cells and CD11b⁺Ly6C⁺CD40^{neg} cells were used for comparison.

The fluorescent glucose-analog 2-deoxy-2-[(7-nitro-2,1,3-benzoxadiazol-4-yl) amino]-D-glucose (2-NBDG) was used to measure the glucose uptake at the level of individual cells. 2-NBDG is taken up by glucose transporters but cannot be fully utilized for glycolysis and thus accumulates within cells. The fluorescence generated by 2-NBDG can then be measured in a quantitative fashion²⁶³. The uptake of 2-NBDG was significantly elevated in

CD11b⁺Ly6C⁺CD40⁺ cells compared to Clec4F⁺ cells and CD11b⁺Ly6C⁺CD40^{neg} cells (Fig. 36A,B). This suggested that CD40⁺ cells should display more glycolytic activity. We therefore FACSsorted CD11b⁺Ly6C⁺CD40⁺, CD11b⁺Ly6C⁺CD40^{neg} and Clec4F⁺ Kupffer cells and subjected them to metabolic analysis employing the Seahorse XF analyzer platform. This platform measures the oxygen consumption (OCR) and extracellular acidification rate (ECAR) of live cells thereby providing information about the mitochondrial respiration and glycolysis. This allows evaluation key aspects of cellular metabolism. The results obtained show that CD11b⁺Ly6C⁺CD40⁺ cells had by far the highest glycolytic capacity. Addition of glucose to these cells led to rapid acidification of the medium, which was dependent on glycolysis because addition of 2-deoxyglucose (which serves as inhibitor of hexokinase) stopped acidification (Fig. 36C). Importantly, CD11b⁺Ly6C⁺CD40^{neg} cells showed a weaker glycolysis and Clec4F⁺ Kupffer cells had almost no measurable glycolytic capacity (Fig. 36C), which is consistent with their lack of glucose uptake shown in (A).

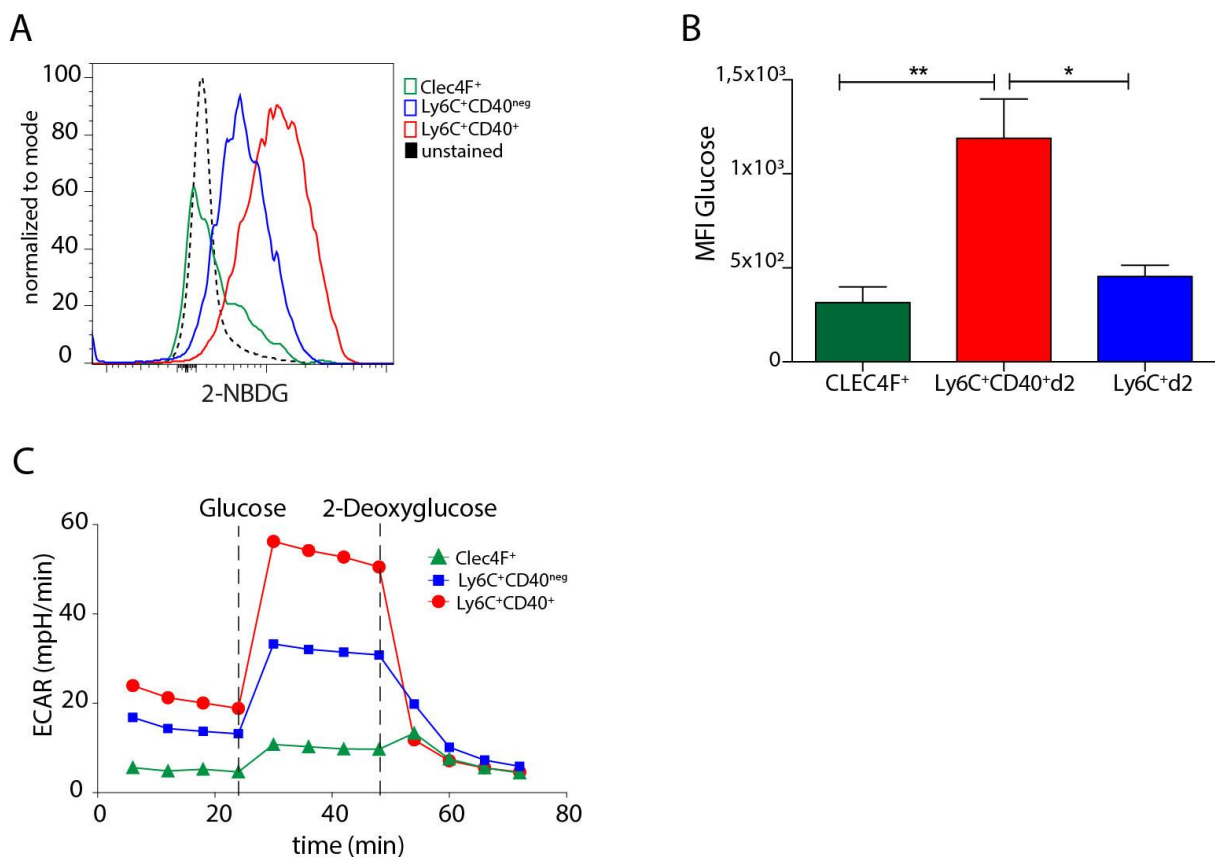


Figure 36: (A-C) CD11b⁺Ly6C⁺CD40⁺ cells have a higher glycolytic capacity than Kupffer cells or CD11b⁺Ly6C⁺CD40^{neg} cells.

(A,B) 2-NBDG (glucose) uptake by hepatic CD11b⁺ cell populations determined by flow cytometry, and quantification (B); representative results from ≥ 5 experiments. (C) Glucose stress test FACSsorted Clec4F⁺ Kupffer cells compared to hepatic CD11b⁺Ly6C⁺CD40⁺ cells or CD11b⁺Ly6C⁺CD40^{neg} cells. (A-C) Pooled data from 3 independent experiments (n=4); Mann-Whitney t test. ***p < 0.001.

In order to use glucose in glycolytic processes glucose needs to enter the cells. There was no upregulation in glucose transporter expression detectable in the RNA sequencing (suppl. Table

14). This indicates that CD11b⁺Ly6C⁺CD40^{neg} cells have a glucose transport mechanism that hasn't been described so far or that their uptake is more efficient.

In the next step the cellular respiration was analyzed by measuring the mitochondrial membrane potential with the MitoProbe DiIC₁(5), a cationic cyanine dye that accumulates in the cells depending on the respective membrane potential. No significant differences between the three analyzed groups were detectable. Nevertheless, the heterogeneous composition of the CD11b⁺Ly6C⁺CD40^{neg} cells was illustrated again, as their peak was really broad spanning several log steps (Fig. 37A,B). In addition to the membrane potential the mitochondrial mass was assessed. No significant differences were detected either (Fig. 37C).

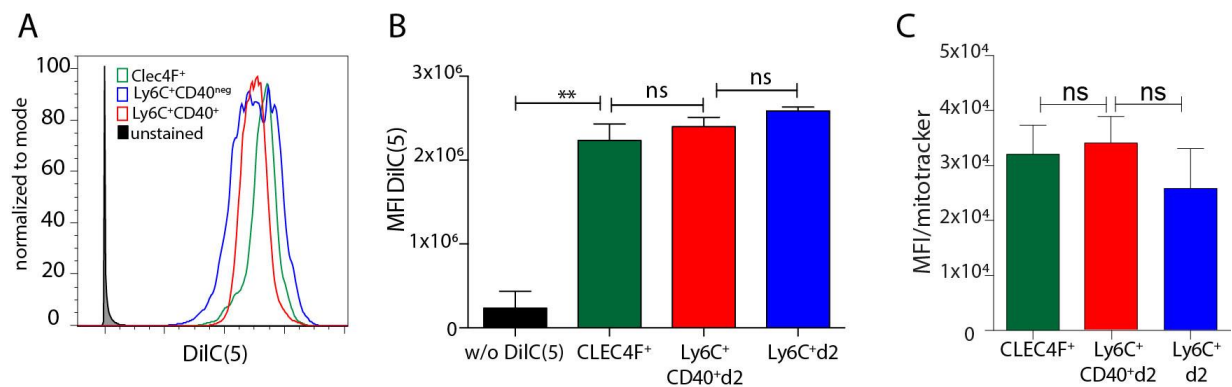


Figure 37: (A-C) Mitochondrial respiration is not elevated in CD11b⁺Ly6C⁺CD40⁺ cells.

(A,B) Mitochondrial membrane potential in different hepatic CD11b⁺ cell populations isolated at steady state (Clec4F⁺ Kupffer cells) or d2 after TLR9-L application determined by fluorescence activity of the potentiometric DiIC(5) dye measured by flow cytometry, and quantification of fluorescence intensity (B); (C) Mitochondrial mass in different hepatic CD11b⁺ cells measured by flow cytometry with Mitotracker-Green. (A-C) Pooled data from 3 independent experiments (n=4); Mann-Whitney t test. ***p < 0.001.

Huang et al. (2013)⁷⁴ described the proliferation of T cells in the liver outside of lymph nodes. The expansion of T cells is restricted to iMATEs and did not require antigen-presentation but was further increased if T cells recognized their specific antigen. CD11b⁺Ly6C⁺CD40⁺ cells appeared rapidly after TLR9-L application and led me to investigate whether these cells were involved in T cell proliferation.

An elevated glycolytic potential has been linked to an increased capability of dendritic cells to activate T cells²⁶⁴ via both TCR and co-stimulatory signaling. Co-stimulatory receptors on T cells like CD28 bind to co-stimulatory molecules on myeloid cells like CD86. Importantly, I found that CD11b⁺Ly6C⁺CD40⁺ cells had increased of CD86 and other co-stimulatory molecules like CD68 and Tim4 compared to CD11b⁺Ly6C⁺CD40^{neg} cells and Clec4F⁺Kupffer cells (Fig. 38). This was shown with FACS analysis and partially in the RNA seq data. It indicated that CD11b⁺Ly6C⁺CD40⁺ cells might provide an immune-metabolic stimulus to CD8 T cells.

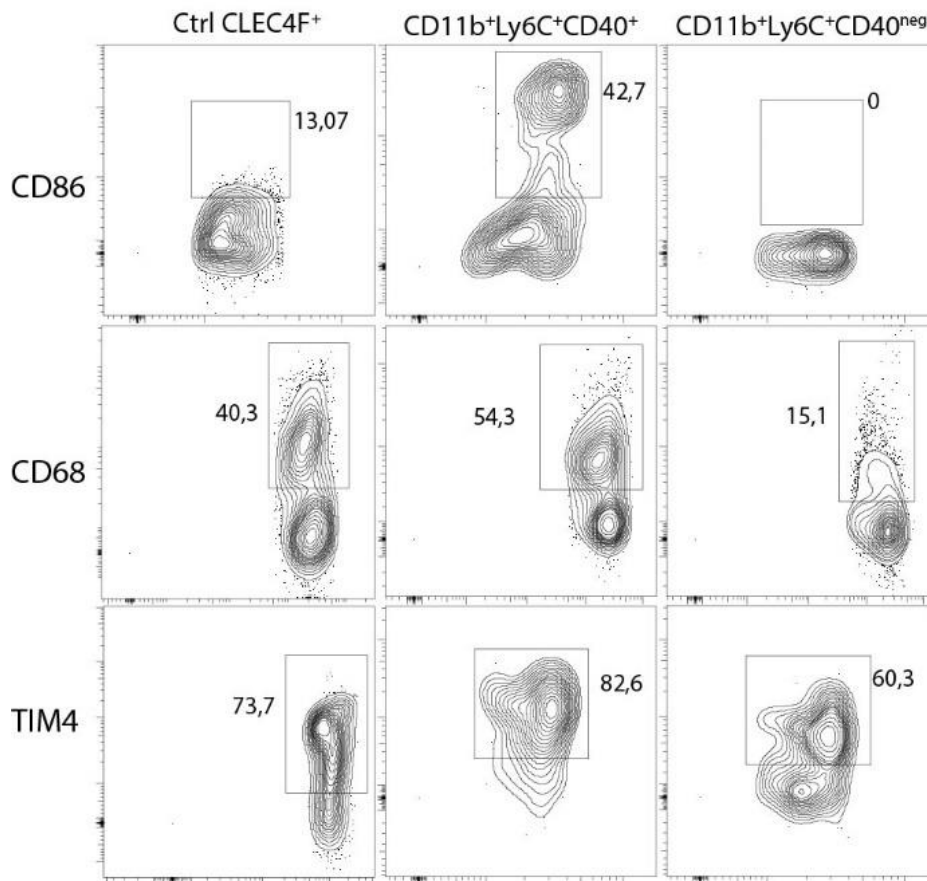


Figure 38: FACS analysis of the expression of CD86, CD68 and Tim4 on CD11b⁺Ly6C⁺CD40⁺ cells, CD11b⁺Ly6C⁺CD40^{neg} cells and Clec4F⁺ Kupffer cells. Data are representative for 3 independent experiments.

However, I wondered whether the increased glycolytic capacity of CD11b⁺Ly6C⁺CD40⁺ cells themselves might have a stimulatory function on CD8 T cells even in the absence of antigen-specific stimulation through the T cell receptor. To this end, I investigated the effect of the glycolytic potential of myeloid cells on T cells during vitro co-incubation assays. FACSsorted CD8 T cells were incubated with CD11b⁺Ly6C⁺CD40⁺ cells, CD11b⁺Ly6C⁺CD40^{neg} cells and Clec4F⁺ Kupffer cells. I found a significantly increased expression of the cytotoxic enzyme granzyme B (GzmB) in CD8⁺ T cells that were incubated with CD11b⁺Ly6C⁺CD40⁺ cells (**Fig. 39A**). The incubation with CD11b⁺Ly6C⁺CD40^{neg} cells and Clec4F⁺ Kupffer cells did not influence GzmB expression in T cells. Also, the T cell activation marker CD25 was significantly upregulated compared to CD11b⁺Ly6C⁺CD40^{neg} cells and T cells without activation stimulus. The difference between CD11b⁺Ly6C⁺CD40⁺ and Clec4F⁺ Kupffer cells was not significant (**Fig. 39B**). Furthermore, a sustained induction of CD8⁺ T cell proliferation was only induced by CD11b⁺Ly6C⁺CD40⁺ cells (**Fig. 39C**). CD11b⁺Ly6C⁺CD40^{neg} cells stimulated T cell proliferation, but only little increase in numbers was detected and the numbers started to decline after 48 hours (**Fig. 39C**). Clec4F⁺ Kupffer cells had a regulatory effect on activated CD8⁺ T cells. They did reduce T cell numbers about 25% within 48 hours (**Fig. 39C**). T cells that were not incubated with FACSsorted myeloid cells rapidly lost their proliferative potential and displayed reduced cell numbers over the time analyzed (**Fig. 39C**).

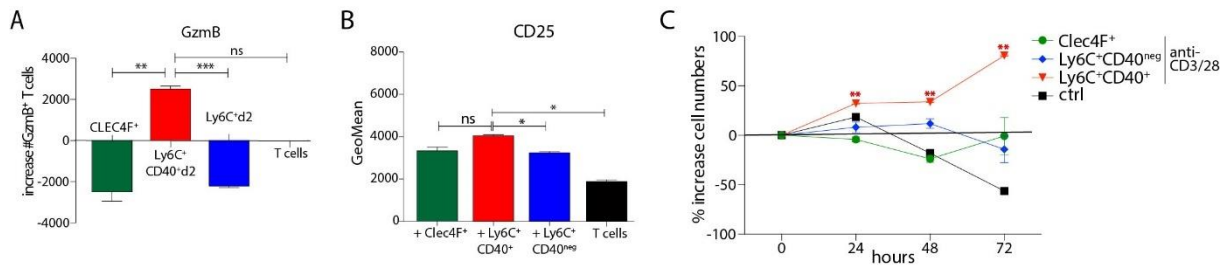


Figure 39: (A,B) Influence of $CD11b^+Ly6C^+CD40^+$, $CD11b^+Ly6C^+CD40^{neg}$ and $Clec4F^+$ Kupffer cells on CD8 T cells. **(A)** Expression levels of GzmB in activated polyclonal CD8 T cells in presence of FACSsorted $Clec4F^+$ Kupffer cells compared to hepatic $CD11b^+Ly6C^+CD40^+$ cells or $CD11b^+Ly6C^+CD40^{neg}$ cells. **(B)** Expression levels of CD25 on activated polyclonal CD8 T cells in presence of FACSsorted $Clec4F^+$ Kupffer cells compared to hepatic $CD11b^+Ly6C^+CD40^+$ cells and $CD11b^+Ly6C^+CD40^{neg}$ cells. **(C)** Time kinetics of expansion of activated CD8 T cells co-cultured with FACSsorted hepatic $CD11b^+$ cells. **(A-C)** Pooled data from 3 independent experiments ($n=4$); Mann-Whitney t test. $***p < 0.001$.

The results did show that $CD11b^+Ly6C^+CD40^+$ cells are metabolically highly active and have an elevated potential for the induction of T cell activation and proliferation compared to Kupffer cells and other inflammatory myeloid cells. Even though CD86 was the only costimulatory molecule that was differentially expressed on $CD11b^+Ly6C^+CD40^+$ cells and its expression was only detected on 40% of the $CD11b^+Ly6C^+CD40^+$ cells, $CD11b^+Ly6C^+CD40^+$ cells were the only ones to induce T cell population expansion in vitro.

5 Discussion

In this thesis I demonstrate the dynamic nature of the myeloid cells that form iMATEs after TLR9-L application, identify a new surrogate marker for iMATEs and attempt to elucidate the mechanisms determining expansion of T cells within iMATEs.

The liver is not a classical secondary lymphoid organ but its location makes it a frontline sentinel. Even though the induction of immune tolerance and hypo-responsiveness would be the primary response to foreign patterns of it has the unique capacity to induce a rapid and robust immune response as well²¹. The complex interactions between the members of the liver resident cell populations enable this finely tuned balance²⁶⁵. The low abundance of MHCs and co-stimulatory molecules additionally attribute to creating an environment in the liver that rather dampens immune responses²⁶⁶. T cells can get activated locally and will expand but they miss licensing cytotoxic effector functions¹⁴. The expression of PD-L1 by LSECs even drives them toward tolerance¹⁶. Furthermore it has been described that DCs that directly interact with LSECs induce T cell tolerance⁹². It can be described as a default to immune non-responsiveness or tolerance^{29,42,93}.

Liver function and integrity rely on the balance between immunity and tolerance. Excessive inflammation due to non-pathogenic molecules inducing tissue damage and remodelling has to be avoided without disabling pathogens clearance²⁶⁷. Insufficient immunity prepares the ground for chronic infections and cancer²⁶⁸. The application of TLR9-L does break the immunological tolerance in the liver but simultaneously does cause excessive inflammation and liver damage⁷⁴. The intrahepatic structures that arise due to this application are local hubs for a short-term CTL population expansion⁷⁴. They have no to little effect on the liver health and disappear without leaving scar tissue behind. All these findings indicated a dynamic regulation of induction of immunity and re-establishment of immune tolerance.

5.1 iMATEs arise within an immunogenic window

The initial Kupffer cell disappearance followed by recruitment of inflammatory monocytes from the circulation led to the hypothesis that an immunogenic window was formed by TLR9-L application. This requires a temporal silencing of the hepatic tolerance that is set to default. This TLR9-L provides the required stimulus that induces Kupffer cell disappearance as well as the recruitment of myeloid cells that are responsible for a low-level inflammation and immunity. Kupffer cells as frontline sentinels take up TLR9L and secrete TNF that induces the recruitment of myeloid cells to the liver²⁶⁹. Apart from inducing TNF secretion TLR9L also triggers the disappearance of Kupffer cells. The reason and mechanism for this event remain elusive so far. It can be hypothesized that the disappearance of the Kupffer cells leaves behind a non-tolerogenic gap that is quickly filled with immigrating inflammatory monocytes. Furthermore, the Kupffer cell disappearance disrupts ongoing tolerance mechanism²⁷⁰. Even though, LSECs, HSCs and hepatocytes are also secreting anti-inflammatory cyto- and chemokines, with the Kupffer cells thus the majority of regulating cells missing after TLR9-L application, it seems unlikely that the remaining regulating cells can keep up the tolerogenic environment. Furthermore, LSECs have been shown to secrete TNF α upon stimulation with

TLR9-L²⁷¹ which is a driver of iMATE formation. This opens a window of opportunity for inflammatory monocytes to migrate into the liver, cluster with others and secrete inflammatory cyto- and chemokines for their part recruiting further immune cells. What seems as a feed forward loop of inflammatory signaling and could lead to excessive inflammation and liver damage is silenced within a short period of time. The inflammatory stimuli of the inflammatory myeloid cells are not strong enough to suppress the reemerging hepatic tolerance leading to the disappearance of iMATEs. The processes leading to iMATE formation are now reversed: inflammatory myeloid cells disappear and Kupffer cells reemerge.

The results indicated that the TLR9-L induced disappearance of Kupffer cells enables iMATE formation. To test this hypothesis, TLR9-L uptake into Kupffer cells was blocked with poly-I^{272,273}. The decelerated loss of Kupffer cells in poly-I and TLR9-L treated animals did confirm the correlation of TLR9-L application and Kupffer cells disappearance. Furthermore, the influx of inflammatory myeloid cells was retarded until day 3 linking the immigration of myeloid cells with the disappearance of Kupffer cells. Not all Kupffer cells were rescued by the application of TLR9L indicating that poly-I had to be used at a higher concentration and for several times. Apparently, the blockade is reversible. Nevertheless, the strong influx of inflammatory monocytes is inhibited. This could be due to either the large number of Kupffer cells present in the hepatic tissue or the absence or low level of chemokines. In follow-up experiments, poly-I could be applied daily over a longer period of time. It would be interesting to see whether TLR9-L will be taken up by other cells, or whether it would remain in the tissue and induce the loss of Kupffer cells as soon as poly-I application is stopped. The recruitment of inflammatory monocytes might be completely abolished. Thus, Clec4F⁺ Kupffer cell depletion and subsequent replenishment imprinted a transitory proinflammatory signature in the hepatic microenvironment, suggesting that such changes in the cellular composition could explain the rapid infiltration of phagocyte precursors⁴⁸. The formation of iMATEs on the other hand is not directly dependent on the disappearance of Kupffer cells. This was confirmed by the application of TLR3 and 4 that did induce Kupffer cell disappearance but no iMATE formation. This indicates that not the activation of Kupffer cells but of another cell population triggers the formation of iMATEs. Alternatively, the activation of Kupffer cells with TLR9L is more pronounced and therefore induces TNF secretion and Kupffer cell death / disappearance.

In conclusion it can be hypothesized that the disappearance of Kupffer cells together with the subsequent recruitment of monocyte-derived macrophages induced by the application of TLR9L open the immunogenic window that allows for the expansion of the T cell population.

5.2 The dynamic changes in the composition of hepatic myeloid cells after TLR9-L application

The hepatic myeloid cells found at steady state conditions are mostly Kupffer cells, defined by their expression of Clec4F and lack of Ly6C⁸⁷. Further phenotypical analysis did not result into the homogenous group of cells they are normally reverted to²⁷⁴, but several different ones, all of them CD11b⁺Clec4F⁺ Ly6C^{neg} but with different expression of CX₃CR1, MHCII, F4/80 or Ly6A. This heterogeneity in liver macrophages has been described before and is attributed to the origin, the location, environmental stimuli and time of establishing residence^{48,275-278}. In

Kupffer cells it is mostly attributed to their different origin²⁷⁹. Kupffer cells in a not yet challenged liver almost exclusively originate from yolk-sac derived precursors that seed the liver before birth^{280,281}. These cells have a self-renewing potential that is driven by M-CSF and reside within the vasculature which led researchers to name them “sessile Kupffer cells”²⁷⁸. The remaining Kupffer cells are derived from either the bone-marrow, fetal liver macrophages or tissue-macrophages²⁸¹. They share the same morphology and phagocytic properties, but only the not-yolk-sac derived engage into inflammatory responses. In addition, the discovered heterogeneity could be linked to hepatic zonation just recently described by S Ben-Moshe et al.(2019)²⁸². This zonation influences gene expression as well as epigenetic features in hepatocytes as well as non-parenchymal cells. Alternatively different differential stages, as they are subject to continuous renewing processes⁴⁷, could cause this heterogeneity. Either way the group of Kupffer cells is even more diverse than described before²⁷⁹. Just recently published data on the human liver cell atlas support these results. N Aizarani et al. (2019)²⁸³ used single-cell RNA-sequencing to map all human liver cells and detected heterogeneous cell populations and previously unknown cell subtypes, supporting the hypothesis of the high plasticity of hepatic myeloid cells. Even though human liver cells were used for this work, similar results can be expected with murine livers.

The hepatic CD11b⁺Ly6C^{neg} and CD11b⁺Ly6C⁺cells detected under steady state conditions are subdivided into even more groups due to their differential expression of MHCII, F4/80, CCR2, CX₃CR1. This has been confirmed elsewhere, as the simple classification into Ly6C⁺ and Ly6C^{neg} comprises a multitude of different cell groups that are found in the liver like DCs, moDCs, macrophages, monocyte-derived macrophages, inflammatory monocytes and others²⁵⁵.

The application of TLR9-L induces drastic changes in the hepatic population of myeloid cells. The Clec4F⁺Kupffer cells vanish within 24 hours and the CD11b⁺Ly6C⁺cells expand their population about 20-fold, the CD11b⁺Ly6C^{neg} cells about 4 to 5-fold. Most of the CD11b⁺Ly6C⁺cells did co-express CCR2 which points towards bone-marrow derived myeloid cells that were recruited from peripheral blood²⁸⁴. The low co-expression of CX₃CR1 was also in line with this assumption²⁸⁵. Only few of the CD11b⁺Ly6C^{neg} cells were positive for CCR2. This indicates that they either use another mechanism of immigration or that they are derived from hematopoietic liver resident precursor cells that were activated due to the disappearance of the Kupffer cells²⁸⁶. Some of them might even be Kupffer cells that did not disappear but changed their surface marker expression profile. None of the additional markers chosen for further phenotypic characterization was suited to be used as a biomarker for iMATE – forming cells, as their expression was not exclusively linked to iMATE formation. Nevertheless, this additional phenotypic analysis did substantiate the diversity of hepatic myeloid cells before and after TLR9-L application. Especially after the application of TLR9-L both cells with pro-inflammatory (CD135, CD115, MHCI, CD86) but also regulatory phenotypes (CD273, CD274, VSIG4), as well as cells of different differential states and functions are present. This might be influenced by the zonation of the liver. S Ben-Moshe et al.(2019)²⁸² just recently described the influence of location within the liver on gene expression as well as epigenetic features in hepatocytes as well as non-parenchymal cells. Furthermore, hepatic myeloid cells have been

described to be less mature than cells from other secondary lymphoid organs¹⁴. Consequently, additional phenotypic or functional differentiation steps are more likely to happen.

BrdU pulse chase experiments could not confirm the hypothesis of local proliferation of myeloid cells supporting the strong increase in numbers of myeloid cells. This was in line with previous research that did show local proliferation of tissue resident cells only in the context of self-maintenance²⁸⁷ with an exception of macrophages in adipose tissue²⁸⁸. This result does contribute to the heterogeneity of cells as local population expansion would produce hubs of homogenous cells.

5.3 iMATE specific gene set reflect its local microenvironment

Laser capture microdissection was performed on TLR9-L treated livers to isolate iMATEs from liver tissue and from these tissue sample then generate by subsequent micro-array analysis transcriptomic profiles of iMATEs as compared to normal liver tissue. The set of genes differentially expressed in iMATEs that was obtained, included genes involved in co-stimulation of T cells, inflammatory responses, cell recruitment and lymphocyte antigen along with genes for regulatory and metabolic processes. They help to further characterize iMATE structures.

Sl2a6 also known as Glut9 is a glucose and urate acid transporter that is highly expressed by hepatocytes^{218,219} and leukocytes²⁸⁹. Glut9 is also expressed in hepatocytes. This implies that its expression in leukocytes is highly elevated, as the iMATE sections are compared to untreated liver tissue that is mainly formed by hepatocytes. Urate acid is involved in metabolic processes, immunoregulation and -stimulation. It is an antioxidant that is transported by Glut9 when activated by increased ROS-levels²⁹⁰ as well as a danger signal elicited by dying cells²⁹¹. Within the iMATEs its high expression is probably induced by ROS. Glut9 might contribute to the phenomenon of little liver damage despite the massive influx of inflammatory cells.

The upregulation of genes involved in chemotaxis and cell recruitment most likely supports immigration of myeloid cells from the circulation to the liver. CXCL10 is potently chemotactic for immune cells and recent data state that it mainly affects macrophages²⁹² whereas others stress its effect on lymphocytes²⁹³. Either way it is upregulated and drives cell recruitment. CCRL2 stimulates chemotaxis of DCs and macrophages to the site of inflammation²¹¹ and has already been described in the context of TLR signaling²¹².

The group of genes that are involved in regulatory processes are a product of the iMATE environment. The TLR9-L application only transiently overrode the hepatic tolerance.

None of the analyzed surface markers defined a distinct cell population exclusively found within iMATEs, apart from CD40. Nevertheless, they are in line with iMATE functionality. The sialoglycoprotein CD24 modulates growth and differentiation signals. It provides both costimulatory signals for T cells as well as regulatory^{294,295}, balancing immunity versus tolerance. CD84, the signaling lymphocytic activation molecule (SLAM) family member 5 is ubiquitously expressed within the hematopoietic lineage and engages in receptor-mediated signaling as a homophilic adhesion molecule. SLAMs are essential for the regulation of both innate and adaptive immunity²⁹⁶. The highest levels of expression have been documented on monocytes²⁹⁷. It is of

special interest that CD84 inhibits the proteolytic degradation of IRF8 a transcription factor that was also found to be upregulated within iMATEs. CD244, the signaling lymphocytic activation molecule (SLAM) family member 4 belongs to the same family of immunoregulatory receptors like CD84. CD244 is expressed on several hematopoietic cells and its expression on monocytes has been described to influence immune tolerance mechanisms²⁹⁸. CD191, the macrophage inflammatory protein 1 alpha receptor (MIP-1 α R) is a member of the beta chemokine receptor family. Besides MIP-1 α it also binds to 'regulated on activation normal T expressed and secreted' protein (RANTES), monocyte chemoattractant protein 3 (MCP-3) and myeloid progenitor inhibitory factor-1 (MPIF-1). The ligation induces signaling that impacts on the recruitment of effector immune cells to the site of inflammation. Recently published data describe increasing expression of CCR1 during the monocyte to macrophage differentiation¹⁷⁷. This is in line with the large portion of monocyte-derived macrophages found after TLR9L application. Tetraspanin 25 (CD53) is a member of the transmembrane 4 family which mediates signals in the regulation of cell development, activation, growth and motility and complexes with integrins and influence growth regulation. Just recently CD53 was reported as a novel correlate of a proinflammatory phenotype, with its expression being regulated by cytokines²⁹⁹. Additionally, LPS induced expression of CD53 has been observed³⁰⁰, indicating that TLR9-L might have a similar effect. Increased surface expression of the above-mentioned molecules may participate in the delivery of activation signals to T cells that result in local T cell proliferation and cell expansion.

The gene ontology analysis of the transcriptome profiles of CD40⁺ cells pointed towards a role of lipids and lipoprotein metabolism. It detected elevated regulation of plasma lipoprotein particles and response to IFN γ as well as monooxygenase and lipid transport activity. These findings can be explained by recent research. York et al. (2015)³⁰¹ linked decreased lipid de novo synthesis and increased lipid import to stimulation with IFN. The influence of IFN signaling reached into the gene expression regulation and is thought to limit the availability of lipid metabolites to pathogens³⁰². Lipids are needed for both proliferation, as a part of newly forming membranes, as well as energy source for highly active cells.

In conclusion the gene expression data analysis showed that the application of TLR9L induces the immigration of proinflammatory, metabolically highly active cells whose genetic expression profile gets shaped by their environment.

5.4 CD40 is a surrogate marker for a distinct myeloid cell population with specific properties involved in iMATE formation

The gene array of iMATE-forming myeloid cells identified the costimulatory molecule CD40 as a potential biomarker. It was upregulated only within iMATEs (laser-capture microdissection), it was not found on Kupffer cells and only transiently appeared on hepatic CD11b⁺Ly6C⁺myeloid cells isolated 48 hours after TLR9-L application. Further analysis did show that it was only upregulated upon the application of TLR9-L and not others like TLR3 or TLR4-L. CD40 expression after TLR9-L application was only detected in the liver and not in spleen or blood. All these results pointed towards an important role of CD40 in the induction of CTL expansion in the liver.

Nevertheless, the proof of concept experiments with CD40^{-/-} mice did not support this hypothesis. Neither iMATE formation nor hepatic CTL expansion were substantially affected. This indicates that additional costimulatory molecules or T cell activation processes were involved in the T cell expansion within iMATEs. These results were confirmed by using CD40L^{-/-} mice with the same experimental setup.

Even though CD40 cannot be used as a biomarker it still is a marker that defines a distinct cell population within the liver. Additional phenotypic characterization did tell something about the ontogeny as well as the function. The expression of several surface proteins involved in cell recruitment, adhesion and transmigration (CX₃CR1¹⁶¹, CD107b¹⁸⁷, CD97³⁰³, CD102³⁰⁴) apart from CCR₂ and CD11b indicate that CD11b⁺Ly6C⁺CD40⁺ cells are recruited from the circulation. The absence of CD40 expression on myeloid cells in the blood suggests that the upregulation of CD40 expression is part of a maturation or differentiation process within the liver. The receptor-type tyrosine-protein kinase Flt3 (CD135) that is primarily found on immature hematopoietic cells³⁰⁵ is also expressed at low levels on some of the CD40⁺ cells supporting the hypothesis of immigrating immature myeloid cells. The expression of low to intermediate levels of CD86 and XCR1 point towards an involvement of CD11b⁺Ly6C⁺CD40⁺ cells in the activation of CTL population expansion. The heavily glycosylated glycoprotein macrofialin (CD68) marks mononuclear phagocytes. Even though its scavenger function still awaits its confirmation it is potentially involved in antigen processing and presentation³⁰⁶ and therefore used to describe macrophage-like cells. Already this first analysis of CD11b⁺Ly6C⁺CD40⁺ cells paints a picture of a cell population with unique features. The expression of CD68, and CD86 was also confirmed by the data of the RNA sequencing. The picture that is painted with the results of the RNA sequencing is neither black nor white. There is a long list of cyto- / chemokines and their receptors which are rather stimulatory and pro-inflammatory. There is a strong signature of IFN- and TNF-signaling and an upregulation of costimulatory molecules like CD40, OX40 or CD86. In the list of the surface markers stimulatory molecules (CD18, CD205, CD69) are upregulated next to regulatory molecules (CD274, CD273). The analysis of coregulated genes by WGCNA classified the differentially regulated genes into four modules, that describe the role of the upregulated (1 and 2) and downregulated (3 and 4) genes in CD11b⁺Ly6C⁺CD40⁺ cells. The results from the various high-content assays employed in this thesis do not come to a unifying conclusion on the classification of CD11b⁺Ly6C⁺CD40⁺ cells. The expression of markers like CD11b, MHCII and CD68, as well as the strong upregulation of M1-type related genes like Nos2, Il-12 β , Stat1 or Il-6 would argue for a classification of CD11b⁺Ly6C⁺CD40⁺ cells as macrophages^{101,105,307}. On the other hand, there are transcription factors (BatF3, IRF3-8, Stat5, PU.1) and surface markers (CD11c, CD8a, Dectin1, CD40) pointing towards a DC-like progeny^{122,132,308-311}. The functional assays also did not help to reach a final decision on this question. Their high expression of CCR2 and Ly6C suggest that CD11b⁺Ly6C⁺CD40⁺ cells are derived from circulating inflammatory monocytes that are recruited into the liver¹⁰⁴. Given the rapid development of circulating monocytes into CD11b⁺Ly6C⁺CD40⁺ cells and their disappearance after 1 to 2 days, suggest that this transient differentiation process represents a so far unrecognized dynamics in the organ-specific development of immune stimulatory cells.

KEGG-pathway analysis highlighted the increased production of proinflammatory mediators and the upregulation of metabolic pathways, which could be confirmed by metabolic and functional assays. The CD11b⁺Ly6C⁺CD40⁺ myeloid cells took up more glucose and their glycolytic capacity was superior to CD11b⁺Ly6C⁺myeloid or Clec4F⁺ Kupffer cells. These factors describe higher glycolytic activity that might be linked to a cellular metabolic polarization that is known as the Warburg effect^{266,312} or aerobic glycolysis. The cells choose glycolysis over the TCA cycle for generation of energy and metabolic building blocks. Considering the tightly packed iMATEs without any vascularization the Warburg effect is not likely the reason for elevated glycolysis. In addition, polarization of macrophages towards the pro-inflammatory M1 type was linked with increased glucose uptake and glycolysis as well as a disrupted Krebs cycle inducing the secretion of proinflammatory cytokines like TNF α , IL-6 or ROS³¹³. The increased glucose uptake in macrophages is due to an overexpression of the glucose transporters (GLUT) 1³¹⁴. In CD11b⁺Ly6C⁺CD40⁺ cells overexpression of Glut 2 and 6 was detected. Their increased glycolytic activity was also accompanied by upregulation of most of the genes involved in glycolysis like hexokinase and phosphofruktokinase³¹⁵. The modulation of the metabolism is a central player during immune cell activation. Its rewiring due to changes in environmental metabolites influences the diversity of functions and responses^{313,316}. The pro-inflammatory polarization of CD11b⁺Ly6C⁺CD40⁺ cells is also driven by changes in other metabolic processes like fatty acid synthesis – the key enzyme Acsl1 is upregulated – and glutamine catabolism – elevated expression of its main transport Slc1a5³¹³. In addition a clear downregulation of genes that are involved in alternative activation towards regulatory activity is detected: CD36 plays a crucial role in metabolic adaptation for alternative polarization³¹⁷ as it takes up triglycerides for FAO that is needed for the Krebs cycle; monoglyceride Lipase (Mgll) catalyzes the final step during lipolysis. Their specific metabolic properties could also be linked to their elevated potential for T cell activation and proliferation induction compared to CD11b⁺Ly6C⁺CD40^{neg} and Clec4F⁺ Kupffer cells. This potential is supported by an upregulation of cytokines, chemokines, their co-stimulatory receptors, interferon signaling and other co-stimulatory molecules like CD86. According to the results of the functional assays they are the key drivers of T cell activation and proliferation. This might be due to metabolic activation of T cells. Their metabolic activity is tightly connected with their activation status. The quiescence exit includes the switch to aerobic glycolysis coupled with the TCA cycle for biosynthesis and energy production^{318,319}. Glucose and glutamine metabolism are key drivers of T cell activation and functional specialization^{320,321}. The strong glycolytic activity of the CD11b⁺Ly6C⁺CD40⁺ cells could influence the glycolytic activity of T cells. This could be further enhanced by IL-2 and IL-15 signaling secreted by CD11b⁺Ly6C⁺CD40⁺ cells³²².

In conclusion even though CD40 expression is not necessary for T cell activation and population expansion, CD11b⁺Ly6C⁺CD40⁺ cells are superior to CD11b⁺Ly6C⁺CD40^{neg} and Kupffer cells in the before mentioned. Together with their homogenous phenotypic profile it leaves them as an attractive surrogate marker with distinct metabolic properties.

5.5 Implications for future research

The present study was initially started to identify a biomarker for iMATE-forming cells that could be measured in peripheral blood. The results obtained provided more insight how the hepatic immune tolerance is overcome by TLR9-L application and why this local activation of T cell immunity is not accompanied by excessive inflammation and liver damage. This knowledge could be useful in the context of chronic liver diseases like HBV, HBC, and parasitic infections with malaria or schistosomiasis or hepatic cancer. All these diseases are characterized by the continuous conversion of effector immune cells into exhausted tolerized cells, the promotion of effector cell death and the education of regulatory cells that all promote clonal deletion, exhaustion or inhibition of T cell immunity³²³. First results into this direction were already achieved by Y Lin et al. (2018)¹⁴⁵ who was able to expand effector CD8⁺T cells within iMATEs induced by systemic application of TLR9-L, that were able to control hepatic tumor growth.

Further studies could address the fate of the Kupffer cells after TLR stimulation in more in detail. The mechanisms determining their rapid disappearance remain unclear, and it needs to be answered whether all Kupffer cells disappear or whether a small population of self-renewing cells survived and are involved in repopulation of the liver with macrophages²⁷⁰. Additional experiments should analyze the influence and involvement of the other liver-resident cells during iMATE formation and disappearance. Even though they might not be directly located within iMATEs it is hard to believe that they are not affected at all. Better understanding of these mechanisms could help to further improve the fine-tuning of iMATEs and prepare the ground to use iMATEs to improve therapeutic vaccination. Analyzing the interaction routes of myeloid cells with hepatocytes could solve the question how hepatocytes avoid an exuberant activation of macrophages within the immunogenic window even though glucose is abundantly present in the liver. It could also disclose whether hepatocytes and macrophages/monocytes are in direct contact to each other or whether the communication is executed via secretion of signaling molecules. It would be of great interest to characterize whether the presence of iMATEs as well as the T cell expansion could be prolonged by repeated TLR9-L application. At first, one would need to detect the perfect timing for additional applications. It is possible that both iMATE preservation and prolonged T cell expansion respond to different time kinetics. It is not known whether T cell expansion happens exclusively within densely clustered iMATEs. In the standard experimental setup for iMATEs, T cell expansion is detected when iMATE disintegration is already well under way. In the following it could be analyzed whether repeated application of TLR9-L has a similar effect, wears off due to memory formation or induces liver damage because restoration of tolerance is affected. Another open question relates to the clustering of the myeloid cells. It is unclear how this tight clustering of cells is achieved. RNA sequencing did not reveal significantly upregulated adhesion molecules. Another possible explanation would be tissue specific peculiarities and could explain why only certain inflammatory stimuli lead to recruitment of inflammatory myeloid cells and iMATE formation.

In addition to that it was not analyzed what predicts the localization of iMATEs within the tissue and whether this localization coincides with Kupffer cell niches. Disappearing Kupffer cells leave an empty space behind – the Kupffer cell niche. Guilliams et al. (2017)³²⁴ hypothesize that there

is only a restricted number of such niches available in the liver. iMATEs could be located within or within the vicinity of these niches. Consequently, reemerging Kupffer cells could be one of the reasons why the iMATEs start to dissolve. The analysis of which cells are taking up the TLR9-L would provide for a deeper understanding of the mechanisms behind this immunogenic window. D Movita et al. (2012)²⁷⁴ described expression of Il-10 and no upregulation of costimulatory molecules like CD80/86 or CD40 and no ROS production by Kupffer cells upon stimulation with TLR9-L. The current these will provide the ground for further studies that will address the mechanisms determining the formation of iMATEs as well as the mechanisms relevant for local T cell activation and expansion.

6 Supplementary

6.1 References

1. Invernizzi, P. Liver auto-immunology: The paradox of autoimmunity in a tolerogenic organ. *Journal of Autoimmunity* **46**, 1–6 (2013).
2. Heymann, F. & Tacke, F. Immunology in the liver—from homeostasis to disease. *Nature Reviews Gastroenterology and Hepatology* **13**, (2016).
3. Madrigal-Matute, J. & Cuervo, A. M. Regulation of Liver Metabolism by Autophagy. *Gastroenterology* **150**, 328–339 (2016).
4. Ding, H. ran, Wang, J. lin, Ren, H. zhen & Shi, X. lei. Lipometabolism and glycometabolism in liver diseases. *Biomed Res. Int.* **2018**, (2018).
5. Campbell, I. Liver: metabolic functions. *Anaesth. Intensive Care Med.* **7**, 51–54 (2006).
6. Rui, L. Energy Metabolism in the Liver. *Compr. Physiol.* **4**, 177–197 (2014).
7. Rines, A. K., Sharabi, K., Tavares, C. D. J. & Puigserver, P. Targeting hepatic glucose metabolism in the treatment of type 2 diabetes. *Nat. Rev. Drug Discov.* **15**, 786–804 (2016).
8. Tall, A ; Yvan-Charvet, L. Cholesterol, inflammation and innate immunity. *Nat. Rev. Immunol.* **15**, 104–116 (2015).
9. Canbay, A., Bechmann, L. & Gerken, G. Lipid metabolism in the liver. *Z. Gastroenterol.* **45**, 35–41 (2007).
10. Tannahill, G. *et al.* Succinate is a danger signal that induces IL-1 β via HIF-1 α . *Nature* **496**, 238–242 (2013).
11. Vandanmagsar, B. *et al.* The NLRP3 inflammasome instigates obesity-induced inflammation and insulin resistance. *Nat. Med.* **17**, 179–189 (2011).
12. Stienstra, R. *et al.* Inflammasome is a central player in the induction of obesity and insulin resistance. *Proc. Natl. Acad. Sci. U. S. A.* **108**, 15324–15329 (2011).
13. Nati, M. *et al.* The role of immune cells in metabolism-related liver inflammation and development of non-alcoholic steatohepatitis (NASH). *Reviews in Endocrine and Metabolic Disorders* **17**, 29–39 (2016).
14. Thomson, A. W. & Knolle, P. A. Antigen-presenting cell function in the tolerogenic liver environment. *Nat. Rev. Immunol.* **10**, 753–766 (2010).
15. Ketan Sheth, paul B. The liver as an immune organ. *Clin. Hepatol. Princ. Pract. Hepatobiliary Dis.* 141–152 (2010). doi:10.1007/978-3-540-93842-2_11
16. Crispe, I. N. Liver antigen-presenting cells. *J. Hepatol.* **54**, 357–365 (2011).
17. Oda, M Yokomori, H Han, J. Y. Regulatory mechanisms of hepatic microcirculation. *clin hemorheol microcirc* **29**, 167–182 (2003).
18. Robinson, M. W., Harmon, C. & O’Farrelly, C. Liver immunology and its role in

- inflammation and homeostasis. *Cell. Mol. Immunol.* **13**, 267–276 (2016).
19. Tedesco, D. & Grakoui, A. Environmental peer pressure: CD4⁺ T cell help in tolerance and transplantation. *Liver Transplant.* **24**, 89–97 (2018).
 20. Dou, L., Ono, Y., Chen, Y. F., Thomson, A. W. & Chen, X. P. Hepatic Dendritic Cells, the Tolerogenic Liver Environment, and Liver Disease. *Semin. Liver Dis.* **38**, 170–180 (2018).
 21. Crispe, I. N. Immune Tolerance in Liver Disease. *Hepatology* **60**, 2109–2117 (2014).
 22. Eckert, C., Klein, N., Kornek, M. & Lukacs-Kornek, V. The complex myeloid network of the liver with diverse functional capacity at steady state and in inflammation. *Front. Immunol.* **6**, (2015).
 23. Vanwolleghem, T. *et al.* Re-evaluation of hepatitis B virus clinical phases by systems biology identifies unappreciated roles for the innate immune response and B cells. *Hepatology* **62**, 87–100 (2015).
 24. Protzer, U. & Knolle, P. “To Be or Not to Be”: Immune Tolerance in Chronic Hepatitis B. (2016). doi:10.1053/j.gastro.2016.09.038
 25. Rock, K. L., Reits, E. & Neefjes, J. Present Yourself! By MHC Class I and MHC Class II Molecules. *Trends Immunol.* **37**, 724–737 (2016).
 26. Tiegs, G. & Lohse, A. W. Immune tolerance: What is unique about the liver. *J. Autoimmun.* **34**, 1–6 (2010).
 27. Liu, K. & Nussenzweig, M. C. Origin and development of dendritic cells. *Immunol. Rev.* **234**, 45–54 (2010).
 28. De Creus, A. *et al.* Low TLR4 Expression by Liver Dendritic Cells Correlates with Reduced Capacity to Activate Allogeneic T Cells in Response to Endotoxin. *J. Immunol.* **174**, 2037–2045 (2005).
 29. Pillarisetty, V. G., Shah, A. B., Miller, G., Bleier, J. I. & DeMatteo, R. P. Liver Dendritic Cells Are Less Immunogenic Than Spleen Dendritic Cells because of Differences in Subtype Composition. *J. Immunol.* **172**, 1009–1017 (2004).
 30. Abe, M., Tokita, D., Raimondi, G. & Thomson, A. W. Endotoxin modulates the capacity of CpG-activated liver myeloid DC to direct Th1-type responses. *Eur. J. Immunol.* **36**, 2483–2493 (2006).
 31. Doherty, D. G. Immunity, tolerance and autoimmunity in the liver: A comprehensive review. *Journal of Autoimmunity* **66**, 60–75 (2016).
 32. León, B., López-Bravo, M. & Ardavin, C. Monocyte-derived dendritic cells. *Semin. Immunol.* **17**, 313–318 (2005).
 33. Biswas, S. K. & Lopez-Collazo, E. Endotoxin tolerance: new mechanisms, molecules and clinical significance. *Trends in Immunology* **30**, 475–487 (2009).
 34. Pillarisetty, V. G., Katz, S. C., Bleier, J. I., Shah, A. B. & DeMatteo, R. P. Natural Killer Dendritic Cells Have Both Antigen Presenting and Lytic Function and in Response to CpG Produce IFN- γ via Autocrine IL-12. *J. Immunol.* **174**, 2612–2618 (2005).
 35. Chen, L. *et al.* Natural killer dendritic cells are an intermediate of developing dendritic

- cells. *J. Leukoc. Biol.* **81**, 1422–1433 (2007).
36. Knolle, P. A. & Limmer, A. Control of immune responses by scavenger liver endothelial cells. *Swiss Med. Wkly.* **133**, 501–6 (2003).
 37. John, B. & Crispe, I. N. Passive and Active Mechanisms Trap Activated CD8 + T Cells in the Liver. *J. Immunol.* **172**, 5222–5229 (2004).
 38. Racanelli, V. & Rehermann, B. The liver as an immunological organ. *Hepatology* **43**, (2006).
 39. Knolle, P. A. *et al.* Induction of cytokine production in naive CD4+ T cells by antigen-presenting murine liver sinusoidal endothelial cells but failure to induce differentiation toward T(h1) cells. *Gastroenterology* **116**, 1428–1440 (1999).
 40. Zhou, Z., Xu, M. J. & Gao, B. Hepatocytes: A key cell type for innate immunity. *Cellular and Molecular Immunology* **13**, 301–315 (2016).
 41. Gregory, S. H. & Wing, E. J. Neutrophil-Kupffer cell interaction: a critical component of host defenses to systemic bacterial infections. *J. Leukoc. Biol.* **72**, 239–48 (2002).
 42. Bertolino, P., McCaughan, G. W. & Bowen, D. G. Role of primary intrahepatic T-cell activation in the 'liver tolerance effect'. *Immunology and Cell Biology* **80**, 84–92 (2002).
 43. Winau, F. *et al.* Ito Cells Are Liver-Resident Antigen-Presenting Cells for Activating T Cell Responses. *Immunity* **26**, 117–129 (2007).
 44. Strober, W. Vitamin A rewrites the ABCs of oral tolerance. *Mucosal Immunology* **1**, 92–95 (2008).
 45. Yu, M. C. *et al.* Inhibition of T-cell responses by hepatic stellate cells via B7-H1-mediated T-cell apoptosis in mice. *Hepatology* **40**, 1312–1321 (2004).
 46. Gale, R. P., Sparkes, R. S. & Golde, D. W. Bone marrow origin of hepatic macrophages (Kupffer cells) in humans. *Science (80-.)*. **201**, 937–938 (1978).
 47. Gomez Perdiguero, E. *et al.* Tissue-resident macrophages originate from yolk-sac-derived erythro-myeloid progenitors. *Nature* **518**, 547–551 (2015).
 48. David, B. A. *et al.* Combination of Mass Cytometry and Imaging Analysis Reveals Origin, Location, and Functional Repopulation of Liver Myeloid Cells in Mice. *Gastroenterology* **151**, 1176–1191 (2016).
 49. Scott, C. L. *et al.* The Transcription Factor ZEB2 Is Required to Maintain the Tissue-Specific Identities of Macrophages. *Immunity* **49**, 312-325.e5 (2018).
 50. Bilzer, M., Roggel, F. & Gerbes, A. L. Role of Kupffer cells in host defense and liver disease. *Liver Int.* **26**, 1175–1186 (2006).
 51. Knolle, P. A. The liver as a lymphoid organ. *Liver Immunol. Princ. Pract.* 55–64 (2014). doi:10.1007/978-3-319-02096-9_5
 52. Knoll, P. *et al.* Human Kupffer cells secrete IL-10 in response to lipopolysaccharide (LPS) challenge. *J. Hepatol.* **22**, 226–229 (1995).
 53. You, Q., Cheng, L., Kedl, R. M. & Ju, C. Mechanism of T cell tolerance induction by

- murine hepatic Kupffer cells. *Hepatology* **48**, 978–990 (2008).
54. Fadok, V. A., Bratton, D. L. & Henson, P. M. Phagocyte receptors for apoptotic cells: recognition, uptake, and consequences. *J. Clin. Invest.* **108**, 957–962 (2001).
 55. Doherty, D. G. Immunity, tolerance and autoimmunity in the liver: A comprehensive review. *J. Autoimmun.* **66**, 60–75 (2016).
 56. Fan, X. & Rudensky, A. Y. Hallmarks of Tissue-Resident Lymphocytes. *Cell* **164**, 1198–1211 (2016).
 57. Doherty, D. G. & O’Farrelly, C. Innate and adaptive lymphoid cells in the human liver. *Immunological Reviews* **174**, 5–20 (2000).
 58. Nemeth, E., Baird, A. W. & O’Farrelly, C. Microanatomy of the liver immune system. *Seminars in Immunopathology* **31**, 333–343 (2009).
 59. Vanderkerken, K. *et al.* Origin and differentiation of hepatic natural killer cells (pit cells). *Hepatology* **18**, 919–925 (1993).
 60. Zimmermann, H. W. *et al.* Frequency and phenotype of human circulating and intrahepatic natural killer cell subsets is differentially regulated according to stage of chronic liver disease. *Digestion* **88**, 1–16 (2013).
 61. Peng, H. & Tian, Z. Re-examining the origin and function of liver-resident NK cells. *Trends Immunol.* **36**, 293–299 (2015).
 62. Groh, V., Steinle, A., Bauer, S. & Spies, T. Recognition of stress-induced MHC molecules by intestinal epithelial $\gamma\delta$ T cells. *Science (80-.)*. **279**, 1737–1740 (1998).
 63. McNamara, H. A. & Cockburn, I. A. The three Rs: Recruitment, retention and residence of leukocytes in the liver. *Clin. Transl. Immunol.* **5**, e123-9 (2016).
 64. Wehr, A. *et al.* Chemokine Receptor CXCR6-Dependent Hepatic NK T Cell Accumulation Promotes Inflammation and Liver Fibrosis. *J. Immunol.* **190**, 5226–5236 (2013).
 65. Geissmann, F. *et al.* Intravascular immune surveillance by CXCR6+ NKT cells patrolling liver sinusoids. *PLoS Biol.* **3**, 0650–0661 (2005).
 66. Doherty, D. G. *et al.* The human liver contains multiple populations of NK cells, T cells, and CD3+CD56+ natural T cells with distinct cytotoxic activities and Th1, Th2, and Th0 cytokine secretion patterns. *J. Immunol.* **163**, 2314–21 (1999).
 67. Kurioka, A., Walker, L. J., Klenerman, P. & Willberg, C. B. MAIT cells: new guardians of the liver. *Clin. Transl. Immunol.* **6**, e132 (2017).
 68. Rahimpour, A. *et al.* Identification of phenotypically and functionally heterogeneous mouse mucosal-associated invariant T cells using MR1 tetramers. *J. Exp. Med.* **212**, 1095–1108 (2015).
 69. Breous, E., Somanathan, S., Vandenberghe, L. H. & Wilson, J. M. Hepatic regulatory T cells and Kupffer cells are crucial mediators of systemic T cell tolerance to antigens targeting murine liver. *Hepatology* **50**, 612–621 (2009).
 70. Jenne, C. N., Urrutia, R. & Kubes, P. Platelets: Bridging hemostasis, inflammation, and immunity. *Int. J. Lab. Hematol.* **35**, 254–261 (2013).

71. Eksioglu, E. A. *et al.* Characterization of HCV interactions with Toll-like receptors and RIG-I in liver cells. *PLoS One* **6**, (2011).
72. Scott, M. J., Chen, C., Sun, Q. & Billiar, T. R. Hepatocytes express functional NOD1 and NOD2 receptors: A role for NOD1 in hepatocyte CC and CXC chemokine production. *J. Hepatol.* **53**, 693–701 (2010).
73. Schwabe, R. F., Seki, E. & Brenner, D. A. Toll-Like Receptor Signaling in the Liver. (2006). doi:10.1053/j.gastro.2006.01.038
74. Huang, L. R. *et al.* Intrahepatic myeloid-cell aggregates enable local proliferation of CD8+T cells and successful immunotherapy against chronic viral liver infection. *Nat. Immunol.* **14**, 574–583 (2013).
75. Graves, D. T. & Jiang, Y. *CHEMOKINES, A FAMILY OF CHEMOTACTIC CYTOKINES.*
76. Karlmark, K. R. *et al.* Hepatic recruitment of the inflammatory Gr1⁺ monocyte subset upon liver injury promotes hepatic fibrosis. *Hepatology* **50**, 261–274 (2009).
77. Sander, L. E. *et al.* Hepatic acute-phase proteins control innate immune responses during infection by promoting myeloid-derived suppressor cell function. *J. Exp. Med.* **207**, 1453–1464 (2010).
78. Sierro, F., M, E., S, R. & Bertolino, P. A Liver Capsular Network of Monocyte-Derived Macrophages Restricts Hepatic Dissemination of Intraperitoneal Bacteria by Neutrophil Recruitment. *Immunity* **47**, 374–388 (2017).
79. Beste, M. T. & Hammer, D. A. Selectin catch-slip kinetics encode shear threshold adhesive behavior of rolling leukocytes. *Proc. Natl. Acad. Sci. U. S. A.* **105**, 20716–20721 (2008).
80. McDonald, B. *et al.* Interaction of CD44 and hyaluronan is the dominant mechanism for neutrophil sequestration in inflamed liver sinusoids. *J. Exp. Med.* **205**, 915–927 (2008).
81. Menezes, G. B. *et al.* Selective Down-Regulation of Neutrophil Mac-1 in Endotoxemic Hepatic Microcirculation via IL-10. *J. Immunol.* **183**, 7557–7568 (2009).
82. Mossanen, J. C. *et al.* Chemokine (C-C motif) receptor 2–positive monocytes aggravate the early phase of acetaminophen-induced acute liver injury. *Hepatology* **64**, 1667–1682 (2016).
83. Moreno, C. *et al.* CCR5 deficiency exacerbates T-cell-mediated hepatitis in mice. *Hepatology* **42**, 854–862 (2005).
84. Tacke, F. *et al.* Monocyte subsets differentially employ CCR2, CCR5, and CX3CR1 to accumulate within atherosclerotic plaques. *J. Clin. Invest.* **117**, 185–194 (2007).
85. Tacke, F. & Randolph, G. J. Migratory fate and differentiation of blood monocyte subsets. *Immunobiology* **211**, 609–618 (2006).
86. Charo, I. F. & Ransohoff, R. M. Mechanisms of disease: The many roles of chemokines and chemokine receptors in inflammation. *New England Journal of Medicine* **354**, 610–621 (2006).
87. Scott, C. L. *et al.* Bone marrow-derived monocytes give rise to self-renewing and fully

- differentiated Kupffer cells. *Nat. Commun.* **7**, (2016).
88. Oo, Y. H., Shetty, S. & Adams, D. H. The role of chemokines in the recruitment of lymphocytes to the liver. *Dig. Dis.* **28**, 31–44 (2010).
 89. Ajami, B., Bennett, J. L., Krieger, C., McNagny, K. M. & Rossi, F. M. V. Infiltrating monocytes trigger EAE progression, but do not contribute to the resident microglia pool. *Nat. Neurosci.* **14**, 1142–1150 (2011).
 90. Yona, Simon; Kim, K; Wolf, Y; Mildner, A; Jung, S. Fate mapping reveals origins and dynamics of monocytes and tissue macrophages under homeostasis. *Immunity* **38**, 79–91 (2013).
 91. Wang, J. & Kubes, P. A Reservoir of Mature Cavity Macrophages that Can Rapidly Invade Visceral Organs to Affect Tissue Repair. *Cell* (2016).
doi:10.1016/j.cell.2016.03.009
 92. Schildberg, F. A., Hegenbarth, S. I., Schumak, B., Limmer, A. & Knolle, P. A. Liver sinusoidal endothelial cells veto CD8 T cell activation by antigen-presenting dendritic cells. *Eur. J. Immunol.* **38**, 957–967 (2008).
 93. Sana, G. *et al.* Adult human hepatocytes promote CD4⁺ T-cell hyporesponsiveness via interleukin-10-producing allogeneic dendritic cells. *Cell Transplant.* **23**, 1127–1142 (2014).
 94. van Furth, R. *et al.* The mononuclear phagocyte system: a new classification of macrophages, monocytes, and their precursor cells. *Bull. World Health Organ.* **46**, 845–852 (1972).
 95. DeKoter, R. P. & Singh, H. Regulation of B lymphocyte and macrophage development by graded expression of PU.1. *Science (80-.).* **288**, 1439–1442 (2000).
 96. Rosenbauer, F. & Tenen, D. G. Transcription factors in myeloid development: Balancing differentiation with transformation. *Nat. Rev. Immunol.* **7**, 105–117 (2007).
 97. Guilliams, M., Mildner, A. & Yona, S. Developmental and Functional Heterogeneity of Monocytes. *Immunity* **49**, 595–613 (2018).
 98. Ginhoux, F. & Jung, S. Monocytes and macrophages: developmental pathways and tissue homeostasis TL - 14. *Nat. Rev. Immunol.* **14 VN-r**, 392–404 (2014).
 99. Ginhoux, F., Schultze, J. L., Murray, P. J., Ochando, J. & Biswas, S. K. New insights into the multidimensional concept of macrophage ontogeny, activation and function. *Nature Immunology* **17**, 34–40 (2016).
 100. Avraham-Davidi, I. *et al.* On-site education of VEGF-recruited monocytes improves their performance as angiogenic and arteriogenic accessory cells. *J. Exp. Med.* **210**, 2611–2625 (2013).
 101. Murray, P. J. *et al.* Macrophage Activation and Polarization: Nomenclature and Experimental Guidelines. *Immunity* **41**, (2014).
 102. Sunderkötter, C. *et al.* Subpopulations of Mouse Blood Monocytes Differ in Maturation Stage and Inflammatory Response. *J. Immunol.* **172**, 4410–4417 (2004).

103. Jakubzick, C. *et al.* Minimal differentiation of classical monocytes as they survey steady-state tissues and transport antigen to lymph nodes. *Immunity* **39**, 599–610 (2013).
104. Movita, D. *et al.* Inflammatory Monocytes Recruited to the Liver within 24 Hours after Virus-Induced Inflammation Resemble Kupffer Cells but Are Functionally Distinct. *J. Virol.* **89**, 4809–4817 (2015).
105. Guillot, A. & Tacke, F. Liver Macrophages: Old Dogmas and New Insights. *Hepatology Commun.* **3**, 730–743 (2019).
106. Ginhoux, F. *et al.* Fate Mapping Analysis Reveals That Adult Microglia Derive from Primitive Macrophages. *Science (80-.).* **701**, 841–845 (2010).
107. Ginhoux, F. & Williams, M. Tissue-Resident Macrophage Ontogeny and Homeostasis. *Immunity* **44**, 439–449 (2016).
108. Gentek, R., Molawi, K. & Sieweke, M. H. Tissue macrophage identity and self-renewal. *Immunol. Rev.* **262**, 56–73 (2014).
109. Rückerl, D. *et al.* Macrophage origin limits functional plasticity in helminth-bacterial co-infection. *PLoS Pathog.* **13**, 1–19 (2017).
110. Hume, D. A., Irvine, K. M. & Pridans, C. The Mononuclear Phagocyte System: The Relationship between Monocytes and Macrophages. *Trends in Immunology* **40**, (2019).
111. Davies, L. C. & Taylor, P. R. Tissue-resident macrophages: Then and now. *Immunology* **144**, (2015).
112. Sica, A. & Strauss, L. Energy metabolism drives myeloid-derived suppressor cell differentiation and functions in pathology. *J. Leukoc. Biol.* **102**, 325–334 (2017).
113. Gordon, S. & Taylor, P. R. Monocyte and macrophage heterogeneity. *Nat. Rev. Immunol.* **5**, 953–964 (2005).
114. Kratochvill, F. *et al.* TNF Counterbalances the Emergence of M2 Tumor Macrophages. *Cell Rep.* **12**, 1902–1914 (2015).
115. Stables, M. J. *et al.* Transcriptomic analyses of murine resolution-phase macrophages. *Blood* **118**, (2011).
116. Fang, W. N., Shi, M., Meng, C. Y., Li, D. D. & Peng, J. P. The Balance between Conventional DCs and Plasmacytoid DCs Is Pivotal for Immunological Tolerance during Pregnancy in the Mouse. *Sci. Rep.* **6**, 1–11 (2016).
117. Merad, M., Sathe, P., Helft, J., Miller, J. & Mortha, A. The Dendritic Cell Lineage: Ontogeny and Function of Dendritic Cells and Their Subsets in the Steady State and the Inflamed Setting. *Annu. Rev. Immunol.* **31**, 563–604 (2013).
118. Waisman, A., Lukas, D., Clausen, B. E. & Yogev, N. Dendritic cells as gatekeepers of tolerance. *Semin. Immunopathol.* **39**, 153–163 (2017).
119. Mildner, A., Yona, S. & Jung, S. A Close Encounter of the Third Kind. Monocyte-Derived Cells. *Adv. Immunol.* **120**, 69–103 (2013).
120. Reis E Sousa, C. Dendritic cells in a mature age. *Nature Reviews Immunology* **6**, 476–483 (2006).

121. Chistiakov, D. A., Orekhov, A. N., Sobenin, I. A. & Bobryshev, Y. V. Plasmacytoid dendritic cells: Development, functions, and role in atherosclerotic inflammation. *Front. Physiol.* **5** JUL, 1–17 (2014).
122. Schlitzer, A. *et al.* Identification of cDC1- and cDC2-committed DC progenitors reveals early lineage priming at the common DC progenitor stage in the bone marrow. *Nat. Immunol.* **16**, 718–728 (2015).
123. Ginhoux, F. *et al.* The origin and development of nonlymphoid tissue CD103+ DCs. *J. Exp. Med.* **206**, 3115–3130 (2009).
124. Schulz, O. *et al.* Intestinal CD103+, but not CX3CR1+, antigen sampling cells migrate in lymph and serve classical dendritic cell functions. *J. Exp. Med.* **206**, 3101–3114 (2009).
125. Shortman, K. & Heath, W. R. The CD8+ dendritic cell subset. *Immunological Reviews* **234**, 18–31 (2010).
126. Lewis, K. L. *et al.* Notch2 receptor signaling controls functional differentiation of dendritic cells in the spleen and intestine. *Immunity* **35**, 780–791 (2011).
127. Seillet, C. & Belz, G. T. *Terminal Differentiation of Dendritic Cells. Advances in Immunology* **120**, (Elsevier Inc., 2013).
128. Amigorena, S. & Savina, A. Intracellular mechanisms of antigen cross presentation in dendritic cells. *Current Opinion in Immunology* **22**, 109–117 (2010).
129. Carenza, C. *et al.* Costimulatory Molecules and Immune Checkpoints Are Differentially Expressed on Different Subsets of Dendritic Cells. *Front. Immunol.* **10**, 1325 (2019).
130. Kastenmüller, K. *et al.* Protective T cell immunity in mice following protein-TLR7/8 agonist-conjugate immunization requires aggregation, type I IFN, and multiple DC subsets. *J. Clin. Invest.* **121**, 1782–1796 (2011).
131. Asselin-Paturel, C., Brizard, G., Pin, J.-J., Brière, F. & Trinchieri, G. Mouse Strain Differences in Plasmacytoid Dendritic Cell Frequency and Function Revealed by a Novel Monoclonal Antibody. *J. Immunol.* **171**, 6466–6477 (2003).
132. Manh, T. P. V., Alexandre, Y., Baranek, T., Crozat, K. & Dalod, M. Plasmacytoid, conventional, and monocyte-derived dendritic cells undergo a profound and convergent genetic reprogramming during their maturation. *Eur. J. Immunol.* **43**, 1706–1715 (2013).
133. Smith, C. M. *et al.* Cognate CD4+ T cell licensing of dendritic cells in CD8+ T cell immunity. *Nat. Immunol.* **5**, 1143–1148 (2004).
134. Jonuleit, H., Schmitt, E., Schuler, G., Knop, J. & Enk, A. H. Induction of interleukin 10-producing, nonproliferating CD4+ T cells with regulatory properties by repetitive stimulation with allogeneic immature human dendritic cells. *J. Exp. Med.* **192**, 1213–1222 (2000).
135. Schmidt, S. V., Nino-Castro, A. C. & Schultze, J. L. Regulatory dendritic cells: There is more than just immune activation. *Frontiers in Immunology* **3**, (2012).
136. Rydström, A. & Wick, M. J. Monocyte Recruitment, Activation, and Function in the Gut-Associated Lymphoid Tissue during Oral Salmonella Infection. *J. Immunol.* **178**, 5789–

- 5801 (2007).
137. Cheong, C. *et al.* Microbial stimulation fully differentiates monocytes to DC-SIGN/CD209 + dendritic cells for immune T cell areas. *Cell* **143**, 416–429 (2010).
 138. Chow, K. V., Lew, A. M., Sutherland, R. M. & Zhan, Y. Monocyte-Derived Dendritic Cells Promote Th Polarization, whereas Conventional Dendritic Cells Promote Th Proliferation. *J. Immunol.* **196**, 624–636 (2016).
 139. Sacher, T. *et al.* CpG-ODN-induced inflammation is sufficient to cause T-cell-mediated autoaggression against hepatocytes. *Eur. J. Immunol.* **32**, 3628–3637 (2002).
 140. Kakimi, K. *et al.* Blocking chemokine responsive to γ -2/interferon (IFN)- γ inducible protein and monokine induced by IFN- γ activity in vivo reduces the pathogenetic but not the antiviral potential of hepatitis B virus-specific cytotoxic T lymphocytes. *J. Exp. Med.* **194**, 1755–1766 (2001).
 141. Limmer, A. *et al.* Cross-presentation of oral antigens by liver sinusoidal endothelial cells leads to CD8 T cell tolerance. *Eur. J. Immunol.* **35**, 2970–2981 (2005).
 142. Bertolino, P., McCaughan, G. W. & Bowen, D. G. Role of primary intrahepatic T-cell activation in the ‘liver tolerance effect’. *Immunol. Cell Biol.* **80**, 84–92 (2002).
 143. Crispe, I. N. & Pierce, R. H. Killer T cells find meaningful encounters through iMATEs. *Nat. Immunol.* **14**, 533–534 (2013).
 144. Ehltling, C. *et al.* MAPKAP kinase 2 regulates IL-10 expression and prevents formation of intrahepatic myeloid cell aggregates during cytomegalovirus infections. *J. Hepatol.* **64**, 380–389 (2016).
 145. Lin, Y.-C. *et al.* Induction of liver-specific intrahepatic myeloid cells aggregation expands CD8 T cell and inhibits growth of murine hepatoma. *Oncoimmunology* **7**, e1502129 (2018).
 146. Macosko, E. Z. *et al.* Highly parallel genome-wide expression profiling of individual cells using nanoliter droplets. *Cell* **161**, 1202–1214 (2015).
 147. Love, M. I., Huber, W. & Anders, S. Moderated estimation of fold change and dispersion for RNA-seq data with DESeq2. *Genome Biol.* **15**, (2014).
 148. Langfelder, P. & Horvath, S. WGCNA: an R package for weighted correlation network analysis. *BMC Bioinformatics* **9**, 559 (2008).
 149. Langfelder, P. & Horvath, S. Eigengene networks for studying the relationships between co-expression modules. *BMC Syst. Biol.* **1**, 54 (2007).
 150. Shannon, P. *et al.* Cytoscape: A software Environment for integrated models of biomolecular interaction networks. *Genome Res.* **13**, 2498–2504 (2003).
 151. Zhenjiawang, Z. *et al.* BART: A transcription factor prediction tool with query gene sets or epigenomic profiles. *Bioinformatics* **34**, 2867–2869 (2018).
 152. Zhou, Q. *et al.* A mouse tissue transcription factor atlas. *Nat. Commun.* **8**, (2017).
 153. Fletcher, M. N. C. *et al.* Master regulators of FGFR2 signalling and breast cancer risk. *Nat. Commun.* **4**, (2013).

154. Subramanian, A. *et al.* Gene set enrichment analysis: A knowledge-based approach for interpreting genome-wide expression profiles. *Proc. Natl. Acad. Sci. U. S. A.* **102**, 15545–15550 (2005).
155. Zhou, Y. *et al.* Metascape provides a biologist-oriented resource for the analysis of systems-level datasets. *Nat. Commun.* **10**, (2019).
156. Li, L. *et al.* The spleen in liver cirrhosis: Revisiting an old enemy with novel targets. *J. Transl. Med.* **15**, 1–10 (2017).
157. Haisma, H. J. *et al.* Polyinosinic acid enhances delivery of adenovirus vectors in vivo by preventing sequestration in liver macrophages. *J. Gen. Virol.* **89**, 1097–1105 (2008).
158. Gao, B. & Yin, S. Toll-like receptor 3 in liver diseases. *Gastroenterol. Res. Pract.* **2010**, 1–6 (2010).
159. Yan, J. The role of the liver in sepsis. **33**, 498–510 (2014).
160. Austyn, J. M. & Gordon, S. F4/80, a monoclonal antibody directed specifically against the mouse macrophage. *Eur. J. Immunol.* **11**, 805–815 (1981).
161. Landsman, L. *et al.* CX3CR1 is required for monocyte homeostasis and atherogenesis by promoting cell survival. *Blood* **113**, 963–972 (2009).
162. Lee, M., Lee, Y., Song, J., Lee, J. & Chang, S. Y. Tissue-specific role of CX3CR1 expressing immune cells and their relationships with human disease. *Immune Netw.* **18**, 1–19 (2018).
163. Imai, T. *et al.* Identification and molecular characterization of fractalkine receptor CX3CR1, which mediates both leukocyte migration and adhesion. *Cell* **91**, 521–530 (1997).
164. Bakos, E. *et al.* CCR2 Regulates the Immune Response by Modulating the Interconversion and Function of Effector and Regulatory T Cells. *J. Immunol.* **198**, 4659–4671 (2017).
165. Mackay, C. R. Chemokines: Immunology's high impact factors. *Nat. Immunol.* **2**, 95–101 (2001).
166. Neefjes, J., Jongstra, M. L. M., Paul, P. & Bakke, O. Towards a systems understanding of MHC class I and MHC class II antigen presentation. *Nat. Rev. Immunol.* **11**, 823–836 (2011).
167. Chen, C., Gault, L. S. and N. N. Molecular cloning and expression of early T cell costimulatory molecule-1 and its characterization as B7-2 molecule. *J. Immunol.* **152**, 4929–4936 (1994).
168. Steinman, K. I. I. W.-P. H. H. M. Expression of B7 Costimulator Molecules on Mouse Dendritic Cells. in *Dendritic Cells in Fundamental and Clinical Immunology* (ed. Banchereau, Jacques, D. S.) 65–70 (Springer, Boston, MA, 2001). doi:<https://doi.org/10.1007/978-1-4615-1971-3>
169. Foks, A. C. *et al.* Blockade of Tim-1 and Tim-4 enhances atherosclerosis in low-density lipoprotein receptor-deficient mice. *Arterioscler. Thromb. Vasc. Biol.* **36**, 456–465 (2016).

170. Shaw, T. N. *et al.* Tissue-resident macrophages in the intestine are long lived and defined by Tim-4 and CD4 expression. *J. Exp. Med.* (2018). doi:10.1084/jem.20180019
171. van de Laar, L. *et al.* Yolk Sac Macrophages, Fetal Liver, and Adult Monocytes Can Colonize an Empty Niche and Develop into Functional Tissue-Resident Macrophages. *Immunity* **44**, 755–768 (2016).
172. Matsumura, Y. *et al.* Expression of CD134 and CD134 ligand in lesional and nonlesional psoriatic skin. *Arch. Dermatol. Res.* **294**, 563–566 (2003).
173. Karulf, M., Kelly, A., Weinberg, A. D. & Gold, J. A. OX40 Ligand Regulates Inflammation and Mortality in the Innate Immune Response to Sepsis. *J. Immunol.* **185**, 4856–4862 (2010).
174. Bierer, B. E., Peterson, A., Barbosa, J., Seed, B. & Burakoff, S. J. Expression of the T-cell surface molecule CD2 and an epitope-loss CD2 mutant to define the role of lymphocyte function-associated antigen 3 (LFA-3) in T-cell activation. *Proc. Natl. Acad. Sci.* **85**, 1194–1198 (1988).
175. Wolf, Y., Anderson, A. C. & Kuchroo, V. K. TIM3 comes of age as an inhibitory receptor. *Nat. Rev. Immunol.* **1**, (2019).
176. Gorman, J. V. & Colgan, J. D. Regulation of T cell responses by the receptor molecule Tim-3. *Immunol. Res.* **59**, 56–65 (2014).
177. Kaufmann, A., Salentin, R., Gemsa, D. & Sprenger, H. Increase of CCR1 and CCR5 expression and enhanced functional response to MIP-1 α during differentiation of human monocytes to macrophages. *J. Leukoc. Biol.* **69**, 248–252 (2001).
178. Marlin, S. D. & Springer, T. A. Intercellular Adhesion molecule-1 (ICAM-1) is a Ligand for Lymphocyte Function-Associated Antigen 1 (LFA-1). *Cell* **51**, 813–819 (1987).
179. Kawamura, A. *et al.* Increased Expression of Monocyte CD11a and Intracellular Adhesion Molecule-1 in Patients with Initial Atherosclerotic Coronary Stenosis. *Circ. J.* **68**, 6–10 (2004).
180. Schittenhelm, L., Hilken, C. M. & Morrison, V. L. B2 Integrins As Regulators of Dendritic Cell, Monocyte, and Macrophage Function. *Front. Immunol.* **8**, (2017).
181. Jing Yang, Barbara C. Furie, B. F. The Biology of P-Selectin Glycoprotein Ligand-1: Its Role as a Selectin Counterreceptor in Leukocyte-Endothelial and Leukocyte-Platelet Interaction. *Thromb. Haemost.* **81**, 1–7 (1999).
182. Holness, C. L. & Simmons, D. L. Molecular cloning of CD68, a human macrophage marker related to lysosomal glycoproteins. *Blood* **81**, 1607–1613 (1993).
183. Ammon, C. *et al.* Comparative analysis of integrin expression on monocyte-derived macrophages and monocyte-derived dendritic cells. *Immunology* **100**, 364–9 (2000).
184. Osugi, Y., Vuckovic, S. & Hart, D. N. J. Myeloid blood CD11C+ dendritic cells and monocyte-derived dendritic cells differ in their ability to stimulate T lymphocytes. *Blood* **100**, 2858–2866 (2002).
185. Cuervo, A. M. & Dice, J. F. Unique properties of lamp2a compared to other lamp2 isoforms. *J. Cell Sci.* **113**, 4441–4450 (2000).

186. Huynh, K. K. *et al.* LAMP proteins are required for fusion of lysosomes with phagosomes. *EMBO J.* **26**, 313–324 (2007).
187. Min, B. K., Suk, K. & Lee, W. H. Stimulation of CD107 affects LPS-induced cytokine secretion and cellular adhesion through the ERK signaling pathway in the human macrophage-like cell line, THP-1. *Cell. Immunol.* **281**, 122–128 (2013).
188. Simmons, D. The role of ICAM expression in immunity and disease. *Cancer Surv.* **24**, 141–155 (1995).
189. Ifn-, A. I., Schroder, K., Hertzog, P. J., Ravasi, T. & Hume, D. A. IFN Gamma. *J. Leukoc. Biol.* **75**, 163–89 (2004).
190. Kim, S. Y. *et al.* Pro-inflammatory hepatic macrophages generate ROS through NADPH oxidase 2 via endocytosis of monomeric TLR4-MD2 complex. *Nat. Commun.* **8**, (2017).
191. Masson, D. & Tschopp, J. A family of serine esterases in lytic granules of cytolytic T lymphocytes. *Cell* **49**, 679–685 (1987).
192. Wensink, A. C., Hack, C. E. & Bovenschen, N. Granzymes Regulate Proinflammatory Cytokine Responses. *J. Immunol.* **194**, 491–497 (2015).
193. Nuvolone, M. *et al.* Cystatin F is a biomarker of prion pathogenesis in mice. *PLoS One* **12**, 1–25 (2017).
194. Hamilton, G., Colbert, J. D., Schuettelkopf, A. W. & Watts, C. Cystatin F is a cathepsin C-directed protease inhibitor regulated by proteolysis. *EMBO J.* **27**, 499–508 (2008).
195. Schoenen, H. *et al.* Mincle is essential for recognition and adjuvanticity of the mycobacterial cord factor and its synthetic analogue trehalose-. *J. Immunol.* **184**, 2756–2760 (2010).
196. Matsumoto, M. *et al.* A novel LPS-inducible C-type lectin is a transcriptional target of NF-IL6 in macrophages. *J. Immunol.* **163**, 5039–48 (1999).
197. Yamasaki, S. *et al.* Mincle is an ITAM-coupled activating receptor that senses damaged cells. *Nat. Immunol.* **9**, 1179–1188 (2008).
198. Wicovsky, A. *et al.* Tumor necrosis factor receptor-associated factor-1 enhances proinflammatory TNF receptor-2 signaling and modifies TNFR1-TNFR2 cooperation. *Oncogene* **28**, 1769–1781 (2009).
199. Tsitsikov, E. N. *et al.* TRAF1 Is a Negative Regulator of TNF Signaling. *Immunity* **15**, 647–657 (2001).
200. Raul Elgueta, Micah J. Benson, Victor C. de Vries, Anna Wasiuk, Yanxia Guo, and R. J. N. Molecular mechanism and function of CD40/CD40L engagement in the immune system. *Immunol Rev* **229**, (2009).
201. Megan, J., Patterson, M., Johnson, M. H., Zimonjic, D. B. & Graubert, T. A. Characterization of Ly-6M, a novel member of the Ly-6 family of hematopoietic proteins. *Blood* **95**, 3125–3132 (2000).
202. Loughner, C. L. *et al.* Organization, evolution and functions of the human and mouse Ly6/uPAR family genes. *Hum. Genomics* **10**, 10 (2016).

203. LeClair, K. P., Palfree, R. G., Flood, P. M., Hammerling, U. & Bothwell, A. Isolation of a murine Ly-6 cDNA reveals a new multigene family. *EMBO J.* **5**, 3227–3234 (1986).
204. Henderson, S. C., Kamdar, M. M. & Bamezai, A. Ly-6A.2 Expression Regulates Antigen-Specific CD4 + T Cell Proliferation and Cytokine Production. *J. Immunol.* **168**, 118–126 (2002).
205. Lin, K. W. *et al.* The roles of interleukin-1 and interleukin-1 receptor antagonist in antigen-specific immune responses. *J. Biomed. Sci.* **9**, 26–33 (2002).
206. Zahedi, K., Seldin, M. F., Rits, M., Ezekowitz, R. A. & Whitehead, A. S. Mouse IL-1 receptor antagonist protein. Molecular characterization, gene mapping, and expression of mRNA in vitro and in vivo. *J. Immunol.* **146**, 4228–33 (1991).
207. Josephs, M. D. *et al.* Modulation of the acute phase response by altered expression of the IL-1 type 1 receptor or IL-1ra. *Am. J. Physiol. - Regul. Integr. Comp. Physiol.* **278**, 824–830 (2000).
208. Michelucci, A. *et al.* Immune-responsive gene 1 protein links metabolism to immunity by catalyzing itaconic acid production. *Proc. Natl. Acad. Sci. U. S. A.* **110**, 7820–7825 (2013).
209. Stawowczyk, M., Van Scoy, S., Kumar, K. P. & Reich, N. C. The interferon stimulated gene 54 promotes apoptosis. *J. Biol. Chem.* **286**, 7257–7266 (2011).
210. Fensterl, V. *et al.* Interferon-induced Ifit2/ISG54 protects mice from lethal VSV neuropathogenesis. *PLoS Pathog.* **8**, (2012).
211. Zabel, B. A. *et al.* Mast cell-expressed orphan receptor CCRL2 binds chemerin and is required for optimal induction of IgE-mediated passive cutaneous anaphylaxis. *J. Exp. Med.* **205**, 2207–2220 (2008).
212. Shimada, T., Matsumoto, M., Tatsumi, Y., Kanamaru, A. & Akira, S. A novel lipopolysaccharide inducible C-C chemokine receptor related gene in murine macrophages. *FEBS Lett.* **425**, 490–494 (1998).
213. Sidahmed, A. M. E. *et al.* CXCL10 contributes to p38-mediated apoptosis in primary T lymphocytes in vitro. *Cytokine* **59**, 433–441 (2012).
214. Angiolillo, A. L. *et al.* Human interferon-inducible protein 10 is a potent inhibitor of angiogenesis in vivo. *J. Exp. Med.* **182**, 155–62 (1995).
215. Ishibashi, K., Suzuki, M., Sasaki, S. & Imai, M. Identification of a new multigene four-transmembrane family (MS4A) related to CD20, HTm4 and β subunit of the high-affinity IgE receptor. *Gene* **264**, 87–93 (2001).
216. Cruse, G. *et al.* The CD20 homologue MS4A4 directs trafficking of KIT toward clathrin-independent endocytosis pathways and thus regulates receptor signaling and recycling. *Mol. Biol. Cell* **26**, 1711–1727 (2015).
217. Phay, J. E., Hussain, H. B. & Moley, J. F. Cloning and expression analysis of a novel member of the facilitative glucose transporter family, SLC2A9 (GLUT9). *Genomics* **66**, 217–220 (2000).
218. Keembiyehetty, C. *et al.* Mouse glucose transporter 9 splice variants are expressed in

- adult liver and kidney and are up-regulated in diabetes. *Mol. Endocrinol.* **20**, 686–697 (2006).
219. Preitner, F. *et al.* Glut9 is a major regulator of urate homeostasis and its genetic inactivation induces hyperuricosuria and urate nephropathy. *Proc. Natl. Acad. Sci. U. S. A.* **106**, 15501–15506 (2009).
 220. Le, M. P. T., Shafiu, M., Mu, W. & Johnson, R. J. SLC2A9 - A fructose transporter identified as a novel uric acid transporter. *Nephrol. Dial. Transplant.* **23**, 2746–2749 (2008).
 221. Stout, R. D. & Suttles, J. The many roles of CD40 in cell-mediated inflammatory responses. *Immunol. Today* **17**, 487–492 (1996).
 222. Murray, S. *et al.* CD40 is required for protective immunity against liver stage Plasmodium infection1. *J. Immunol.* **194**, 2268–2279 (2015).
 223. Quezada, S. A., Jarvinen, L. Z., Lind, E. F. & Noelle, R. J. CD40/CD154 Interactions at the Interface of Tolerance and Immunity. *Annu. Rev. Immunol.* **22**, 307–328 (2004).
 224. Rocha, N. & Neefjes, J. MHC class II molecules on the move for successful antigen presentation. *EMBO Journal* **27**, 1–5 (2008).
 225. Villadangos, J. A. Presentation of antigens by MHC class II molecules: Getting the most out of them. *Molecular Immunology* **38**, 329–346 (2001).
 226. Wilcox, R. A. *et al.* Cutting Edge: Expression of Functional CD137 Receptor by Dendritic Cells. *J. Immunol.* **168**, 4262–4267 (2002).
 227. Hendriks, J. *et al.* CD27 is required for generation and long-term maintenance of T cell immunity. *Nat. Immunol.* **1**, 433–440 (2000).
 228. Bowen, M. A., Lee, R. K., Miragliotta, G., Nam, S. Y. & Podack, E. R. Structure and expression of murine CD30 and its role in cytokine production. *J. Immunol.* **156**, 442–9 (1996).
 229. Riches, D. W., Chan, E. D. & Winston, B. W. TNF-alpha-induced regulation and signalling in macrophages. *Immunobiology* **195**, 477–90 (1996).
 230. Winston, B. W., Lange-Carter, C. A., Gardner, A. M., Johnson, G. L. & Riches, D. W. H. Tumor necrosis factor α rapidly activates the mitogen-activated protein kinase (MAPK) cascade in a MAPK kinase-dependent, c-Raf-1-independent fashion in mouse macrophages. *Proc. Natl. Acad. Sci. U. S. A.* **92**, 1614–1618 (1995).
 231. Settles, M. *et al.* Different capacity of monocyte subsets to phagocytose Iron-Oxide nanoparticles. *PLoS One* **6**, (2011).
 232. Sprangers, S., Vries, T. J. D. & Everts, V. Monocyte Heterogeneity: Consequences for Monocyte-Derived Immune Cells. *J. Immunol. Res.* **2016**, (2016).
 233. Grewal, I. S. & Flavell, R. A. Cd40 and Cd154 in Cell-Mediated Immunity. *Annu. Rev. Immunol.* **16**, 111–135 (1998).
 234. Noelle, R. J. The role of gp39 (CD40L) in immunity. *Clin. Immunol. Immunopathol.* **76**, S203–S207 (1995).

235. Bénéchet, A. P. *et al.* Dynamics and genomic landscape of CD8+ T cells undergoing hepatic priming. *Nature* **574**, 200–205 (2019).
236. WM Bayliss, E. S. The mechanism of Pancreatic Secretion. *Proc. Soc. Exp. Biol. Med.* **31**, 178–179 (1902).
237. WH Häcki. Secretin. *Clin Gastroenterol.* **9**, 609–32 (1980).
238. Khazen, W. *et al.* Expression of macrophage-selective markers in human and rodent adipocytes. *FEBS Lett.* **579**, 5631–5634 (2005).
239. Wu, N. *et al.* The secretin/secretin receptor axis modulates liver fibrosis through changes in TGF- β 1 biliary secretion. *Hepatology* **64**, 865–879 (2016).
240. Afroze, S. *et al.* The physiological roles of secretin and its receptor. *Ann. Transl. Med.* **1**, 29 (2013).
241. K Sato, F Meng, J Venter, H Francis, S Glaser, G. A. Secretin and Secretin Receptor Are Required for Inflammatory Cell-Cell Communication via Extracellular Vesicles Between Cholangiocytes Treated with Lipopolysaccharide. *Faseb J.* (2017).
242. Guo, B., Godzik, A. & Reed, J. C. Bcl-G, a Novel Pro-apoptotic Member of the Bcl-2 Family. *J. Biol. Chem.* **276**, 2780–2785 (2001).
243. Giam, M., Okamoto, T., Mintern, J. D., Strasser, A. & Bouillet, P. Bcl-2 family member Bcl-G is not a proapoptotic protein. *Cell Death Dis.* **3**, (2012).
244. Nakamura, M., Nakagawa, M. & Watanabe, J. Ubiquitin-like protein MNSF β negatively regulates T Cell function and survival. *Immunol. Invest.* **44**, 1–12 (2015).
245. Watanabe, J., Nakagawa, M., Watanabe, N. & Nakamura, M. Ubiquitin-like protein MNSF β covalently binds to Bcl-G and enhances lipopolysaccharide/interferon γ -induced apoptosis in macrophages. *FEBS J.* **280**, 1281–1293 (2013).
246. G Jia, J Gonzalo, C Lloyd, L Kremer, L lu, C Martinez-A, B. W. Distinct Expression and Function of the Novel Mouse Chemokine Monocyte Chemotactic Protein-5 in Lung Allergic Inflammation By. *J. Exp. Med.* **184**, 1939–1951 (1996).
247. Sarafi, M. N., Garcia-Zepeda, E. A., MacLean, J. A., Charo, I. F. & Luster, A. D. Murine monocyte chemoattractant protein (MCP)-5: A novel CC chemokine that is a structural and functional homologue of human MCP-1. *J. Exp. Med.* **185**, 99–109 (1997).
248. Katsounas, A., Schlaak, J. F. & Lempicki, R. A. CCL5: A double-edged sword in host defense against the hepatitis C virus. *Int. Rev. Immunol.* **30**, 366–378 (2011).
249. Fantuzzi, L., Tagliamonte, M., Gauzzi, M. C. & Lopalco, L. Dual CCR5/CCR2 targeting: opportunities for the cure of complex disorders. *Cell. Mol. Life Sci.* (2019). doi:10.1007/s00018-019-03255-6
250. Guyon, A. CXCL12 chemokine and its receptors as major players in the interactions between immune and nervous systems. *Front. Cell. Neurosci.* **8**, 1–10 (2014).
251. Liu, C. *et al.* Elevated expression of chemokine CXCL13 in chronic hepatitis B patients links to immune control during antiviral therapy. *Front. Immunol.* **8**, 1–11 (2017).
252. Lahoud, M. H. *et al.* DEC-205 is a cell surface receptor for CpG oligonucleotides. *Proc.*

- Natl. Acad. Sci. U. S. A.* **109**, 16270–16275 (2012).
253. Radjabova, V., Mastroeni, P., Skjødt, K., Zaccane, P. & Bono, B. De. TARM1 is a novel LRC-encoded ITAM receptor that co- stimulates pro-inflammatory cytokine secretion by macrophages and neutrophils. **195**, 3149–3159 (2016).
254. Tomlinson, M. G. *et al.* Characterization of mouse CD53: Epitope mapping, cellular distribution and induction by T cell receptor engagement during repertoire selection. *Eur. J. Immunol.* **25**, 2201–2205 (1995).
255. Kubes, P. & Jenne, C. Immune Responses in the Liver. *Annu. Rev. Immunol.* **36**, (2018).
256. Locke, D., Chen, H., Liu, Y., Liu, C. & Kahn, M. L. Lipid rafts orchestrate signaling by the platelet receptor glycoprotein VI. *J. Biol. Chem.* **277**, 18801–18809 (2002).
257. Zhao, S., Fung-Leung, W. P., Bittner, A., Ngo, K. & Liu, X. Comparison of RNA-Seq and microarray in transcriptome profiling of activated T cells. *PLoS One* **9**, (2014).
258. Grajales-Reyes, G. E. *et al.* Batf3 maintains autoactivation of Irf8 for commitment of a CD8 α + conventional DC clonogenic progenitor. *Nat. Immunol.* **16**, 708–717 (2015).
259. Roy, S. K. *et al.* MEKK1 plays a critical role in activating the transcription factor C/EBP- β -dependent gene expression in response to IFN- γ . *Proc. Natl. Acad. Sci. U. S. A.* **99**, 7945–7950 (2002).
260. Akira, S. *et al.* A nuclear factor for IL-6 expression (NF-IL6) is a member of a C/EBP family. *EMBO J.* **9**, 1897–1906 (1990).
261. Colas, C., Ung, P. M.-U. & Schlessinger, A. SLC Transporters: Structure, Function, and Drug Discovery. *Medchemcomm* **7**, 1069–1081 (2016).
262. Everts, Bart; Eyal Amiel; Redmann, Veronika; Pearce, Erika L.; Pearce, E. J. TLR-driven early glycolytic reprogramming via the kinases TBK1-IKKe supports the anabolic demands of dendritic cell activation. *Nat. Immunol.* **15**, 323–332 (2014).
263. Zhufang Shena, C. Z. Y. W. (2-deoxy-2-[(7-nitro-2,1,3-benzoxadiazol-4-yl) amino]-D-glucose. *J. Biochem. Biophys. Methods* **64**, 207–2015 (2005).
264. Pearce, E. L. & Pearce, E. J. Metabolic pathways in immune cell activation and quiescence. *Immunity* **38**, 633–643 (2013).
265. Jenne, C. N. & Kubes, P. Immune surveillance by the liver. *Nat. Immunol.* **14**, 996–1006 (2013).
266. Krawczyk, C. M. *et al.* Toll-like receptor-induced changes in glycolytic metabolism regulate dendritic cell activation. *Blood* **115**, 4742–4749 (2010).
267. Robinson, M. W., Harmon, C. & O’Farrelly, C. Liver immunology and its role in inflammation and homeostasis. *Cell. Mol. Immunol.* **13**, 267–276 (2016).
268. Xia, A., Zhang, Y., Xu, J., Yin, T. & Lu, X. J. T Cell Dysfunction in Cancer Immunity and Immunotherapy. *Frontiers in immunology* **10**, 1719 (2019).
269. Bonnardel, J. *et al.* Stellate Cells, Hepatocytes, and Endothelial Cells Imprint the Kupffer Cell Identity on Monocytes Colonizing the Liver Macrophage Niche. *Immunity* **51**, 638-654.e9 (2019).

270. Heymann, F. *et al.* Liver inflammation abrogates immunological tolerance induced by Kupffer cells. *Hepatology* **62**, 279–291 (2015).
271. Wu, J. *et al.* Toll-like receptor-induced innate immune responses in non-parenchymal liver cells are cell type-specific. *Immunology* **129**, 363–374 (2010).
272. Haisma, H. J. *et al.* Polyinosinic acid enhances delivery of adenovirus vectors in vivo by preventing sequestration in liver macrophages. *J. Gen. Virol.* **89**, 1097–1105 (2008).
273. Liu, Y. P. *et al.* Polyinosinic acid decreases sequestration and improves systemic therapy of measles virus. *Cancer Gene Ther.* **19**, 202–211 (2012).
274. Movita, D. *et al.* Kupffer cells express a unique combination of phenotypic and functional characteristics compared with splenic and peritoneal macrophages. *J. Leukoc. Biol.* **92**, 723–733 (2012).
275. Ray, K. Mapping the cells in the liver — uncharted subtypes and heterogeneity. *Nat. Rev. Gastroenterol. Hepatol.* **16**, 513 (2019).
276. Tacke, F. & Zimmermann, H. W. Macrophage heterogeneity in liver injury and fibrosis. *J. Hepatol.* **60**, 1090–1096 (2014).
277. Blériot, C. & Ginhoux, F. Understanding the Heterogeneity of Resident Liver Macrophages. **10**, 1–6 (2019).
278. Klein, I. *et al.* Kupffer cell heterogeneity: Functional properties of bone marrow-derived and sessile hepatic macrophages. *Blood* **110**, 4077–4085 (2007).
279. Kinoshita, M. *et al.* Characterization of two F4/80-positive Kupffer cell subsets by their function and phenotype in mice. *J. Hepatol.* **53**, 903–910 (2010).
280. Naito, M., Hasegawa, G. & Takahashi, K. Development, differentiation, and maturation of kupffer cells. *Microsc. Res. Tech.* **39**, 350–364 (1997).
281. van de Laar, L. *et al.* Yolk Sac Macrophages, Fetal Liver, and Adult Monocytes Can Colonize an Empty Niche and Develop into Functional Tissue-Resident Macrophages. *Immunity* **44**, (2016).
282. Ben-moshe, S. & Itzkovitz, S. Spatial heterogeneity in the mammalian liver. *Nat. Rev. Gastroenterol. Hepatol.* (2019). doi:10.1038/s41575-019-0134-x
283. Aizarani, N. *et al.* A human liver cell atlas reveals heterogeneity and epithelial progenitors. *Nature* **572**, 199–204 (2019).
284. Vanbervliet, B. *et al.* Sequential involvement of CCR2 and CCR6 ligands for immature dendritic cell recruitment: Possible role at inflamed epithelial surfaces. *Eur. J. Immunol.* **32**, 231–242 (2002).
285. Platt, A. M., Bain, C. C., Bordon, Y., Sester, D. P. & Mowat, A. M. An Independent Subset of TLR Expressing CCR2-Dependent Macrophages Promotes Colonic Inflammation. *J. Immunol.* **184**, 6843–6854 (2010).
286. Röszer, T. Understanding the Biology of Self-Renewing Macrophages. *Cells* **7**, 103 (2018).
287. Schulz, C. *et al.* A lineage of myeloid cells independent of myb and hematopoietic stem

- cells. *Science (80-.)*. **335**, 86–90 (2012).
288. Amano, S. U. *et al.* Local proliferation of macrophages contributes to obesity-associated adipose tissue inflammation. *Cell Metab.* **19**, 162–171 (2014).
 289. Karim, S., Adams, D. H. & Lalor, P. F. Hepatic expression and cellular distribution of the glucose transporter family. *World J. Gastroenterol.* **18**, 6771–6781 (2012).
 290. Itahana, Y. *et al.* The uric acid transporter SLC2A9 is a direct target gene of the tumor suppressor p53 contributing to antioxidant defense. *Oncogene* **34**, 1799–1810 (2014).
 291. Shi, Y. Caught red-handed: Uric acid is an agent of inflammation. *J. Clin. Invest.* **120**, 1809–1811 (2010).
 292. Tomita, K. *et al.* CXCL10-Mediates Macrophage, but not Other Innate Immune Cells-Associated Inflammation in Murine Nonalcoholic Steatohepatitis. *Sci. Rep.* **6**, 1–13 (2016).
 293. Chen, L. J., Lv, J., Wen, X. Y. & Niu, J. Q. CXC chemokine IP-10: A key actor in liver disease? *Hepatal. Int.* **7**, 798–804 (2013).
 294. Chen, G. Y., Tang, J., Zheng, P. & Liu, Y. CD24 and siglec-10 selectively repress tissue damage - Induced immune responses. *Science (80-.)*. **323**, 1722–1725 (2009).
 295. Zhou, Q. *et al.* CD24 is a genetic modifier for risk and progression of multiple sclerosis. *Proc. Natl. Acad. Sci. U. S. A.* **100**, 15041–15046 (2003).
 296. Agod, Z. *et al.* Signaling lymphocyte activation molecule family 5 enhances autophagy and fine-tunes cytokine response in monocyte-derived dendritic cells via stabilization of interferon regulatory factor 8. *Front. Immunol.* **9**, (2018).
 297. Karampetsou, M. P., Comte, D., Kis-Toth, K., Kyttaris, V. C. & Tsokos, G. C. Expression patterns of signaling lymphocytic activation molecule family members in peripheral blood mononuclear cell subsets in patients with systemic lupus erythematosus. *PLoS One* **12**, 1–17 (2017).
 298. Mak, A. *et al.* Brief report: Decreased expression of CD244 (SLAMF4) on monocytes and platelets in patients with systemic lupus erythematosus. *Clin. Rheumatol.* **37**, 811–816 (2018).
 299. Tippett, E., Cameron, P. U., Marsh, M. & Crowe, S. M. Characterization of tetraspanins CD9, CD53, CD63, and CD81 in monocytes and macrophages in HIV-1 infection. *J. Leukoc. Biol.* **93**, 913–920 (2013).
 300. Kim, T.-R. *et al.* LPS-induced CD53 expression: a protection mechanism against oxidative and radiation stress. *Mol. Cells* **17**, 125–31 (2004).
 301. York, A., William, K., Argus, J., Stetson, D. & Bensinger, S. Limiting cholesterol biosynthetic flux spontaneously engages type I IFN signaling. *Physiol. Behav.* **163**, 1716–1729 (2015).
 302. Minton, K. Immunometabolism: The antiviral effect of limiting lipids. *Nat. Rev. Immunol.* **16**, 76 (2016).
 303. Van Pel, M., Hagoort, H., Hamann, J. & Fibbe, W. E. CD97 is differentially expressed on

- murine hematopoietic stem- and progenitor-cells. *Haematologica* **93**, 1137–1144 (2008).
304. Steiner, O. *et al.* Differential Roles for Endothelial ICAM-1, ICAM-2, and VCAM-1 in Shear-Resistant T Cell Arrest, Polarization, and Directed Crawling on Blood–Brain Barrier Endothelium. *J. Immunol.* **185**, 4846–4855 (2010).
 305. Waskow, C., Liu, K., Ginhoux, F., Merad, M. & Nussenzweig, M. FMS-like tyrosine kinase 3 is required for dendritic cell development in peripheral lymphoid tissues. *Nat. Immunol.* **9**, 676–683 (2008).
 306. Chistiakov, D. A., Killingsworth, M. C., Myasoedova, V. A., Orekhov, A. N. & Bobryshev, Y. V. CD68/macrosialin: Not just a histochemical marker. *Lab. Investig.* **97**, 4–13 (2017).
 307. Galli, S. J., Borregaard, N. & Wynn, T. A. Phenotypic and functional plasticity of cells of innate immunity: Macrophages, mast cells and neutrophils. *Nat. Immunol.* **12**, 1035–1044 (2011).
 308. Schönheit, J. *et al.* PU.1 Level-Directed Chromatin Structure Remodeling at the *Irf8* Gene Drives Dendritic Cell Commitment. *Cell Rep.* **3**, 1617–1628 (2013).
 309. Liu Yong-Jun, Kanzler, H., Soumelis, V. & Gilliet, M. Dendritic cell lineage, plasticity and cross-regulation. *Nat. Immunol.* **2**, 585–589 (2001).
 310. Chopin, M. *et al.* Transcription Factor PU.1 Promotes Conventional Dendritic Cell Identity and Function via Induction of Transcriptional Regulator DC-SCRIPT. *Immunity* **50**, 77-90.e5 (2019).
 311. Yamazaki, C. *et al.* Critical Roles of a Dendritic Cell Subset Expressing a Chemokine Receptor, XCR1. *J. Immunol.* **190**, 6071–6082 (2013).
 312. Warburg, O. On the origin of cancer cells. *Science (80-)*. **123**, 309–314 (1956).
 313. Stunault, M. I., Bories, G., Guinamard, R. R. & Ivanov, S. Metabolism plays a key role during macrophage activation. *Mediators Inflamm.* **2018**, (2018).
 314. Freemerman, A. J. *et al.* Metabolic reprogramming of macrophages: Glucose transporter 1 (GLUT1)-mediated glucose metabolism drives a proinflammatory phenotype. *J. Biol. Chem.* **289**, 7884–7896 (2014).
 315. Rodríguez-Prados, J.-C. *et al.* Substrate Fate in Activated Macrophages: A Comparison between Innate, Classic, and Alternative Activation. *J. Immunol.* **185**, 605–614 (2010).
 316. O’Neill, L. A. J. & Pearce, E. J. Immunometabolism governs dendritic cell and macrophage function. *J. Exp. Med.* **213**, 15–23 (2016).
 317. Huang, S. C. C. *et al.* Cell-intrinsic lysosomal lipolysis is essential for alternative activation of macrophages. *Nat. Immunol.* **15**, 846–855 (2014).
 318. Tan, H. *et al.* Integrative Proteomics and Phosphoproteomics Profiling Reveals Dynamic Signaling Networks and Bioenergetics Pathways Underlying T Cell Activation. *Immunity* **46**, 488–503 (2017).
 319. Wang, R. *et al.* The Transcription Factor Myc Controls Metabolic Reprogramming upon T Lymphocyte Activation. *Immunity* **35**, 871–882 (2011).

320. Ditoro, D. *et al.* Differential IL-2 expression defines developmental fates of follicular versus nonfollicular helper T cells. *Science* (80-.). **361**, (2018).
321. Verbist, K. C. *et al.* Metabolic maintenance of cell asymmetry following division in activated T lymphocytes. *Nature* **532**, 389–393 (2016).
322. Chapman, N. M., Boothby, M. R. & Chi, H. Metabolic coordination of T cell quiescence and activation. *Nat. Rev. Immunol.* (2019). doi:10.1038/s41577-019-0203-y
323. Zheng, M. & Tian, Z. Liver-Mediated Adaptive Immune Tolerance. *Front. Immunol.* **10**, (2019).
324. Guilliams, M. & Scott, C. L. Does niche competition determine the origin of tissue-resident macrophages? *Nature Reviews Immunology* **17**, 451–460 (2017).

6.2 Table of figures

Figure 1: Anatomical location of hepatic antigen-presenting cells (APCs) and the factors that regulate their function11.”	9
Figure 2: (A,B) Two different views on the hematopoietic development.	15
Figure 3: 3D image of an iMATE with T cells (pink: CD31 for vessels, yellow: Ly6C for inflammatory monocytes, turquoise: CD8 for T cells).	19
Figure 4: (A-D) Hepatic myeloid cells after the application of TLR9-L.	44
Figure 5: (A-C) Analysis of CD11b ⁺ cells after the application of TLR9-L.	45
Figure 6: The immunogenic window.	45
Figure 7: (A-C) Influence of TLR9-L on the myeloid cells in blood, spleen, kidney and lymph nodes.	46
Figure 8: (A-C) Kupffer cell disappearance is slowed down by additional poly-I treatment.	48
Figure 9: (A-B) Effect of poly-I application on myeloid cells in spleen and blood.	48
Figure 10: (A-E) Analysis of myeloid cells after the application of different TLR ligands.	50
Figure 11: FACS analysis of one and 12h pulse chase experiment with BrdU and TLR9-L.	51
Figure 12: (A-C) Cytokine expression in different organs after the application of TLR9L at day 2.	52
Figure 13: (A,B) Phenotypic analysis of myeloid cells at steady state and two and six days after TLR9-L application.	54
Figure 14: Quantification of marker expression at steady state and two days after the application of TLR9-L in CD11b ⁺ cells.	55
Figure 15: Quantification of marker expression at steady state and two days after the application of TLR9-L in CD11b ⁺ cells.	56
Figure 16: Quantification of marker expression at steady state and two days after the application of TLR9-L in CD11b ⁺ cells.	Fehler! Textmarke nicht definiert.
Figure 17: Quantification of marker expression at steady state and two days after the application of TLR9-L in CD11b ⁺ cells.	Fehler! Textmarke nicht definiert.
Figure 18: Quantification of marker expression at steady state and two days after the application of TLR9-L in CD11b ⁺ cells.	Fehler! Textmarke nicht definiert.
Figure 19: (A-B) Visualization of the overlap of the significantly up-regulated genes.	58
Figure 20: Genetic expression profiles of hepatic cells.	59
Figure 21: (A,B) Upregulated CD40 expression after the application of TLR9-L.	59
Figure 22: (A-C) Upregulated Ly6A expression after the application of TLR9-L.	60
Figure 23: (A,B) Upregulated MHCII expression after the application of TLR9-L.	60
Figure 24: Principal component analysis in 3 dimensions, colored by time and shaped by cell type.	61
Figure 25: Volcano plots of the gene differential expression.	62
Figure 26: (A-B) Transient expression of CD40 on hepatic CD11b ⁺ Ly6C ⁺ cells after TLR9-L application.	63
Figure 27: Expression of CD40 and Ly6C on CD11b ⁺ cells in spleen and blood.	63
Figure 28: Expression of TNF receptors under steady state conditions and after the application of TLR9-L.	65
Figure 29: (A,B) FACS analysis of co-expressing markers on CD11b ⁺ Ly6C ⁺ cells.	66
Figure 30: (A-B) CD40 expression after the application of different TLR-L.	66
Figure 31: Expression of CD154 on hepatic myeloid	67
Figure 32: Cytokine expression profile of FACSsorted cells.	68
Figure 33: (A-C) Effect of TLR9-L on hepatic myeloid cells of CD40 ^{-/-} and CD40L ^{-/-} mice.	69
Figure 34: Workflow of bioinformatic analysis.	69
Figure 35: (A-B) Bioinformatic analysis of gene expression data of CD11b ⁺ Ly6C ⁺ CD40 ^{neg} and Clec4F ⁺ Kupffer cells.	70
Figure 36: (A,B) Additional analysis of gene expression data of CD11b ⁺ Ly6C ⁺ CD40 ⁺ cells compared to Clec4F ⁺ Kupffer cells.	75
Figure 37: (A-B) Transcription factor analysis of data from CD11b ⁺ Ly6C ⁺ CD40 ⁺ cells compared to Clec4F ⁺ Kupffer cells.	76
Figure 38: (A-D) Gene co-regulation analysis of genes differentially expressed in CD11b ⁺ Ly6C ⁺ CD40 ⁺ cells compared to Clec4F ⁺ Kupffer cells.	77

Figure 39: (A-D) CD11b⁺Ly6C⁺CD40⁺ cells have a higher glycolytic capacity than Kupffer cells or CD11b⁺Ly6C⁺CD40^{neg} cells. _____ 80

Figure 40: (A-C) No elevated respiratory capacity of CD11b⁺Ly6C⁺CD40⁺ cells. _____ 81

Figure 41: FACS analysis of the expression of CD86, CD68 and Tim4 on CD11b⁺Ly6C⁺CD40⁺ cells, CD11b⁺Ly6C⁺CD40^{neg} cells and Clec4F⁺ Kupffer cells. Data are representative for 3 experiments. _____ 82

Figure 42: (A,B) Influence of CD11b⁺Ly6C⁺CD40⁺, CD11b⁺Ly6C⁺CD40^{neg} and Clec4F⁺ Kupffer cells on CD8 T cells. _____ 83

6.3 Index of tables

Table 1: The 20 most affected genes of the microarray at day 2. _____ 74

Table 2: Differentially regulated transcription factors. _____ 75

Table 3: Number of differentially expressed genes in the different combinations. _____ 78

Table 4: Genes specific for CD11b⁺Ly6C⁺CD40⁺ cells. _____ 79

6.4 Supplementary Tables

		Mouse	6	7	8	11	12	13	14	15	17	18	19	20	21	22	23	24	16		
Hepatocytes	Day2		4	1	7	0	0	0	0	0	0	0	0	0	0	0	0	0	0	0	
	Day3		0	0	0	2	2	2	1	1	0	0	0	0	0	0	0	0	0	0	0
	Day4		0	0	0	0	0	0	0	0	2	2	3	3	0	0	0	0	0	0	0
	Day5		0	0	0	0	0	0	0	0	0	0	0	0	1	2	2	3	0	0	0
iMATEs	Day2		2	4	6	0	0	0	0	0	0	0	0	0	0	0	0	0	0	0	0
	Day3		0	0	0	4	4	3	0	0	0	0	0	0	0	0	0	0	0	0	0
	Day4		0	0	0	0	0	0	0	0	3	4	0	0	0	0	0	0	0	0	3
	Day5		0	0	0	0	0	0	0	0	0	0	0	0	5	4	4	0	0	0	0

Supplementary Table 1: Tissue sections of the different mice and areas.

Genes affected by	nSignGenes			%SignGenes
	nTotal	nUp	nDown	
differential expression in iMATEs versus Hepatocytes at day 2	1773	775	998	10.11
differential expression in iMATEs versus Hepatocytes at day 3	1067	270	797	6.09
differential expression in iMATEs versus Hepatocytes at day 4	1312	462	850	7.48
differential expression in iMATEs versus Hepatocytes at day 5	123	16	107	0.7
differential expression in iMATEs at day 2 versus the average of all Hepatocytes	2484	1062	1422	14.17
differential expression in iMATEs at day 3 versus the average of all Hepatocytes	3478	1790	1688	19.84
differential expression in iMATEs at day 4 versus the average of all Hepatocytes	3283	1710	1573	18.72
differential expression in iMATEs at day 5 versus the average of all Hepatocytes	639	252	387	3.64
differential expression in iMATEs at day 3 versus day2	250	143	107	1.43
differential expression in iMATEs at day 4 versus day2	133	78	55	0.76
differential expression in iMATEs at day 5 versus day2	232	65	167	1.32

differential expression in Hepatocytes at day 3 versus day2	164	107	57	0.94
differential expression in Hepatocytes at day 4 versus day2	12	3	9	0.07
differential expression in Hepatocytes at day 5 versus day2	4	3	1	0.02

Supplementary Table 2: Overall differentially expressed genes. Genes are considered significant if adjusted p-values <0.05.

	No. of differentially expressed genes	No. of up-regulated genes	No. of down-regulated genes
CD11b ⁺ Ly6C ⁺ CD40 ⁺ vs CD11b ⁺ Clec4F ⁺ Ly6C ^{neg}	3463	1407	2056
CD11b ⁺ Ly6C ⁺ CD40 ⁺ vs CD11b ⁺ Ly6C ⁺ d2	299	129	170
CD11b ⁺ Clec4F ⁺ Ly6C ^{neg} vs CD11b ⁺ Ly6C ⁺ d2	13	13	0

Supplementary Table 3: Results of all performed RNA sequencing experiments.

Genes	log2FC	p-value	p-adj	Log2TPM	aliases
<i>Sct</i>	7,34958155	0,0001499	0,00051546	2,97527774	Secretin
<i>Bcl2l14</i>	6,940000328	7,49-10	5,35E-09	3,818813606	apoptosis regulator Bcl-G
<i>Adgrg5</i>	6,67073306	9,48-08	5,43E-07	3,23661161	adhesion G-protein coupled receptor G5
<i>Prm1</i>	6,636621139	1,58-09	1,09E-08	3,421490325	Protamine 1
<i>Ccl12</i>	6,486464658	8,89-29	2,50E-27	6,474326289	C-C motif chemokine ligand 12
<i>Defb52</i>	6,390371122	3,22-60	3,53E-58	9,087795643	defensin beta 52
<i>Gp6</i>	6,165039892	1,10-14	1,24E-13	4,393987102	glycoprotein 6
<i>Anpep</i>	6,141982643	1,18-09	8,29E-09	2,157234785	aminopeptidase M
<i>Il12b</i>	6,110508923	1,33-12	1,24E-11	3,530112631	Interleukin 12 beta
<i>Ffar2</i>	6,078304068	3,22-07	1,73E-06	2,4593503	free fatty acid receptor
<i>Ido1</i>	5,969147615	8,73-07	4,36E-06	1,99588914	Indoleamine-2,3 Dioxygenase
<i>Ly75</i>	5,838958359	2,53-07	1,38E-06	1,163604201	lymphocyte antigen 75
<i>Vdr</i>	5,832513893	1,85-07	1,02E-06	1,44571324	Vitamin D receptor
<i>Tnp2</i>	5,741808039	5,40-11	4,33E-10	4,465184548	transition protein 2
<i>Kcnn4</i>	5,654750997	1,52-11	1,28E-10	3,149816256	potassium channel protein 4
<i>Saa3</i>	5,575415865	7,84-63	9,63E-61	12,16526162	serum amyloid 3
<i>Tmem171</i>	5,567094093	2,45-07	1,34E-06	2,649514131	transmembrane protein
<i>Gpmb</i>	5,528374633	2,17-06	1,02E-05	2,868504087	glycoprotein
<i>Rhov</i>	5,466091902	4,36-07	2,29E-06	2,289613834	Ras homolog family member V
<i>Rmi2</i>	5,442766154	2,78-06	1,29E-05	1,353908328	open reading frame
<i>Ptgs2os2</i>	5,387869521	4,15-07	2,19E-06	2,249937887	prostaglandin-endoperoxide synthase 2;

Supplementary Table 4: The 20 most upregulated genes comparing CD11b+Ly6C+CD40+ cells at day 2 with Clec4F+KCs under steady state conditions.

Genes	log2FC	pvalue	padj	Log2TPM	aliases
<i>Colec10</i>	-6,67434102	9,14E-12	7,85E-11	2,622425156	collectin
<i>Adrb1</i>	-6,7443938	2,49E-08	1,53E-07	2,53561442	adrenoreceptor beta 1
<i>Nkd1</i>	-6,74842266	4,03E-15	4,70E-14	3,04153021	NKD inhibitor of Wnt signlaing pathway 1

<i>Il13ra2</i>	-6,75691208	4,16E-10	3,05E-09	2,83746061	Interleukin 13 receptor subunit alpha 2
<i>Mcc</i>	-6,78747043	2,89E-10	2,15E-09	1,96631715	MCC Regulator Of WNT Signaling Pathway
<i>Tmem132e</i>	-6,7878564	7,11E-11	5,62E-10	2,5622778	transmembrane protein 132E
<i>Tcf7l1</i>	-6,81976614	7,15E-16	8,82E-15	3,37333619	Transcription Factor 7 Like 1
<i>Tmem56</i>	-6,87588768	9,82E-13	9,29E-12	3,74714957	transmembrane protein 56
<i>Ppfia2</i>	-7,0657665	8,32E-11	6,53E-10	1,83775214	PTPRF Interacting Protein Alpha 2
<i>Dnah8</i>	-7,15280056	3,82E-11	3,10E-10	1,36005754	Dynein Axonemal Heavy Chain 8
<i>Ston1</i>	-7,16495952	6,24E-11	4,97E-10	2,42798132	Stonin 1
<i>Pik3c2b</i>	-7,17197357	1,15E-11	9,77E-11	3,53035599	Phosphatidylinositol-4-Phosphate 3-Kinase Catalytic Subunit Type 2 Beta
<i>Ttc28</i>	-7,2209217	2,42E-11	2,01E-10	1,55737944	Tetratricopeptide Repeat Domain 28
<i>Cav1</i>	-7,24166055	9,15E-12	7,86E-11	2,98412738	Caveolin 1
<i>Ntn4</i>	-7,28712939	5,54E-12	4,87E-11	4,15644277	Netrin 4
<i>Vstm4</i>	-7,34842675	7,12E-12	6,20E-11	2,96366709	V-Set And Transmembrane Domain Containing 4
<i>Pcolce2</i>	-7,4019567	3,22E-12	2,91E-11	2,64100578	Procollagen C-Endopeptidase Enhancer 2
<i>Ankrd29</i>	-7,478509	2,99E-12	2,71E-11	2,50451368	Ankyrin Repeat Domain 29
<i>Chp2</i>	-7,51722905	3,20E-12	2,90E-11	3,11460533	Calcineurin Like EF-Hand Protein 2
<i>St6galnac3</i>	-7,6081805	4,54E-13	4,43E-12	3,94827396	ST6 N-Acetylgalactosaminide Alpha-2,6-Sialyltransferase 3

Supplementary Table 5: The 20 most downregulated genes comparing CD11b+Ly6C+CD40+ cells at day 2 with Clec4F+KCs under steady state conditions.

Genes	Log2FoldChange	p-value	p-adj
<i>Ccl12</i>	6,486465	8,89E ⁻²⁹	2,50E ⁻²⁷
<i>Ccl22</i>	3,96616	2,218 ⁻⁰³	5,925 ⁻⁰³
<i>Ccl5</i>	3,96165	1,21E ⁻¹⁴³	1,44E ⁻¹⁴⁰
<i>Ccr7</i>	3,837886	3,29 ⁻⁰⁴	1,06 ⁻⁰³
<i>Ccr2</i>	3,763255	1,29E ⁻³⁶	5,50E ⁻³⁵
<i>Cxcl11</i>	3,693161	2,63E ⁻²⁴	5,64E ⁻²³
<i>Ccl3</i>	3,387046	1,82E ⁻²⁸	5,08E ⁻²⁷
<i>Ccl4</i>	3,23802	1,14E ⁻⁴²	6,19E ⁻⁴¹
<i>Ccl8</i>	3,108213	2,726 ⁻⁰³	7,119 ⁻⁰³
<i>Ccr1</i>	2,827669	5,68E ⁻⁰⁸	3,36E ⁻⁰⁷
<i>Ccr12</i>	2,726271	1,54E ⁻³²	5,27E ⁻³¹
<i>Ccl2</i>	2,695946	2,87E ⁻¹³	2,87E ⁻¹²
<i>Cxcl9</i>	2,342395	3,95E ⁻³¹	1,25E ⁻²⁹
<i>Ccl9</i>	2,214091	2,77E ⁻⁰⁷	1,50E ⁻⁰⁶
<i>Isg20</i>	3,157117	1,62E ⁻³²	5,52E ⁻³¹
<i>Cxcr4</i>	1,802777	5,18E ⁻⁰⁵	1,94 ⁻⁰⁴
<i>Cxcl2</i>	1,623257	1,29E ⁻⁰⁵	5,34E ⁻⁰⁵
<i>Tgfa</i>	-3,165445	1,43E ⁻⁰⁷	8,01E ⁻⁰⁷
<i>Tnfaip1</i>	-3,207461	1,41E ⁻⁶²	1,70E ⁻⁶⁰
<i>Cxcl1</i>	-4,019875	1,92E ⁻²²	3,72E ⁻²¹

<i>Ccl24</i>	-4,379429	8,77E ⁻²⁶	2,06E ⁻²⁴
<i>Cxcl13</i>	-5,971218	6,09E ⁻¹⁸	8,67E ⁻¹⁷
<i>Cxcl12</i>	-6,277776	1,74E ⁻⁴⁸	1,19E ⁻⁴⁶

Supplementary Table 6: Chemokines and receptors differentially regulated in CD11b⁺Ly6C⁺CD40⁺ cells compared to Clec4F⁺Kupffer cell.

Genes	Log2FoldChange	p-value	p-adj
Cd40	4,14151814	4,59 ⁻³¹	3,95E ⁻²⁹
Cd274 (PDL1)	3,61239714	2,12 ⁻²³	1,02E ⁻²¹
Cd7	2,738611505	2,135709 ⁻⁰³	8,032891 ⁻⁰³
Cd86	2,208234712	1,66 ⁻¹⁵	3,85E ⁻¹⁴
Itgax (CD11c)	3,32235512	3,36 ⁻⁰⁷	2,94E ⁻⁰⁶
Cd74	3,246436555	2,00 ⁻¹⁵	4,60E ⁻¹⁴
Tnfrsf4 (OX40)	3,1756283	3,5167 ⁻⁰³	8,9327 ⁻⁰³
Cd69	3,080541568	4,42 ⁻¹¹	6,64E ⁻¹⁰
Cd74	3,616544	3,44 ⁻²⁴	7,31E ⁻²³
Cd69	3,198555	1,49 ⁻¹⁸	2,22E ⁻¹⁷
Cd53	2,38424	2,31 ⁻⁴⁴	1,32E ⁻⁴²
Cd34	-1,76634	2,934 ⁻⁰³	0,007599
Cd9	-1,972961	2,39 ⁻²⁵	5,44E ⁻²⁴
Cd36	-3,018269	1,51 ⁻²⁵	3,49E ⁻²⁴
Cd81	-3,54	1,25 ⁻²³	2,58E ⁻²²
Icam2 (CD102)	-3,540551944	3,61 ⁻²¹	1,44E ⁻¹⁹
Cd27	-3,61517	1,79 ⁻⁰⁵	7,23E ⁻⁰⁵
S1pr1 (CD363)	-3,708924	1,40 ⁻¹²	1,31E ⁻¹¹
Cd209b	-4,669297	5,45 ⁻⁰⁷	2,82E ⁻⁰⁶
Cd55	-5,434695	8,40 ⁻⁴⁰	4,10E ⁻³⁸
Mcam(CD146)	-5,494036	1,20 ⁻¹⁴	1,34E ⁻¹³
Cd59a	-5,494708	5,26 ⁻⁴⁰	2,60E ⁻³⁸
Cd5l	-5,593434	1,30 ⁻¹⁸¹	2,45E ⁻¹⁷⁸
Clec4f	-5,992594	3,76 ⁻¹⁹⁷	1,24E ⁻¹⁹³
Cd207	-6,185497	1,53 ⁻²⁶	3,78E ⁻²⁵
Vsig4	-6,520186	1,75 ⁻⁷⁷	3,42E ⁻⁷⁵
Cd163	-6,65995	7,24 ⁻¹⁴	7,63E ⁻¹³

Supplementary Table 7: Surface markers differentially regulated in CD11b⁺Ly6C⁺CD40⁺ cells compared to Clec4F⁺Kupffer cell.

Genes	Log2FoldChange	p-value	p-adj
<i>Il12b</i>	6,110509	1,33E ⁻¹²	1,24E ⁻¹¹
<i>Il1rn</i>	4,466613	2,69E ⁻⁵⁷	2,70E ⁻⁵⁵
<i>Il4i1</i>	4,217903	3,31E ⁻⁰⁶	1,52E ⁻⁰⁵
<i>Il27</i>	3,869522	3,47E ⁻²³	6,98E ⁻²²
<i>Il12rb2</i>	3,509197	1,9 ⁻⁰⁴	6,4 ⁻⁰⁴
<i>Il15ra</i>	2,481224	2,54E ⁻²¹	4,61E ⁻²⁰
<i>Il18</i>	2,284814	1,13E ⁻⁰⁹	7,91E ⁻⁰⁹
<i>Il10ra</i>	2,171028	9,72E ⁻²⁰	1,56E ⁻¹⁸

<i>Il6</i>	1,905244	2,86E ⁻⁰⁵	1,12 ⁻⁰⁴
<i>Il1b</i>	1,266207	2,86E ⁻¹⁰	2,13E ⁻⁰⁹
<i>Il1a</i>	-2,189725	2,12E ⁻¹⁵	2,53E ⁻¹⁴
<i>Il17rc</i>	-3,544996	3,15E ⁻⁰⁶	1,44E ⁻⁰⁵
<i>Il6st</i>	-3,817353	3,63E ⁻²⁶	8,73E ⁻²⁵
<i>Il33</i>	-4,043921	5,19E ⁻⁰⁷	2,70E ⁻⁰⁶
<i>Il1r1</i>	-6,203315	2,17E ⁻¹²	1,99E ⁻¹¹
<i>Il13ra2</i>	-6,756912	4,16E ⁻¹⁰	3,05E ⁻⁰⁹

Supplementary Table 8: Interleukins and receptors differentially regulated in CD11b+Ly6C+CD40+ cells compared to Clec4F+ Kupffer cell.

symbol	logFC	adj.P.Val	genefamily	genename	RNA Seq
Acbd4	-1.2	7.5e-08		acyl-Coenzyme A binding domain containing 4	
Ghr	-1.4	7.5e-08	Secreted	growth hormone receptor	
Cpt1a	-1.1	1.8e-08		carnitine palmitoyltransferase 1a, liver	
Serpinf1	-2.0	1.1e-08	Secreted	serine (or cysteine) peptidase inhibitor, clade F,	
Cyp2d22	-2.1	1.8e-08		cytochrome P450, family 2, subfamily d, polypeptid	x
Adtrp	-2.2	1.8e-08		androgen dependent TFPI regulating protein	
Tlcd2	-2.5	1.3e-08		TLC domain containing 2	x
Rarres2	-2.6	5.7e-08	Secreted	retinoic acid receptor responder (tazarotene induc	x
Pttg1ip	-2.7	1.4e-08		pituitary tumor-transforming 1 interacting protein	x
Agpat2	-2.7	1.4e-08		1-acylglycerol-3-phosphate O-acyltransferase 2 (ly	upregulated
Apoc4	-2.9	3.6e-09	Secreted	apolipoprotein C-IV	x
Col18a1	-2.9	1.1e-08	Secreted	collagen, type XVIII, alpha 1	x
Tmprss6	-3.0	1.8e-08	peptidase	transmembrane serine protease 6	x
Serpina6	-3.0	7.5e-08	Secreted	serine (or cysteine) peptidase inhibitor, clade A,	
Cyp8b1	-3.1	7.0e-09		cytochrome P450, family 8, subfamily b, polypeptid	
Apoa2	-3.3	3.0e-08	Secreted	apolipoprotein A-II	x
Cyp2d10	-3.6	1.8e-08		cytochrome P450, family 2, subfamily d, polypeptid	
Abcb4	-3.6	5.2e-08	transporter	ATP-binding cassette, sub-family B (MDR/TAP), memb	x
C8g	-3.8	5.2e-08	transporter	complement component 8, gamma polypeptide	x
Apoa1	-4.0	7.5e-08	Secreted	apolipoprotein A-I	x

Supplementary Table 9: The 20 most affected genes of the microarray at day 3; data were compared to the differentially expressed genes comparing KCs with CD11b+Ly6C+CD40+ cells at day 2

symbol	logFC	adj.P.Val	genefamily	genename	RNA Seq
S100a4	2.3	5.6e-08		S100 calcium binding protein A4	x
Spi1	1,9	3.1e-08		spleen focus forming virus (SFFV) proviral integra	x
Pik3r5	1.5	1.8e-07	kinase	phosphoinositide-3-kinase, regulatory subunit 5, p	x
Ghr	-1.4	5.9e-07	Secreted	growth hormone receptor	
Slc25a15	-1.8	4.2e-08	transporter	solute carrier family 25 (mitochondrial carrier or	

Cyp2j5	-1.8	4.0e-07		cytochrome P450, family 2, subfamily j, polypeptid	
Dpyd	-2.0	2.9e-07		dihydropyrimidine dehydrogenase	x
Masp2	-2.0	5.9e-07	peptidase	mannan-binding lectin serine peptidase 2	
Igfbp4	-2.0	5.9e-07	Secreted	insulin-like growth factor binding protein 4	x
Adtrp	-2.1	4.8e-07		androgen dependent TFPI regulating protein	
Aldh8a1	-2.3	2.9e-07		aldehyde dehydrogenase 8 family, member A1	x
Otc	-2.4	3.2e-07		ornithine transcarbamylase	
Abcb11	-3.1	4.4e-07	transporter	ATP-binding cassette, sub-family B (MDR/TAP), memb	
C4bp	-3.2	1.8e-07		complement component 4 binding protein	
Pxmp2	-3.3	6.9e-07		peroxisomal membrane protein 2	
Slc22a1	-3.6	1.8e-07	transporter	solute carrier family 22 (organic cation transport	x
Ehhadh	-3.6	1.8e-07		enoyl-Coenzyme A, hydratase/3-hydroxyacyl Coenzyme	
Cyp2c54	-3.6	2.9e-07		cytochrome P450, family 2, subfamily c, polypeptid	
Cyp4a14	-3.9	4.2e-08		cytochrome P450, family 4, subfamily a, polypeptid	
Cyp4a10	-4.4	3.6e-07		cytochrome P450, family 4, subfamily a, polypeptid	

Supplementary Table 10: The 20 most affected genes of the microarray at day 4; data were compared to the differentially expressed genes comparing KCs with CD11b+Ly6C+CD40+ cells at day 2

symbol	logFC	adj.P.Val	genefamily	genename	RNA seq
Arrb2	1.1	1.4e-04		arrestin, beta 2	
Mical1	1.2	2.1e-04		microtubule associated monooxygenase, calponin and	x
Ltb	1.3	1.4e-04		lymphotoxin B	
Gimap3	2.3	1.2e-05		GTPase, IMAP family member 3	
Ctsw	2.3	4.3e-05	peptidase	cathepsin W	
H2-Ob	1.4	6.5e-05		histocompatibility 2, O region beta locus	
Laptm5	1.5	1.8e-05		lysosomal-associated protein transmembrane 5	
Emp3	1.9	1.9e-04		epithelial membrane protein 3	x
Coro1a	2.6	4.9e-05		coronin, actin binding protein 1A	x
H2-Eb1	2.9	7.1e-05		histocompatibility 2, class II antigen E beta	
Asgr2	-0.7	6.5e-05		asialoglycoprotein receptor 2	
Ptprf	-0.8	2.0e-04	phosphatase	protein tyrosine phosphatase, receptor type, F	
AI317395	-1.2	7.1e-05	peptidase	expressed sequence AI317395	
Tmem19	-1.2	1.1e-04		transmembrane protein 19	
Ociad2	-1.4	1.2e-04		OCIA domain containing 2	
Dpys	-1.4	1.5e-04		dihydropyrimidinase	
C1ra	-1.6	1.2e-04	peptidase	complement component 1, r subcomponent A	x
Insig2	-1.7	1.7e-04		insulin induced gene 2	x
Adtrp	-1.9	1.0e-05		androgen dependent TFPI regulating protein	
Retsat	-2.5	1.0e-05		retinol saturase (all trans retinol 13,14 reductas	x

Supplementary Table 11: The 20 most affected genes of the microarray at day 5; data were compared to the differentially expressed genes comparing KCs with CD11b+Ly6C+CD40+ cells at day 2

Genes	Degree	Log2FC	P adj	Log2TPM
<i>Cebpb</i>	177	1,60098	8,8 ⁻¹²	9,79639
<i>Irf8</i>	49	1,33033	1,3 ⁻¹²	8,46819
<i>Irf5</i>	148	3,04194	2 ⁻¹⁰⁸	8,337
<i>Mrpl28</i>	107	1,24915	3,8 ⁻⁰⁷	8,23895
<i>Batf3</i>	31	2,11211	6,4 ⁻¹⁰	8,08337
<i>Ikzf1</i>	75	2,37304	1,5 ⁻¹¹	8,0297
<i>Batf</i>	47	2,14657	1,9 ⁻¹³	7,89074
<i>Nfkbib</i>	34	1,73725	8,7 ⁻¹⁴	7,75116
<i>Tgif1</i>	111	1,89143	1,4 ⁻¹⁵	7,69762
<i>Stat1</i>	166	3,49817	1,1 ⁻⁴⁴	7,63159
<i>Arid5a</i>	58	2,46906	6,2 ⁻¹⁷	7,47778
<i>Nr1h3</i>	29	1,19268	1,6 ⁻⁰⁵	7,40305
<i>Hmgn3</i>	34	3,0341	1 ⁻¹¹	7,17734
<i>Relb</i>	63	2,06045	9 ⁻⁰⁸	7,02261
<i>Mlx</i>	121	1,2504	7,8 ⁻⁰⁹	6,6256
<i>Lyl1</i>	54	1,95676	5,4 ⁻¹⁴	6,55138
<i>Bhlhe40</i>	38	1,98209	4,9 ⁻⁰⁶	6,13232
<i>Mier2</i>	46	1,57891	3,7 ⁻⁰⁹	6,1277
<i>Zfp524</i>	31	1,24795	1,93 ⁻⁰³	6,12726
<i>Nfkb2</i>	35	1,98378	7,2 ⁻⁰⁹	5,9975
<i>Hmgb2</i>	27	1,38792	1,4 ⁻⁰⁶	5,98098

Supplementary Table 12: Transcription factors affected downstream of differentially regulated genes in CD11b+Ly6C+CD40+ cells compared to Clec4F+ Kupffer cells. (degree = number of targets)

Genes	Log2FC	p adj
<i>Bcl2a1d</i>	4,94714	2,34382 ⁻²⁹
<i>Slc2a6</i>	4,72117	3,40252 ⁻⁴²
<i>Bcl2a1a</i>	4,64386	1,74607 ⁻⁵³
<i>Spib</i>	4,45513	1,062222 ⁻⁰³
<i>Traf1</i>	4,20703	2,20866 ⁻³⁸
<i>Cd40</i>	4,17224	2,67887 ⁻⁴⁸
<i>Ciita</i>	4,1008	5,01466 ⁻¹⁹
<i>Xcr1</i>	3,97568	1,39912 ⁻⁰³
<i>Ccl5</i>	3,96165	1,4448 ⁻¹⁴⁰
<i>Cd52</i>	3,81788	2,8305 ⁻¹⁰⁰
<i>Cd74</i>	3,61654	7,30607 ⁻²³
<i>Cd274</i>	3,5576	7,42262 ⁻³⁸
<i>Stat1</i>	3,49817	1,07783 ⁻⁴⁴
<i>Cd69</i>	3,19856	2,22022 ⁻¹⁷
<i>Isg20</i>	3,15712	5,5246 ⁻³¹
<i>Irf5</i>	3,04194	1,8403 ⁻¹⁰⁸
<i>Irf7</i>	2,84458	4,42939 ⁻⁵⁷
<i>Ccl2</i>	2,72627	5,27242 ⁻³¹
<i>Isg15</i>	2,6812	1,13233 ⁻⁶¹

CD52	2,38424	1,3245 ⁻⁴²
------	---------	-----------------------

Supplementary Table 13: IRF8 target signature expressed in CD11b⁺Ly6C⁺CD40⁺ cells.

Genes	log2FoldChange	p value	p adj	Log2TPM
Slc2a6	4,721166861	6,01E-44	3,40E-42	6,8538525
Slc4a11	4,089193834	0,0013859	0,0039177	0,9732412
Slc7a11	3,976825751	5,06E-08	3,01E-07	2,0421601
Slc28a2	3,817096522	2,07E-13	2,09E-12	3,8264232
Slc16a3	3,652679698	1,55E-36	6,58E-35	6,9740793
Slc2a1	3,324413494	4,52E-23	9,03E-22	4,9975236
Slc36a3os	3,18057681	9,82E-16	1,20E-14	6,5789037
Slc16a10	3,046423178	4,57E-10	3,32E-09	2,9793848
Slc38a1	2,506252609	1,17E-07	6,61E-07	2,5452592
Slc29a3	2,321974093	4,96E-15	5,73E-14	4,1774244
Slc35c2	2,303455786	4,03E-22	7,64E-21	7,5361196
Slc25a13	1,921835574	0,0012779	0,0036434	2,729395
Slc1a5	1,913554155	1,92E-06	9,13E-06	3,9439572
Slc11a1	1,782069818	1,58E-07	8,81E-07	7,2250922
Slc15a4	1,625424072	4,95E-12	4,40E-11	5,8924999
Slc6a6	1,527505187	1,44E-11	1,21E-10	5,8987687
Slc35c1	1,447462654	5,40E-08	3,20E-07	5,0432051
Slc25a20	1,441856751	2,26E-08	1,39E-07	5,8853621
Slc26a2	1,422600562	0,0002709	0,0008865	3,4685289
Slc15a3	1,368805286	2,14E-07	1,18E-06	7,5584758
Slc52a2	1,292832311	0,0006076	0,0018644	4,2562494
Slc31a1	1,273881261	2,37E-08	1,46E-07	6,4136413
Slc12a9	1,156980615	0,001021	0,0029785	4,030917
Slc8b1	1,11461362	1,88E-05	7,59E-05	6,4301132
Slc7a8	1,05807218	0,0018283	0,0049812	4,56381
Slc25a12	1,025357996	0,0011373	0,0032837	3,8991127
Slc25a45	1,014546332	1,94E-05	7,80E-05	5,9259497
Slc43a2	-1,013914035	0,0001029	0,000364	9,1177401
Slc50a1	-1,143999582	5,65E-13	5,46E-12	8,7515697
Slc39a10	-1,267182986	0,0022368	0,0059689	2,7716369
Slc38a2	-1,410779586	9,66E-11	7,56E-10	5,7703172
Slc38a10	-1,44252906	5,86E-07	3,01E-06	4,749099
Slc35a1	-1,637902556	7,84E-09	5,09E-08	5,3126906
Slc37a3	-1,883043352	0,0003554	0,0011386	2,888062
Slc36a4	-1,941694963	4,02E-08	2,42E-07	4,7929792
Slc35b3	-1,95300411	1,53E-09	1,06E-08	5,4571034
Slc35d1	-2,121003459	0,000663	0,0020172	2,3438289
Slc25a35	-2,307367217	4,32E-05	0,0001632	3,3781283

Slc22a15	-2,368880173	0,0019005	0,0051585	2,235384
Slc25a29	-2,526931165	1,33E-05	5,52E-05	3,5175844
Slc7a5	-2,946431012	1,34E-06	6,52E-06	2,5750958
Slc2a8	-3,094636617	7,13E-17	9,31E-16	4,5599706
Slc17a9	-3,290521493	0,0008104	0,002413	1,9966675
Slc12a2	-3,295669292	1,49E-06	7,19E-06	1,8658524
Slc44a1	-3,534051008	1,48E-12	1,38E-11	3,8368878
Slc9a9	-3,539374198	6,05E-23	1,20E-21	4,2288884
Slc27a3	-3,736074927	0,0016038	0,0044405	1,8500146
Slc46a1	-3,989138632	1,67E-18	2,47E-17	4,1964095
Slc16a2	-4,114144322	7,11E-08	4,13E-07	2,2022345
Slc29a1	-4,119803832	5,38E-57	5,36E-55	8,2311769
Slc22a17	-4,150775682	0,0010797	0,0031354	1,1260609
Slco1b2	-4,194627866	0,0007763	0,0023301	1,3745511
Slco2b1	-4,287500351	1,05E-06	5,19E-06	1,8992111
Slc26a10	-4,352613019	2,07E-34	7,89E-33	4,9569531
Slco2a1	-4,398365528	1,26E-23	2,58E-22	4,7851205
Slc5a3	-4,449730815	3,96E-16	4,92E-15	2,1385374
Slc43a3	-4,617585859	7,91E-27	1,99E-25	9,7130147
Slc12a5	-4,693960573	7,88E-10	5,61E-09	4,5481144
Slc16a9	-4,735078521	0,0001603	0,000548	1,2252947
Slc40a1	-4,77842372	4,04E-67	5,59E-65	6,3420594
Slc45a3	-4,827299112	1,70E-09	1,17E-08	2,8190674
Slc16a12	-4,959344465	0,0002076	0,0006937	1,015009
Slc9a3r2	-5,309103389	1,02E-15	1,24E-14	7,7507566
Slc24a5	-5,453342715	1,07E-27	2,83E-26	4,446546
Slc35g2	-5,477233141	1,24E-06	6,07E-06	2,5048186
Slc10a6	-5,56695592	7,78E-07	3,92E-06	2,297682
Slc18b1	-6,061164394	6,86E-08	4,00E-07	2,2605409
Slc39a8	-6,389751476	3,50E-42	1,87E-40	4,3935872

Supplementary Table 14: Glucose transporters differentially expressed in CD11b+Ly6C+CD40+ cells compared to Clec4F+Kupffer cells.

6.5 Index of supplementary Tables

Supplementary Table 1: Tissue sections of the different mice and areas.	114
Supplementary Table 2: Overall differentially expressed genes. Genes are considered significant if adjusted <i>p</i> -values <0.05.	115
Supplementary Table 3: Results of all performed RNA sequencing experiments.	115
Supplementary Table 4: The 20 most upregulated genes comparing CD11b+Ly6C+CD40+ cells at day 2 with Clec4F+KCs under steady state conditions.	115
Supplementary Table 5: The 20 most downregulated genes comparing CD11b+Ly6C+CD40+ cells at day 2 with Clec4F+KCs under steady state conditions.	116
Supplementary Table 6: Chemokines and receptors differentially regulated in CD11b+Ly6C+CD40+ cells compared to Clec4F+Kupffer cell.	117
Supplementary Table 7: Surface markers differentially regulated in CD11b+Ly6C+CD40+ cells compared to Clec4F+Kupffer cell.	117
Supplementary Table 8: Interleukins and receptors differentially regulated in CD11b+Ly6C+CD40+ cells compared to Clec4F+Kupffer cell.	118
Supplementary Table 9: The 20 most affected genes of the microarray at day 3; data were compared to the differentially expressed genes comparing KCs with CD11b+Ly6C+CD40+ cells at day 2	118
Supplementary Table 10: The 20 most affected genes of the microarray at day 4; data were compared to the differentially expressed genes comparing KCs with CD11b+Ly6C+CD40+ cells at day 2	119
Supplementary Table 11: The 20 most affected genes of the microarray at day 5; data were compared to the differentially expressed genes comparing KCs with CD11b+Ly6C+CD40+ cells at day 2	119
Supplementary Table 12: Transcription factors affected downstream of differentially regulated genes in CD11b+Ly6C+CD40+ cells compared to Clec4F+Kupffer cells. (degree ≡ number of targets)	120
Supplementary Table 13: IRF8 target signature expressed in CD11b+Ly6C+CD40+ cells.	121
Supplementary Table 14: Glucose transporters differentially expressed in CD11b+Ly6C+CD40+ cells compared to Clec4F+Kupffer cells.	122

6.6 Abbreviation

2-NBDG	2-deoxy-2-[(7-nitro-2,1,3-benzoxadiazol-4-yl) amino]-D-glucose
AF	Alexa Fluor
AHR	aryl hydrocarbon receptor
APC	antigen presenting cell
BM	bone marrow
BrdU	Bromodeoxyuridine
Clec	C-type lectin family member
CCR	C-C chemokine receptor type
CD	cluster of differentiation
C/EBP	CCAAT/enhancer binding protein
CpG	CpG – dinucleotide
CSF	colony stimulating factor
CTL	cytotoxic T lymphocyte
d	day
DAMP	danger/damage-associated molecular pattern
DC	dendritic cell
DEG	differentially expressed genes
ECAR	extracellular acidification rate
ELISA	enzyme-linked immunosorbent assay
FACS	fluorescence activated cell sorting
FcR	immunoglobulin receptor
FlowSOM	visualization for cytometry data, by using Self-Organizing Map clustering
Fig	figure
FITC	fluorescein
GFP	green fluorescent protein
GLUT	glucose transporter
GPI	glycophosphatidylinositol
GP(C)R	G-protein coupled receptor

GSEA	gene set enrichment analysis
GzmB	granzyme B
h	hour(s)
HSC	hepatic stellate cells
ICAM	intercellular adhesion molecule
IDO	indoleamine 2,3-dioxygenase
IFN	interferon
IL	interleukin
iNOS	nitric oxide synthase
IRF	interferon regulating factor
iMATE	intrahepatic myeloid cell aggregate for T cell expansion
iv	intravenous
JNK	c-Jun N-terminal kinase
KC	Kupffer cell
LAK	lymphokine activated killing
LAMP	lysosome associated membrane protein
LPS	Lipopolysaccharide
LSEC	liver sinusoidal endothelial cell
MAIT	mucosal-associated invariant T <i>cells</i>
<i>MAMP</i>	microbial associated molecular patterns
MAPK	mitogen activated protein kinase
MCP	monocyte chemoattractant protein
MglI	Monoglyceride Lipase
MHC	major histocompatibility complex
MIP	macrophage inflammatory protein
moDCs	monocyte-derived dendritic cells
MPIF	myeloid progenitor inhibitory factor
MPS	mononuclear phagocyte system
NfκB	Nuclear factor kappa-light-chain-enhancer of activated B cells
NK	natural killer cell

NKT	natural killer T cell
NO	nitric oxide
NPC	non-parenchymal cell
ODN	oligo di-nucleotide
OVA	ovalbumin
PAMP	pathogen-associated molecular pattern
PBS	phosphate buffered saline
PCA	principal component analysis
pDC	plasmacytoid dendritic cell
PE	phycoerythrin
PFA	paraformaldehyde
Poly-I	polyinosinic acid
Poly-IC	polyinosinic:polycytidylic acid
PPR	pattern recognition receptor
Q-VD-O-Ph	carboxy terminal phenoxy group conjugated to valine and aspartate
RANTES	regulated on activation normal T expressed and secreted protein
RFP	red fluorescent protein
RNA	ribonucleic acid
ROS	reactive oxygen species
RT	room temperature
Runx	runt-related transcription factor
SPF	specific pathogen free
TCR	T cell receptor
TGF- β	transforming growth factor beta
T _H	T helper cell
Tim	T-cell immunoglobulin and mucin-domain containing
Tip	TNF/iNOS-producing
TLR	toll-like receptor
TLR-L	toll-like receptor ligand
TMB	3,3',5,5'-Tetramethylbenzidin

TNF	tumor necrosis factor
TNFR	tumor necrosis factor receptor
TRAF	TNF receptor associated factor
TRAIL	TNF-related apoptosis-inducing ligand
T _{reg}	regulatory T cell
VSIG4	V-set and immunoglobulin domain containing 4
WGCNA	weighted gene correlation network analysis
YFP	yellow fluorescent protein
μ	micro

6.7 Prior publications

Excerpts of this work were used at the following congresses:

Pawelka K., Höchst B., Heikenwälder M., Haller D., Knolle P. „Unique functional phenotype of iMATE-defining monocytes.”

Talk at *the European Congress of Immunology, Amsterdam, Netherlands (2018)*

Pawelka K., Tuefferd M., Höchst B., Heikenwälder M., Aerssens J., Knolle P. “Identification of the unique functional phenotype of iMATE-defining monocytes that drive hepatic T cell proliferation.”

Poster at the *Keystone Meeting “Myeloid cells.” Breckenridge, Colorado, USA (2018)*

Pawelka K., Höchst B., Heikenwälder M., Haller D., Knolle P. „Unique functional phenotype of iMATE-defining monocytes and their contribution to local T cell proliferation in the liver.”

Talk at the Annual meeting of *the “Deutsche Gesellschaft für Immunologie”, Erlangen, Germany (2017)*

Pawelka K., Höchst B., Heikenwälder M., Haller D., Knolle P. „Unique functional phenotype of iMATE-defining monocytes and their contribution to local T cell proliferation in the liver.”

Poster at the Annual meeting of *the “Deutsche Gesellschaft für Immunologie”, Hamburg, Germany (2016)*

7 Acknowledgement

There are many people who contributed to this work and enabled its finalization.

I especially want to thank Prof. Percy A Knolle for giving me the opportunity for this dissertation at his institute of molecular immunology. This work would have not been possible without his support on an intellectual but also personal level, all the fruitful discussions and all the opportunities for scientific discourse on conferences he enabled.

I want to thank Prof. Dirk Haller for his helpful supervision as the second reviewer.

I want to thank Prof. Matthias Heikenwalder for the scientific discussions in his role as my mentor.

Furthermore, I want to thank all the members of the institute for their support and help, especially Miriam Bosch, Phillipa Meiser, Sainitin Donakonda, Sandra Lampl, Max Ludemann, Nina Kallin, Silke Hegenbarth and Savvoula Michailidou.

Finally, I want to thank my parents and grandparents who have always been supporting me along my way through difficult and happy times.